PERFORMANCE EVALUATION OF SWAT AND HEC-HMS MATHEMATICAL MODELS FOR ATRAI-KARATOA RIVER BASIN

Master of Engineering Project

By

MD. MONIRUZZAMAN

DEPARTMENT OF WATER RESOURCES ENGINEERING

BANGLADESH UNIVERSITY OF ENGINEERING AND TECHNOLOGY

DHAKA-1000, BANGLADESH

NOVEMBER 2022

PERFORMANCE EVALUATION OF SWAT AND HEC-HMS MATHEMATICAL MODELS FOR ATRAI-KARATOA RIVER BASIN

Master of Engineering Project

By

MD. MONIRUZZAMAN

Student ID: 0416162016 P

DEPARTMENT OF WATER RESOURCES ENGINEERING

BANGLADESH UNIVERSITY OF ENGINEERING AND TECHNOLOGY

DHAKA-1000, BANGLADESH

NOVEMBER 2022

PERFORMANCE EVALUATION OF SWAT AND HEC-HMS MATHEMATICAL MODELS FOR ATRAI-KARATOA RIVER BASIN

Submitted by

Md. Moniruzzaman

(Student ID: 0416162016 P)

In partial fulfillment of the requirement for the degree of
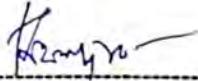
MASTER OF ENGINEERING IN WATER RESOURCES ENGINEERING

DEPARTMENT OF WATER RESOURCES ENGINEERING

BANGLADESH UNIVERSITY OF ENGINEERING AND TECHNOLOGY

DHAKA-1000, BANGLADESH

NOVEMBER 2022

Bangladesh University of Engineering and Technology, Dhaka
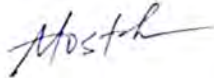## Department of Water Resources Engineering

Certificate of Approval

The project titled **"Performance Evaluation of SWAT and HEC-HMS Mathematical Models for Atrai-Karatoa River Basin"**, submitted by Md. Moniruzzaman, roll no. 0416162016 P, Session April 2016, to the Department of Water Resources Engineering, Bangladesh University of Engineering and Technology, has been accepted as satisfactory in partial fulfillment of the requirements for the degree of Master of Engineering in Water Resources Engineering and approved as to its style and content. Examination held on November 09, 2022.

Dr. Badal Mahalder
Associate Professor
Department of Water Resources Engineering
Bangladesh University of Engineering Technology

Chairman
(Supervisor)

Dr. Md. Mostafa Ali
Professor
Department of Water Resources Engineering
Bangladesh University of Engineering Technology

Member

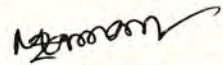---

Dr. Nasreen Jahan
Professor
Department of Water Resources Engineering
Bangladesh University of Engineering Technology

Member

III

CANDIDATE'S DECLARATION

It is hereby declared that this project or any part of it has not been submitted elsewhere for the award of any degree or diploma.

Signature of the Candidate

Md. Moniruzzaman

TABLE OF CONTENTS

LIST OF FIGURES

LIST OF TABLES

LIST OF ABRIVATION

AKRB	Atrai-Karatoa River Basin
BWDB	Bangladesh Water Development Board
CN	Curve Number
DEM	Digital Elevation Model
ET	Evapotranspiration
FAO	Food and Agriculture Organization
GBM	Ganges-Brahmaputra-Meghna
GCM	Global Climate Model
GIS	Geographic Information System
HEC-HMS	Hydraulic Engineering Center – Hydraulic Modeling System
HRU	Hydraulic Response Unit
IPCC	Intergovernmental Panel on Climate Change
IRBs	International River Basins
IWM	Institute of Water Modelling
LULC	Land Use and Land Cover
MOM	Methods of Moment
NASA	National Aeronautics and Space Administration
NOAH	National Organization for Albinism and Hypopigmentation
NWHR	North-West Hydrological Region
NWRM	North-West Regional Model
POWER	Prediction of Worldwide Energy Resources
SCS	Soil Conservation Service
SREC	Special Report on Emissions Scenarios
SRTM	Shuttle Radar Topography Mission
SW	Surface Water
SWAT	Soil and Water Assessment Tool
SWATBF	Soil and Water Assessment Tool Base Flow
UH	Unit Hydrograph
USDA	United State Department of Agriculture

ACKNOWLEDGEMENT

ABSTRACT

The use of mathematical models for simulating the hydrological processes in a catchment scale is getting popular. As a result, numerous hydrological models have been developed by researchers over the years. These complex mathematical models have contributed significantly in understanding the hydrological processes in different scales. Therefore, those models have been providing logical supports to the strategists and policy makers for sustainable watershed management. However, those models were developed based on various theories and assumptions considering distinct goals, therefore, the performances of hydrological models are not similar. Therefore, a comparative study using different hydrological models required to evaluate the performances of different hydrological models applicable to a particular watershed.

In this study, two popular hydrological modeling software SWAT and HEC-HMS have been used to assess the performance of those models in a data limited watershed of Bangladesh. Atrai-Karatoa River system is one of the prominent rivers in the Northwest Hydrological Region (NWHR) of Bangladesh. The Atrai-Karatoa River basin does not have year-round continuous discharge measurements, unlike other rivers in Bangladesh. As a result, utilizing historical climate, land use, and soil data, calibrated and validated hydrological model can be beneficial for estimating runoff for the watershed.

Results from this study revealed that during the calibration and validation phase, the performances of two models were satisfactory and both models were able to reproduce the hydrological characteristics of the Atrai-Karatoa watershed during dry and wet seasons. During calibration (2017–2019) and validation (2013–2016), Coefficient of Determination (R^2) and a Nash Sutcliffe Efficiency (NSE) were found 0.86, 0.75, and 0.84, 0.75, respectively for the SWAT model. During the same periods, the HEC-HMS model results showed the values were 0.70, 0.56, and 0.68, 0.55, respectively during the calibration and validation. These results inferred that high flows were captured well by the SWAT model, while medium flows were captured well by the HEC-HMS model. It is noteworthy that the simulated low flows were close to the observed values by both models. Furthermore, dry and wet seasonal flows were simulated reasonably well by the SWAT model with slight under predicting compared to the observed values. The HEC-HMS model slightly over predicted the dry flow during validation stage and slightly over predicted the wet seasonal peak flows in calibration stage and slightly under predicted the

peak flow during validation stage compared to observed flows. However, overall SWAT model performed better compared with HEC-HMS for the Atrai-Karatoa River Basin.

In addition, in this study peak flows for different return periods have been estimated considering the return period of different rainfall events. Results show that the HEC-HMS estimated flow varied between 5% to 10% compared with the data using observed predicted flow, whereas, the SWAT estimated flow varied between 3% to 6%. These findings indicated that for the Atrai-Karatoa River basin both HEC-HMS and SWAT model performs satisfactorily but between the two models SWAT performed better than the HEC-HMS model.

CHAPTER 1

INTRODUCTION

1.1 Background and Present State of the Problem

Watershed is a geographical area drained to an exit point through a network of streams, which is also a complex and dynamic biophysical system used to plan and manage a project (Elias and Alderton, 2020) In terms of the resources (materials), energy, and information available, a watershed is also a hydrological rejoinder unit and a multidimensional ecological unit. The watershed can be a helpful unit for physical assessments as well as a socioeconomic-political component for the implementation of management methods. The hydrological behavior of any watershed can be understood by using mathematical modelling tools, which has been extensively used for watershed management (Lund et al., 2010). Many environmental transport processes including excess water, water shortage, and dissolved/solid material can be analyzed realistically using hydrologic modeling (Elias and Alderton, 2020). Due to dynamic nature of a watershed and its hydrological processes, no single model can provide the optimum results of hydrological parameters; instead, several models can provide realistic solutions for diverse hydrological conditions (Elias and Alderton, 2020).

Therefore, a comparative study using different hydrological model is required to evaluate the performances of different hydrological models. Among numerous hydrological models, SWAT and HEC-HMS are popular, which have been used extensively to estimate watershed runoff. These are semi-distributed model, which use gridded and non-gridded data to calculate runoff from a basin (Ali et al., 2019).

Several river systems are interlinked among the eight hydrological regions of Bangladesh. Atrai-Karatoa river is a major river system in the North Bengal, located in the North-Western Hydrological Region (NWHR), which used to receive water from the Teesta River and flows to the Ganges River. However, after the 1787 earthquake, the river course was shifted and entered the Brahmaputra/Jamuna River (Nowreen et al., 2020). At present, the Atrai-Karatoa originates from a beel (depressed area) of Baikunthapur in India and initially enters Bangladesh (latitude 26°28' and longitude 88°36') at Bardeshwari in Panchagarh district. It runs towards the south up to Sahamjhiaghat before entering India again and running for 50 km within India. The river re-enters Bangladesh (latitude 25°10' and longitude 88°46') at Naogaon, flows southward, meets the Little Jamuna (this Jamuna is

not the Brahmaputra-Jamuna, it is another river flowing through the district of Naoga) near Rasulpur, and ultimately falls at Hurasagar. This is a long river with a total length of about 455 km. For the present analysis, the river has been divided into two reaches, namely, Karatoa and Atrai. The upper reach is Karatoa, which extends from Panchagarh to Dinajpur before entering into India, and the lower reach is Atrai, when it re-enters into Bangladesh from Naogaon and flows up to its outfalls at Hurasagar River. The river is the main drainage system for a large part of the north-west region of Bangladesh (Nowreen et al., 2020).

Similar to other rivers in Bangladesh, continuous discharge measurements are not available throughout the year for the Atrai-Karatoa River basin (Quader, 1995). Therefore, an established mathematical hydrological model can be useful to forecast runoff though the watershed using recorded climate, land use, and soil data. Literature suggests that few studies have been conducted on the hydrological analysis of the Atrai-Karatoa River basin (Islam et al. 2016; Jahan et al., 2018; Hossain et al., 2020). Moreover, previous studies did not consider the performance evaluation of multiple hydrologic models on this watershed. Therefore, this research aims to use two completely different hydrological models: SWAT and HEC-HMS for Atrai-Karatoa River basin to better understand the model performances by comparing the simulated and observed discharge.

1.2   Objective of the Study

a) The main objective of this study is listed below:

i)   To develop calibrated and validated hydrological models using SWAT and HEC-HMS for estimating surface runoff for Atrai-Karatoa River basin.

ii) To compare the performances of these models by analyzing the results.

b) Possible outcome:

The expected outcome of this research work would be:

Calibrated and validated hydrological models will be developed for Atrai-Karatoa river basin using SWAT and HEC-HMS model. This result will also help the Water Resources Engineers and policy makers for selecting suitable model/models in this hydrological region based on the performances of these models.

1.3   Organization of the Thesis

Chapter 1 is the Introduction to the study. Here, the background, present state of the study, objectives and possible outcomes of the study have been discussed.

Chapter 2 is the Literature Review and related theoretical background. This chapter contains review of hydro-morphological status of the study area, Atrai-Karatoa River Basin. Also, literature of several topics which include review of previous studies for estimating surface runoff and model performance evaluation of different River Basin have been discussed. The basic concepts and theories of different hydrological processes of HEC-HMS and SWAT models are also discussed.

Chapter 3 discuss about the Study Area, where the physical and climatic characteristics of the study area and steps followed in the present study from data collection to model setup, model calibration/validation for estimating surface runoff for the Atrai-Karatoa River Basin have been discussed.

Chapter 4 describes the detail climatic data analysis and procedure followed to setup surface runoff models of Atrai-Karatoa River Basin and process of Calibration and validation of surface runoff models.

Chapter 5 describes the results obtained from this study and evaluate the performance of calibration/validation and discussions made on future climatic change and its impact on the model performance.

Chapter 6 is the Conclusions and Recommendations. This chapter gives a summary of the results obtained in this study and includes recommendations for further study relevant to this topic.

CHAPTER 2

LITERATURE REVIEW AND THEORETICAL BCKGROUND

2.1 General

This chapter provides a brief literature review on Atrai-Karatoa River Basin and comparative study on different hydrological model conducted all over the world. A careful and thorough literature review is essential for conducting research at any level. In this section, available study reports, project documents, published scientific articles have been collected and reviewed to get information on the study area and corresponding water resources related to this study.
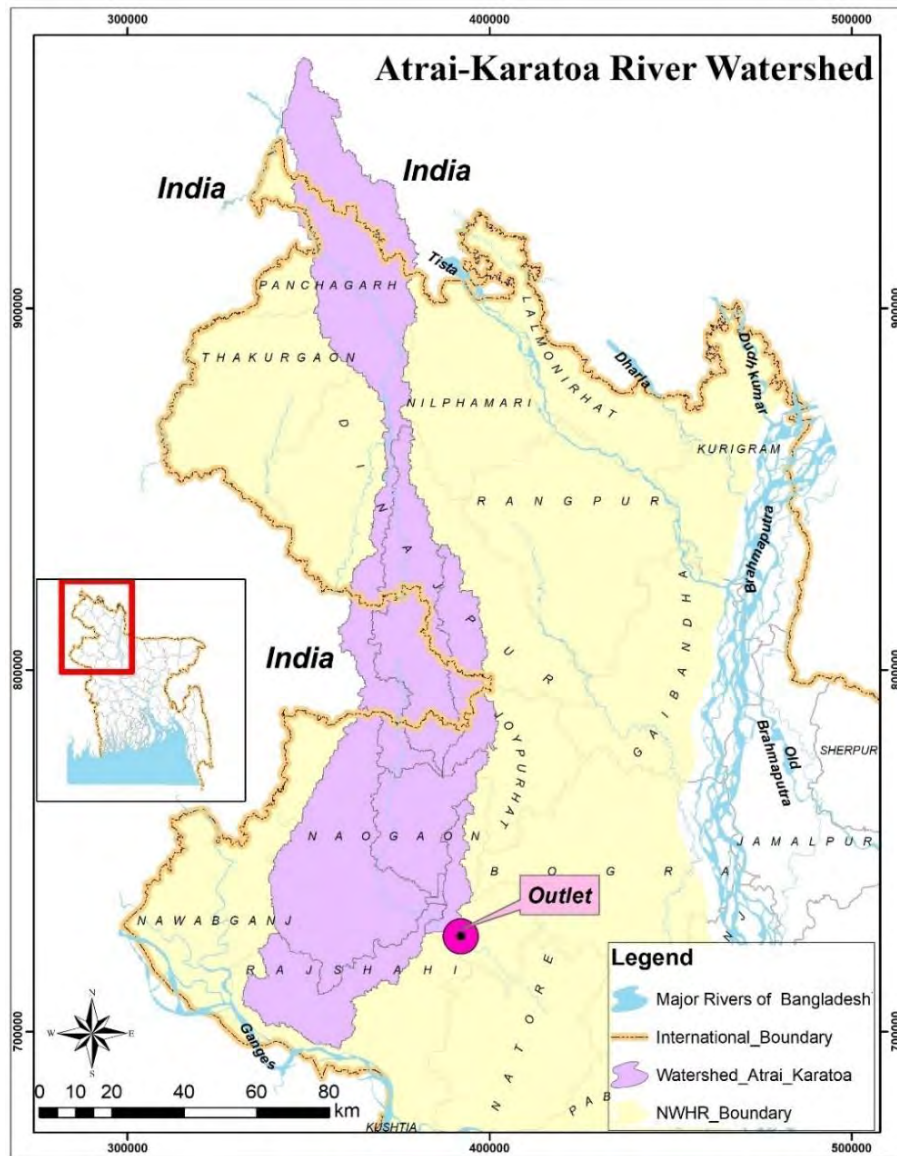
Figure 2. 1: Atrai-Karatoa River Basin

2.2 Previous Studies and Research on River Basin Runoff

Several studies on River runoff have been conducted on several Rivers of Bangladesh by many researchers. According to the literature, there have been few research on the hydrological analysis of the Atrai-Karatoa River basin. Furthermore, earlier research on this watershed did not consider the performance evaluation of several hydrologic models.

2.2.1 Basin wise Surface Runoff Model Studies

Watson et al., (2008) represented a forested watersheds model on the Boreal Plain in Canada. In the study, Soil and Water Assessment Tool (SWAT) model was used for the Willow Creek watershed (15.1 km^2) situated in north central Alberta. The performance of the model for the calibration period (2001–2003) was good where coefficients of efficiency for monthly and daily was found to be 0.89 and 0.81, respectively. However, the study reported that SWAT model did not perform well for the validation period (2004–2006) as the monthly and daily coefficients of efficiency was 0.44 and 0.27, respectively.

Venkatesh et al., (2007) presented that the hydrologic modeling for the development of management scenario and the simulation of the effect of management practices on water and sediment yielding in Gharasu watershed (5793 km^2) using the SWAT model. This basin is located in the northwest of Karkheh River Basin in the far western corner of Iran. In the study, the model was calibrated from 1991 to 1996 and validated from 1997 to 2000. The calibrated model for hydrological conditions was used to assess suspended sediment load. Eventually, the model was used to predict the effect of changing land use and conservation practices on sediment yield within the basin.

Anaba et al., (2016) simulated stream flow for the Murchison Bay catchment as a result of land use changes using SWAT. SWAT model was calibrated and validated for stream flow for extended periods. The Sequential Uncertainty Fitting (SUFI-2) global sensitivity method within SWAT Calibration and Uncertainty Procedures (SWAT- CUP) was used to identify the most sensitive stream flow parameters. The model satisfactorily simulated stream discharge from the catchment. The model performance was determined based on different statistical parameters. The study findings reported satisfactory simulated stream flow. They also reported that if all uncertainties are being minimized, a well calibrated SWAT model can generate reasonable hydrologic simulation results in relation to land use, which is useful to water and environmental resources managers and policy and decision makers.

Gashaw et al. (2018) analyzes the hydrological impacts of Land Use and Land Cover (LULC) changes in the Andassa watershed for the period of 1985–2015 and to predict the LULC change impact on the hydrological status for the year 2045. The hybrid land use classification technique for classifying Landsat images (1985, 2000 and 2015) using the Cellular-Automata Markov (CA- Markov) method for the prediction of 2030 and 2045 LULC states. After that SWAT hydrological model was used for estimating surface runoff. In the study, for isolating the impacts of LULC changes, they used LULC maps independently while keeping the other SWAT inputs constant. The LULC changes during the period of 1985 to 2015, had increased the annual flow by 2.2%, wet seasonal flow by 4.6%, surface runoff by 9.3% and water yield by 2.4%.

Kumar et al. (2018) analyzed the effects of LULC changes on hydrological processes in the Tons River Basin (TRB). Evaluating the impact of LULC changes revealed that there was decrease in surface runoff from 62.29 to 62.14% and lateral flow from 2.39 to 0.261% for the period of 2015 to 2035. The groundwater flow showed a slight increment from 37.42 to 37.62% while the total water yield increased from 774.74 to 776.74 mm. The simulated results for TRB showed that the hydrological processes in the watershed were influenced by LULC changes. It was concluded that the basin's LULC change was not pronounced and was minimally affected by natural and artificial changes

2.2.2 Basin wise Surface Runoff Studies in Bangladesh

Nishat et al. (2009) provided useful insights on future water availability scenarios for downstream nations in anticipation of proposed upstream water resources projects in large international river basins (IRBs). However, they reported that model set up can be challenging due to the large amounts of data requirement on both static states (soils, vegetation, topography, drainage network, etc.) and dynamic variables (rainfall, streamflow, soil moisture, evapotranspiration, etc.) over the basin from multiple nations and data collection agencies. Under such circumstances, satellite remote sensing provides a more pragmatic and convenient alternative because of the vantage of space and easy availability from a single data platform. In the study, MIKE BASIN model was used for the GBM river basins. Using an array of satellite remote sensing data on topography, vegetation, and rainfall from the transboundary regions, it was reported that MIKE BASIN can predict streamflow for Ganges and Brahmaputra rivers satisfactorily for water resources management purposes. According to the study findings, it was reported that

runoff for the Ganges and Brahmaputra rivers follows the trends in the rated discharge for the calibration period. However, monthly flow volume differs from the actual rated flow by (−) 8% to (+) 20% in the Ganges basin, by (−) 15 to (+) 12% in the Brahmaputra basin, and by (−) 15 to (+) 19% in the Meghna Basin.

Ahmed et al. (2011) attempted to establish a basin scale hydrological model for the Ganges basin to predict the impact of climate changes on water resources availability. A water balance model has been setup using physical based, semi- distributed hydrological model SWAT. Temperature and precipitation data from 9 GCMs and two SRES scenarios (A1B and A2) were used along with various input data (e.g., DEM, land use/cover, soil type, weather). Besides, assessment of statistical confidence of the results from different GCM was done utilizing the non-parametric Mann-Whitney U test. It was reported that the average annual flow generated from the Ganges basin is 361,593 Mm^3. The results also indicated that the water availability will decrease during dry period and increase during monsoon. The average annual flow volume increases 22% by 2030, 26% by 2050 and 19% by 2080 for A1B scenario. A similar situation was also reported for A2.

Mohammed et al. (2018) assessed the possible changes in floods in the Bangladesh part of the densely populated Ganges– Brahmaputra–Meghna (GBM) delta at 1.5°C, 2°C, and 4°C global warming. The study was undertaken with the aim of joining the efforts of the global scientific community to assist in the preparation of the upcoming Special Report on 1.5 Degrees by the Intergovernmental Panel on Climate Change. The future changes in the possibilities of peak synchronization of nearby large rivers were assessed for the first time. Results from the study indicated that the flood peaks of the GBM Rivers are more likely to synchronize in the future. Results also indicated that the flood magnitudes may become more severe in the future. At global warming levels of 1.5°C, 2°C, and 4°C, flood flows with a 100-year return period were projected to increase by about 27%, 29%, and 54% for the Ganges; 8%, 24%, and 63% for the Brahmaputra; and 15%, 38%, and 81% for the Meghna, respectively, compared with a baseline condition during 1986–2005.

Khan and Ali (2019) assessed the potential changes to the water balance of the Teesta River basin due to climate change using SWAT. After assessing the results of GCM solutions for 2080s, four scenarios were selected for detail analysis. Wettest, Driest, Warmest and Coolest. Among the selected scenarios, for the wettest scenario, the precipitation increased by 11.71% while it decreased by 1.76% for the driest scenario.

The increase in temperature for the coolest and the warmest scenario was found as 2.24°C and 5.34°C. The developed hydrological model of 1998-2013 timeframe served as the base model output to be compared against climate change model results. Comparing the water balance of the climate change model with the base model, it was reported that the monsoon season will become wetter (as much as 48% increase of precipitation) and the dry season become drier (as much as 43% reduction of precipitation) due to climate change considering all the climate change scenarios. The general trend emerging from the flow analysis is that the Dalia point will experience a more severe shortage of water during the lean season where, as much as 25% decrease of flow has been found even without any upstream controls.

Raihan et al. (2020) used SWAT model to predict stream runoff of Halda Basin in Bangladesh. While the calibrated model's performance was satisfactory (R^2 = 0.80, NSE = 0.71), the model was unable to track the extreme low flow peaks due to the temporal and spatial variability of rainfall which may not be fully captured by using data from one rainfall gauging station. Groundwater delay time, base flow alpha factor and curve number were reported as the most sensitive parameters influencing model performance.

2.2.3 Performance Evaluation Studies of Different Hydrological Models

Cornelissen et al. (2013) conducted a comparative study in the West African Catchment where four models: WaSim, SWAT, UHP-HRU and GR4J, the study analyzed the appropriateness of several model types for predicting scenarios of future discharge behavior in a West African watershed in the context of climate and land use change. In the study, potential sources of uncertainty in tropical catchment hydrological modeling have been identified and reported. For the years 1998 to 2005, all models were calibrated and validated with reasonable accuracy. The model structure and calibration technique created significant discrepancies in the simulation of climate and land use change implications on discharge behavior. Due to changes in land use, all models predict an increase in surface runoff. The use of climate change scenarios resulted in significant difference amongst models, indicating not only the uncertainties in climate change predictions but also a range of probable future changes.

Brirhet et al. (2016) conducted a comparative study on Issen basin (sub-catchment of Aguenza basin) through a comparison of two conceptual hydrological models HEC-HMS with ATHYS. The goal of the study was to determine how adaptable these models are to

the research area so that the chosen model may be used to the entire watershed. The validation phase of the two models yielded good results, with both models being able to simulate the hydrological behavior of the Aguenza watershed during flood events. Furthermore, this research showed that a strong distributed model can outperform a global model for flood forecasting, particularly in terms of volume, as demonstrated in the current study.

Khoi and Nguyen (2016) did a comparative study on Srepok River Catchment, Vietnam, using HEC-HMS and SWAT hydrological models to simulate streamflow in the Srepok River Catchment. The two models were calibrated and validated using streamflow data collected at the Ban Don station between 1981 and 2009. The calibration and validation findings indicate that both models could reasonably represent the streamflow for the study area. For the calibration and validation periods, the model performances using HEC-HMS with value of NSE > 0.62 and R^2 > 0.65, and the SWAT model produced model performance with a value of NSE > 0.72 and R^2 > 0.80. In general, the simulated streamflow produced by the SWAT model was superior to that produced by the HEC-HMS model.

Tegegne et al. (2017) conducted a comparative study on upper Blue Nile River Basin, where the multi-criteria model comparison demonstrated that simple conceptual models fared best in smaller watersheds for recreating observed streamflow in the time domain, whereas the complex model performed best in the largest watershed. For reproducing observed streamflow in the quantile domain, the simple conceptual models performed best for simulation of high, moist, mid-range, and dry-flows in the Gilgelabay watershed; of dry and low-flows in the Gummera and Megech watersheds; and of high flows in the Ribb watershed. The complicated model performed better for the remaining flow ranges of each watershed. The sensitivity of the complex model to the number of partitioned sub-basins was also investigated in this study. They reported that when the number of partitioned sub-basins was increased in the largest watershed, the complicated model's performance improved. Because of its physical variability, this finding suggested that distributed models are particularly suitable for the complex watershed.

Vo et al. (2018) did another comparative study on Vu Gia Thu River Catchment, Vietnam, using Distributed and Lumped model where it implies that each model has their own advantages and limitations regarding data availability and size of the catchment.

Sorman et al. (2020) conducted another comparative study for the Upper Aras Basin, Turkey, where during 2008 to 2015 water years in the hilly headwaters of the Aras Basin in eastern Turkey. Two distinct conceptual hydrologic models (HEC-HMS and HBV) were compared. For both models, Nash-Sutcliffe Efficiency performance on runoff is above 0.8 for calibration and 0.7 for validation. This first implementation and comparison of conceptual hydrologic modeling in the Aras Basin yielded good findings and suggested that other variables be considered in addition to streamflow.

2.3 Hydrological Models

A model is a simplified representation of a complex process or phenomenon. Considering hydrologic cycle, mathematical model is the quantitative expression of observing, analyzing or predicting a process by simulating it through the transformation of rainfall to runoff in catchments. The landscape can be affected numerous ways when water flows over the land surface and through stream channels. Similar to many major rivers in Bangladesh, continuous discharge measurements are not recorded throughout the year for some River basins. These problems can be best evaluated in conjunction with hydrologic simulation. Also, a good calibrated and validated model can be used for hydrologic prediction and determination of runoff for ungauged River basin. SWAT, HEC-HMS, VIC, HBV, MIKE-SHE, LISFLOOD are some widely used hydrologic modeling tool for watershed analysis.

2.4 Considerations for Surface Runoff Modelling using HEC-HMS

2.4.1 Conceptual Basis

HEC-HMS divides a watershed into several sub-basins. Each sub-basin is connected through a junction in a channel. HEC-HMS omits any detailed accounting of movement of water within the soil. It includes models of infiltration from the land surface. But it does not model storage and movement of water vertically within the soil layer. It implicitly combines the near surface flow and overland flow and models this as direct runoff. It does not include a detailed model of interflow or flow in the groundwater aquifer, instead representing only the combined outflow as base flow. Most of the models included in HEC-HMS are event-based models but ModClark model is an exception. It includes both empirical and conceptual models. All models included in HEC-HMS are deterministic. HEC-HMS uses a separate model to represent each component of the runoff process that

is illustrated in Figure 2.2 including:

- Models that compute runoff volume
- Models of direct runoff (overland flow and interflow)
- Models of base flow
- Models of channel flow
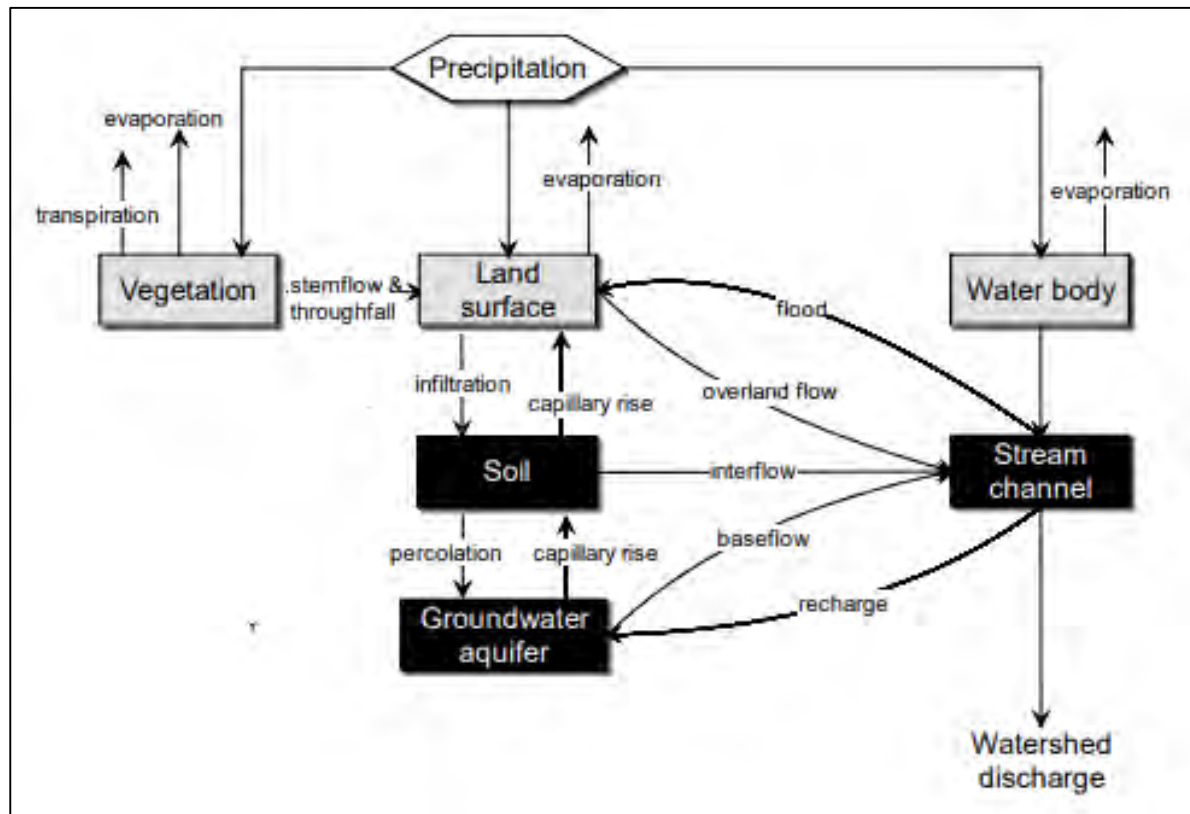
Figure 2. 2: Typical HEC-HMS representation of watershed runoff (Scharffenberg, 2015)

2.4.2 Runoff Volume Computations

SCS Curve Number

In HEC-HMS, there are several methods available for runoff volume computations. In this study, to compute runoff volume Soil Conservation Service (SCS)-Curve Number Method has been used. In hydrological modeling, the runoff estimation is the most important aspect. There are number of empirical methods for its estimation. The most commonly and widely used empirical method is the SCS-Curve Number Method (SCS, 1972) developed by United States Department of Agriculture and Soil Conservation Service (USDA-SCS) to estimate surface runoff. This method is very popular due to its simplicity, flexibility and requirement

of a single parameter called Curve Number (CN) for computation of runoff. Hydrologic soil group number, land use type, vegetation cover is the basic catchment characteristics used for curve number calculations. The curve number has clearly defined ranges and should not be specified with values beyond the defined ranges. This method is recommended for basins that do not have a good flow record for calibration (Brirhet et al., 2016).

Precipitation

Precipitation is an input parameter to the system of storages. Precipitation first contributes to the canopy interception storage. If the canopy storage fills, the excess amount is then available for infiltration.

Infiltration

Infiltration is the process of water movement that enters the soil profile from the ground surface. Water available for infiltration during a time step comes from precipitation that passes through canopy interception, plus water already in surface storage. The volume of infiltration during a time interval is a function of the volume of water available for infiltration, the state (fraction of capacity) of the soil profile, and the maximum infiltration rate-based on soil texture specified by the model user.

Evapotranspiration (ET)

ET is the loss of water from the canopy interception, surface depression, and soil profile storages.

2.4.3 Modelling Direct Runoff

In HEC-HMS the following methods can be used to simulate the process of direct runoff of excess precipitation on a watershed as transformation of precipitation excess into point runoff.

- User-Specified Unit Hydrograph
- Clark's UH
- Snyder's UH
- SCS UH
- ModClark
- Kinematic Wave

In this study, SCS Unit Hydrograph is used for direct runoff among all these methods as Atrai-Karatoa river basin is a data poor basin. Lag hour can be easily calculated from time

of concentration and the range of peaking co-efficient is 0.4 to 0.8 (Hydrologic Engineering Center, 2000).

SCS Unit Hydrograph Method

The Soil Conservation Service (SCS) proposed a parametric Unit Hydrograph (UH) model; this model is included in the program. The model is based upon averages of UH derived from gaged rainfall and runoff for a large number of small agricultural watersheds throughout the US (USDA-NRCS, 2010).

Basic Concepts

The SCS UH model is a dimensionless, single-peaked UH. This dimensionless UH expresses the UH discharge, U_p for any time t, a fraction of T_p, the time to UH peak. Research by the SCS suggests that the UH peak and time of UH peak are related by:

$$U_p = C \frac{A}{T_p} \qquad\qquad 2.1$$

in which A = watershed area; and C = conversion constant (2.08 in SI and 484 in foot-pound system). The time of peak (also known as the time of rise) is related to the duration of the unit of excess precipitation as:

$$T_P = \frac{\Delta t}{2} + t_{lag} \qquad\qquad 2.2$$

in which $\triangle$ t = the excess precipitation duration (which is also the computational interval in the run); and t_{lag}= the basin lag, defined as the time difference between the center of mass of rainfall excess and the peak of the UH. [Note that for adequate definition of the ordinates on the rising limb of the SCS UH, a computational interval, Δt, that is less than 29% of t_{lag} must be used (USACE, 1998).] When the lag time is specified, the program solves Equation 2.2 to find the time of UH peak, and Equation 2.1 to find the UH peak. With Up and T_p known, the UH can be found from the dimensionless form, which is built into the program, by multiplication.

2.4.4 Modelling Channel Flow

This section describes the models of channel flow that are included in the program; these are also known as routing models. The routing models available include:

- Lag
- Muskingum
- Modified Puls, also known as storage routing
- Kinematic wave
- Muskingum Cunge

Each of these models computes a downstream hydrograph, given an upstream hydrograph as a boundary condition. Each does so by solving the continuity and momentum equations. In this study Muskingum method is used for routing model. The routing models that are included are suitable for many but not all flood runoff studies.

Muskingum Method

The Muskingum method is a commonly used hydrologic routing method in situations requiring a variable storage-discharge relationship (Chow et al., 1988). The Muskingum method models the storage volume of flooding in a river channel using a combination of wedge and prism storage. The key parameters in Muskingum routing are K (travel time) and X (weighting coefficient). The value of X depends on the shape of the wedge storage to be modeled, and the value of X ranges from 0 for reservoir type storage to 0.5 for a full wedge. In natural streams, X is between 0 and 0.3 with a mean value near 0.2 (Chow et. al., 1988). K is the time required for an incremental flood wave to traverse its reach, and it may be estimated as the observed time of travel of peak flow through the reach (Chow et.al., 1988).

2.5 Surface Runoff Modelling using SWAT

SWAT is a spatially distributed, continuous time scale watershed scale model developed by Dr. Jeff Arnold for the USDA-ARS. It was developed to predict the impact of land management practices on water, sediment and agricultural chemical yields in large complex watersheds with varying soils, landuse and management conditions over long periods of time. SWAT divides a watershed into sub-watersheds. Each sub-watershed is connected through a stream channel and further divided into Hydrologic Response Unit (HRU). HRU is a unique combination of a soil and a vegetation type in a sub-watershed, and SWAT

14

simulates hydrology, vegetation growth, and management practices at the HRU level. Weather, soil properties, topography, vegetation and land management practices are the most important inputs for SWAT to model hydrologic and water quality in a watershed SWAT allows a basin to be subdivided into sub-basins to evaluate hydrology, weather, sediment yield, nutrients and pesticides, soil temperature, crop growth, tillage and agricultural management practices (Neitsch et al., 2011).

2.5.1 Conceptual Basis

The Soil and Water Assessment Tool (SWAT) is a watershed scale conceptual model (Arnold et al., 1998) which is also a physically based model (Gassman et al., 2007) that can simulate long term water yield and water quality from watersheds with varying soils and land management practices. The SWAT model is applicable for hydrological prediction in both large- and small-scale watersheds. The comprehensive SWAT model is capable of simulating different hydrological components such as climate, hydrology, soil temperature, plant growth, erosion, nutrient transport, pesticide transport, and land management practices (Arnold et al., 1998; Neitsch et al., 2011). The model accounts for spatial details and is a better predictor of long-term yields rather than a single flood event (Arnold et al., 1998). In the SWAT model, a watershed can be partitioned into smaller units on the basis of two-levels of discretization. First, a watershed can be divided into any number of smaller spatial units called sub-watersheds. Thereafter, the sub-watersheds are further subdivided into non- spatial groupings called hydrologic response units (HRUs) on the basis of the identical soil and land use characteristics. Hence, the SWAT model can preserve the spatially distributed parameters of the entire basin (Srinivasan et al., 1998; Neitsch et al., 2011).

2.5.2 Theory on Water Balance

Water balance is the driving force behind everything that happens in the watershed. To accurately predict the movement of pesticides, sediments or nutrients, the hydrologic cycle as simulated by the model must conform to what is happening in the watershed.
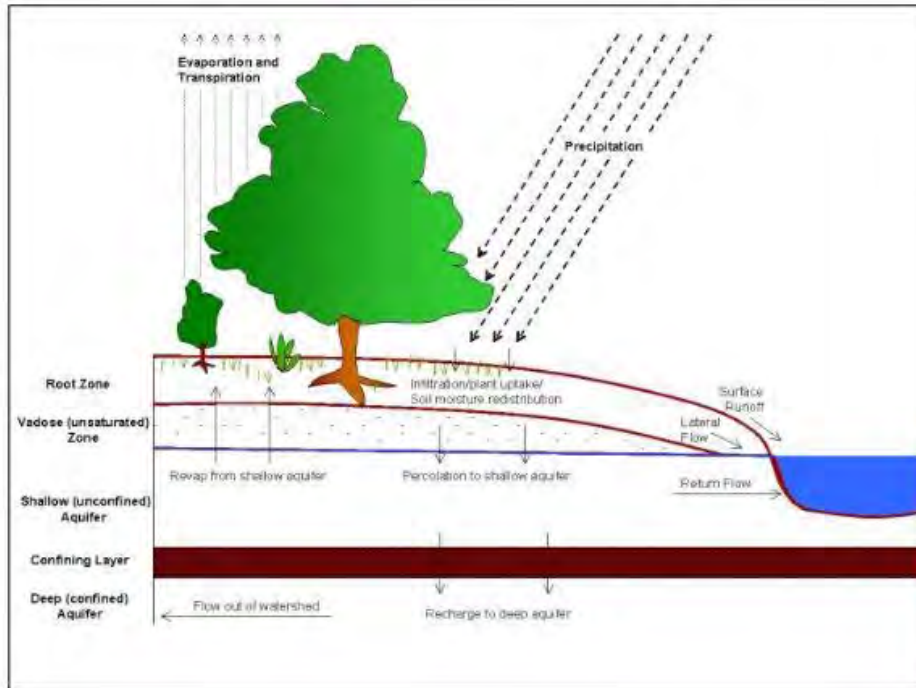
Figure 2. 3: Hydrologic process in SWAT (Neitsch et al., 2011)

The simulation of hydrologic cycle can be separated into land phase and water or routing phase. Land phase controls the amount of water, sediment, nutrient, and pesticide loading to the main channel in each sub-basin whereas routing phase defines the movement of water, sediments, etc. through the channel network of the watershed to the outlet. Schematic of pathways available for water movement in SWAT is shown in the Figure 2.3. It involves various elements such as snow, canopy storage, infiltration, evapotranspiration, lateral subsurface flow, surface runoff etc.

Canopy Storage

Canopy storage is the water intercepted by vegetative surfaces where it is held and made available for evaporation. When using the curve number method to compute surface runoff, canopy storage is taken into account in the term initial abstractions. However, if methods such as Green & Ampt are used to model infiltration and runoff, canopy storage must be modeled separately.
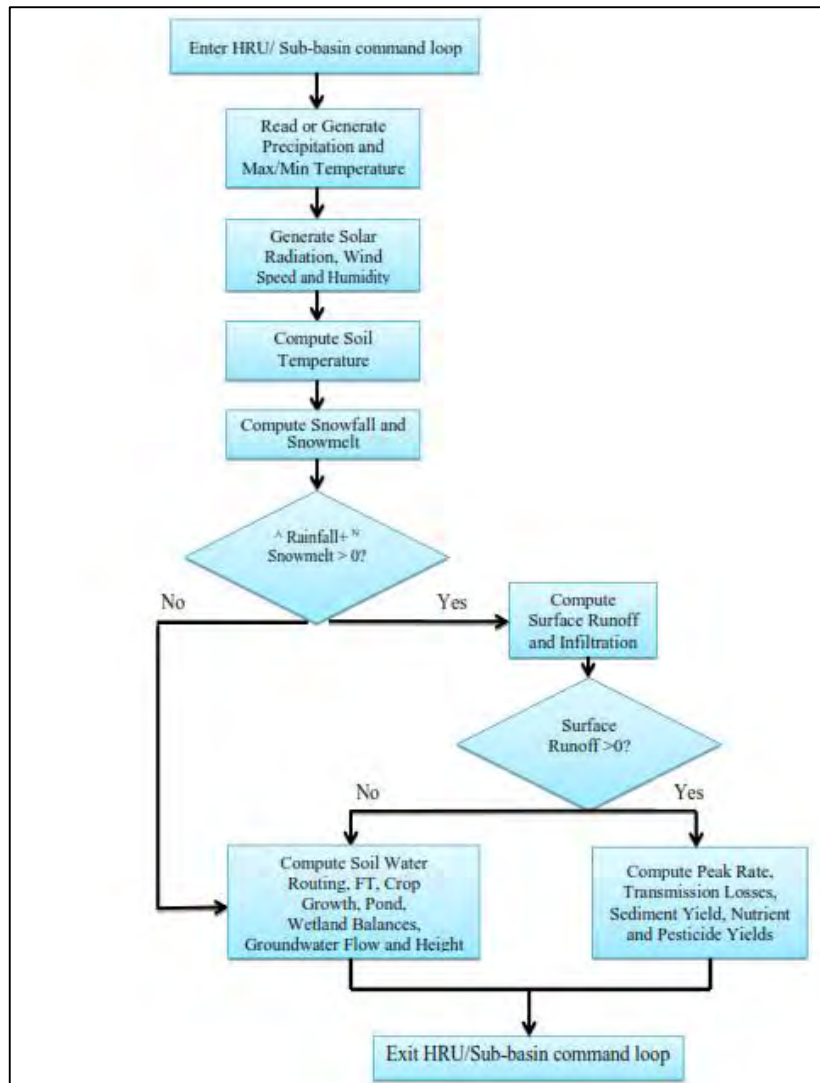
Figure 2. 4: HRU/Sub-basin in command loop (Neitsch et al., 2005)

SWAT allows the user to input the maximum amount of water that can be stored in the canopy at the maximum leaf area index for the land cover. This value and the leaf area index are used by the model to compute the maximum storage at any time in the growth cycle of the land cover/crop.

Infiltration

In the SWAT model, the amount of water infiltrating into the soil profile is calculated indirectly because the surface runoff is computed directly using either of the previously mentioned methods (Neitsch et al., 2011). Hence, the infiltrated water is calculated as a difference between the amount of rainfall and the amount of surface runoff.

Evapotranspiration

The model computes evaporation from soils and plants separately as described by Ritchie (1972). Potential soil water evaporation is estimated as a function of potential evapotranspiration and leaf area index (area of plant leaves relative to the area of the HRU). Actual soil water evaporation is estimated by using exponential functions of soil depth and water content. Plant transpiration is simulated as a linear function of potential evapotranspiration and leaf area index. Numerous methods have been developed to estimate ET. Three of these methods have been incorporated into SWAT: The Penman-Monteith method (Monteith, 1965; Allen, 1986; Allen et al., 1989), the Priestley-Taylor method (Priestley and Taylor, 1972) and the Hargreaves method (Hargreaves et al., 1985; Neitsch et al., 2011). In this study the Hargreaves method is used to compute the ET.

Surface Runoff

Surface runoff, or overland flow, is flow that occurs along a sloping surface. Using daily or sub-daily rainfall amounts, SWAT simulates surface runoff volumes and peak runoff rates for each HRU. Surface runoff component simulates the surface runoff volume and the peak runoff rates provided daily rainfall data are fed. Surface runoff is computed using a modification of the SCS curve number (USDA Soil Conservation Service, 1972) or the Green & Ampt infiltration method (Green and Ampt, 1911). In the curve number method, the curve number varies none linearly with the moisture content of the soil. The curve number drops as the soil approaches the wilting point and increases to near 100 as the soil approaches saturation.

Peak Runoff Rate

The model calculates the peak runoff rate with a modified rational method. The rational method is based on the assumption that if a rainfall of intensity *i* begins at time t = 0 and continues indefinitely, the rate of runoff will increase until the time of concentration, t = t_{conc}, when the entire sub-basin area is contributing to flow at the outlet.

Return Flow

Return flow, or base flow, is the volume of stream flow originating from groundwater. SWAT partitions groundwater into two aquifer systems: a shallow, unconfined aquifer which contributes return flow to streams within the watershed and a deep, confined aquifer which contributes return flow to streams outside the watershed (Arnold et.al., 1993; Neitsch

et al., 2011). Water percolating past the bottom of the root zone is partitioned into two fraction search fraction becomes recharge for one of the aquifers.
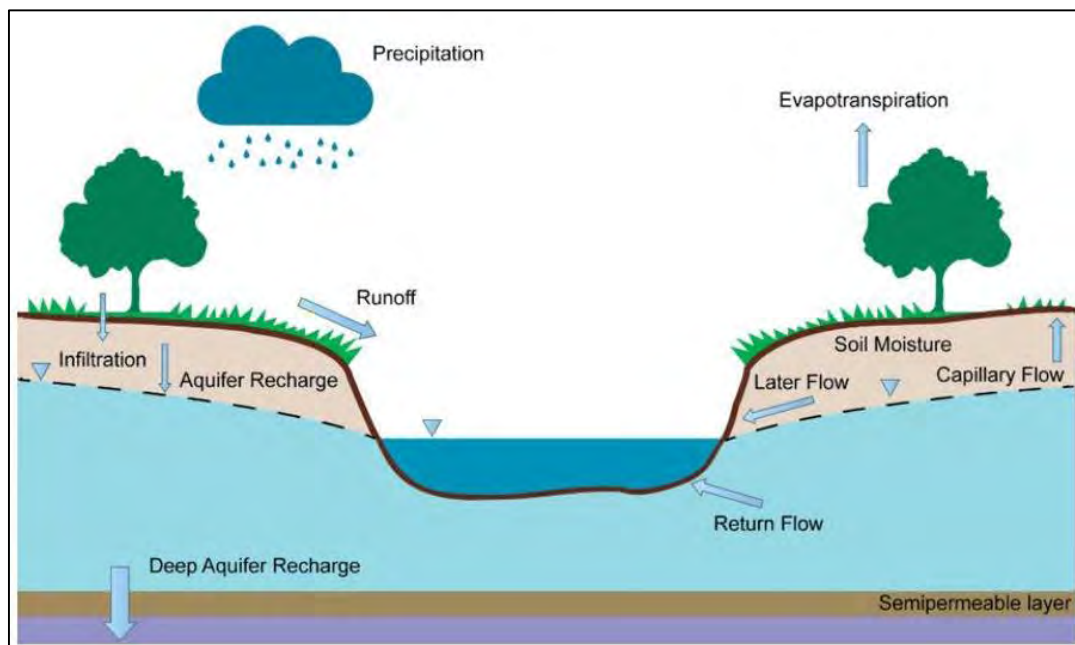
Figure 2. 5: Schematic representation of conceptual water balance of the SWAT model (Neitsch et al., 2011)

In addition to return flow, water stored in the shallow aquifer may replenish moisture in the soil profile in very dry conditions or be directly removed by plant. Water in the shallow or deep aquifer may be removed by pumping.

Routing Phase of Hydrologic Cycle

Once SWAT determines the loading of water, sediment, nutrients and pesticides to the main channel, the loading is routed through the stream network of the watershed using a command structure (Neitsch et al., 2011). Additionally, SWAT also models the transformation of chemicals in the stream and streambed.
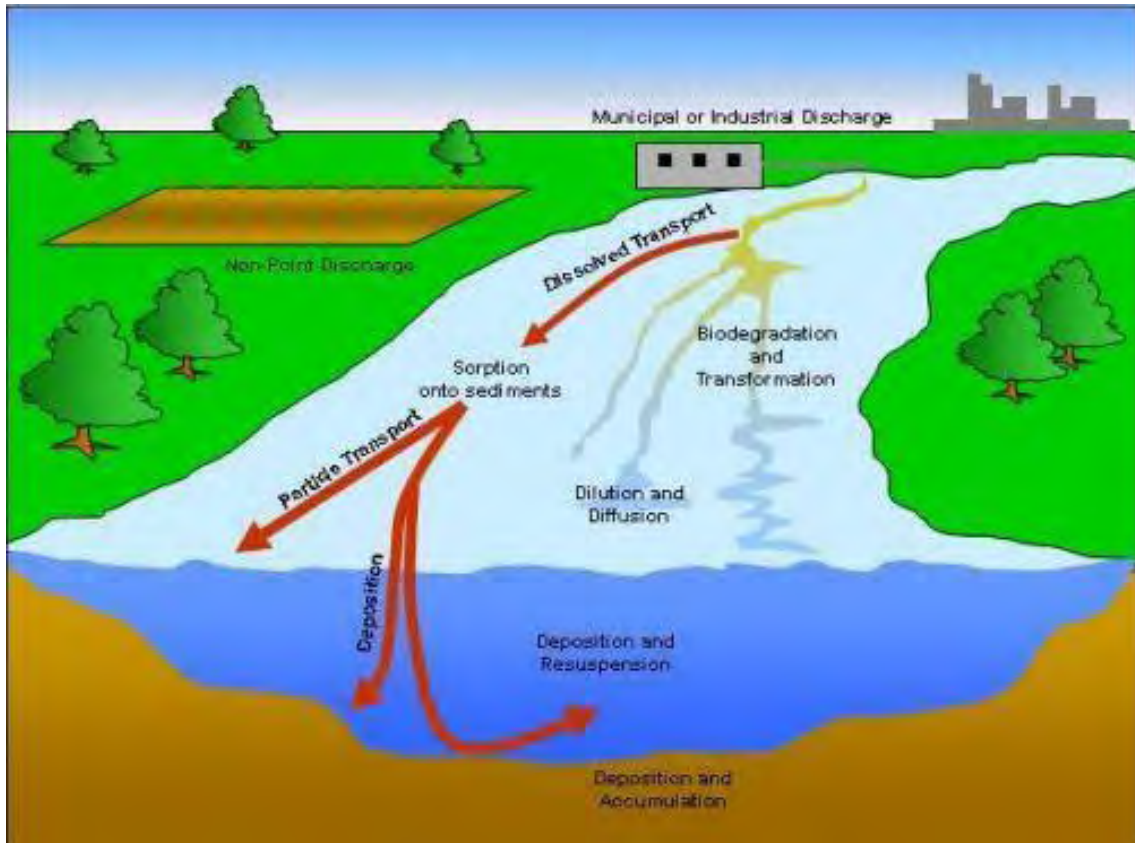
Figure 2. 6: In-stream processes modeled by SWAT (Neitsch et al., 2011)

Routing in the Main Channel or Reach

As water flows downstream, a portion may be lost due to evaporation and transmission through the bed of the channel. Another potential loss is removal of water for agricultural or human use. Flow may be supplemented by the fall of rainfall or addition of water from point source. In SWAT flow is routed using variable storage coefficient method developed by Williams (1969) or the Muskinghum routing method. In this study the routing method selected for SWAT model is Muskingum method due to its simplicity and easy application.

2.5.3 Advantages of Using SWAT Model

The main advantage of SWAT is the capability to run simulations for large watersheds without extensive monitoring data and the capacity to predict changes in hydrological parameters under different management practices and physical environmental factors (Neitsch et al., 2011;). Some advantages of SWAT model had given below:

- Physically based.

- Requires generally available information as input.

- Computationally efficient.

- Capable of being used on un-gauged watersheds.

- Enables users to study long-term impact.

2.6 Summary

Theoretical background of a model has been very important for a research study. It is essential to gather knowledge about how the model simulation is done. It is also necessary to know about the background equation of the model. If the theoretical background is clear, then the proper utilization of the model can be more effectively done.

CHAPTER 3

STUDY AREA AND METHODOGOLOGY

3.1 General

A large number of pre-processing and post processing works are required to set up a hydrological model for a river basin. Researchers face numerous issues during these works. In the present work for Atrai-Karatoa River Basin, initially several types of data such as, Digital Elevation Model (DEM), land use pattern, soil distribution, climate data, and flow time series were collected to setup a hydrological model using HEC-HMS and SWAT model.

3.2 Study Area

Before the great earthquake and flood of 1787, the Atrai-Karatoa River, a transboundary river in Bangladesh, was one of the main branches of the Teesta River. Atrai-Karatoa rapidly deteriorated and was completely cut off from the original Teesta once the Teesta abandoned its old path. Currently, the Atrai-Karatoa originates from Baikunthapur in India and first enters Bangladesh at Bardeshwari in Panchagarh district (latitude 26°28' and longitude 88°36'). It runs about 50 km from Panchagar to Dinajpur before entering India again. At Naogaon (latitude 25°10' and longitude 88°46'), the river re-enters Bangladesh, runs south, and meets the Little Jamuna (this Jamuna is not the Brahmaputra-Jamuna) another river that eventually falls at Hurasagar flows through the Naogaon district, close to Rasulpur, with a total length of around 455 km. The lower reach of the river is known as Atrai, and the upper reach is known as Karatoa River.
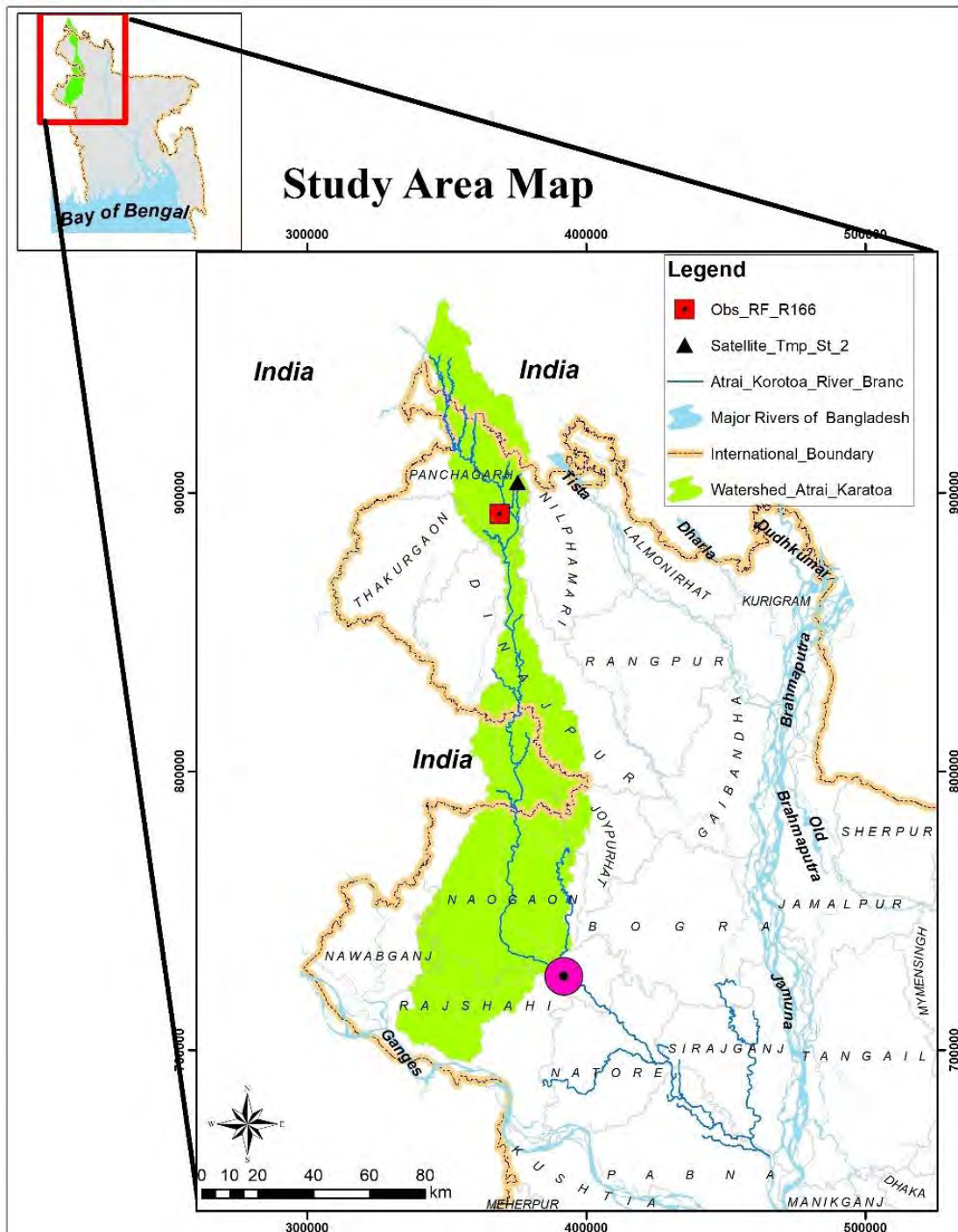
Figure 3. 1: Study Area Map of Atrai-Karatoa River

3.2.1 River System

Upper Karatoa is one of the main rivers of North-West Region. Generated from Himalayan territory, it enters into Bangladesh at Panchagarh. It is flashy in nature and flows through a steeper ground slope. It is a perennial river. The lower part of Upper Karatoa river named as Atrai is flowing through slightly steeper to flat land. Atrai river with several tributaries and distributaries has formed a complex network of rivers before falling into the Hurasagar

river at Baghabari, the single outlet to the Jamuna. Upper part of Atrai river is influenced by local flow and is flashy in nature whereas the lower part is largely influenced by backwater effect of the Jamuna. There are several depressions or beels existing around this river and a number of breaches originate every year from the banks of Atrai. This causes changed flow characteristics every year. Important tributaries of Atrai river system are Ichamati-Jamuna, Lower-Nagor, Nandakuja, Baral and important distributaries are Dhepa, Sib-Barnai and Fakirni (IWM, 2019).

3.2.2 Physiographic characteristics

The Himalayan Piedmont Plains are the alluvial cones of the rivers originating in the Terai region of the Himalayan foothills. The region is bounded by the Mahananda River in the west and the Dinajpur-Karatoa River in the east. The rivers in this region are entrenched in recent alluvial deposits of fine sand and silts with gradients of approximately 0.00091. The alluvial deposits in the south of the Himalayan Peidmont Plains overlay Pleistocene clays of the Barind Tract (River Morphology of Bangladesh - Msrblog, 2019). The Middle Atrai floodplain is an 81 km long valley with the Barind tract rising on both sides. It stretches from Chirirbandar to Mahadebpur. The lower areas of the Middle Atrai floodplain are subject to flash flooding. The Atrai River is entrenched into the clay deposits of the Barind tract, whilst its floodplain consists of sandy material (Morphology Of Bangladesh - Msrblog, 2019).

The Lower Atrai Basin has an approximate area of 3120 km^2. The entire basin is inundated during the rainy season with a depth of water of between 0.6 m to 3.7 m. The western part of the basin is aggrading with silt from the Barind tract (Morphology Of Bangladesh - Msrblog, 2019).

3.2.3 Climatic Characteristics

To quantify the climatic characters of the Atrai-Karatoa River Basin five observed rainfall stations of BWDB [Tentulia (R220), Debiganj (R166), Kantanagar (R180), Hilli (R175) and Manda (R185)] and five satellite stations of NASA-POWER is used these stations provide gridded data which have a spatial resolution of 55 km x 55 km. The climatic parameters are used for this analysis are Precipitation, Temperature and Relative Humidity. The Figure 3.2 shows the climatic station used for this study.
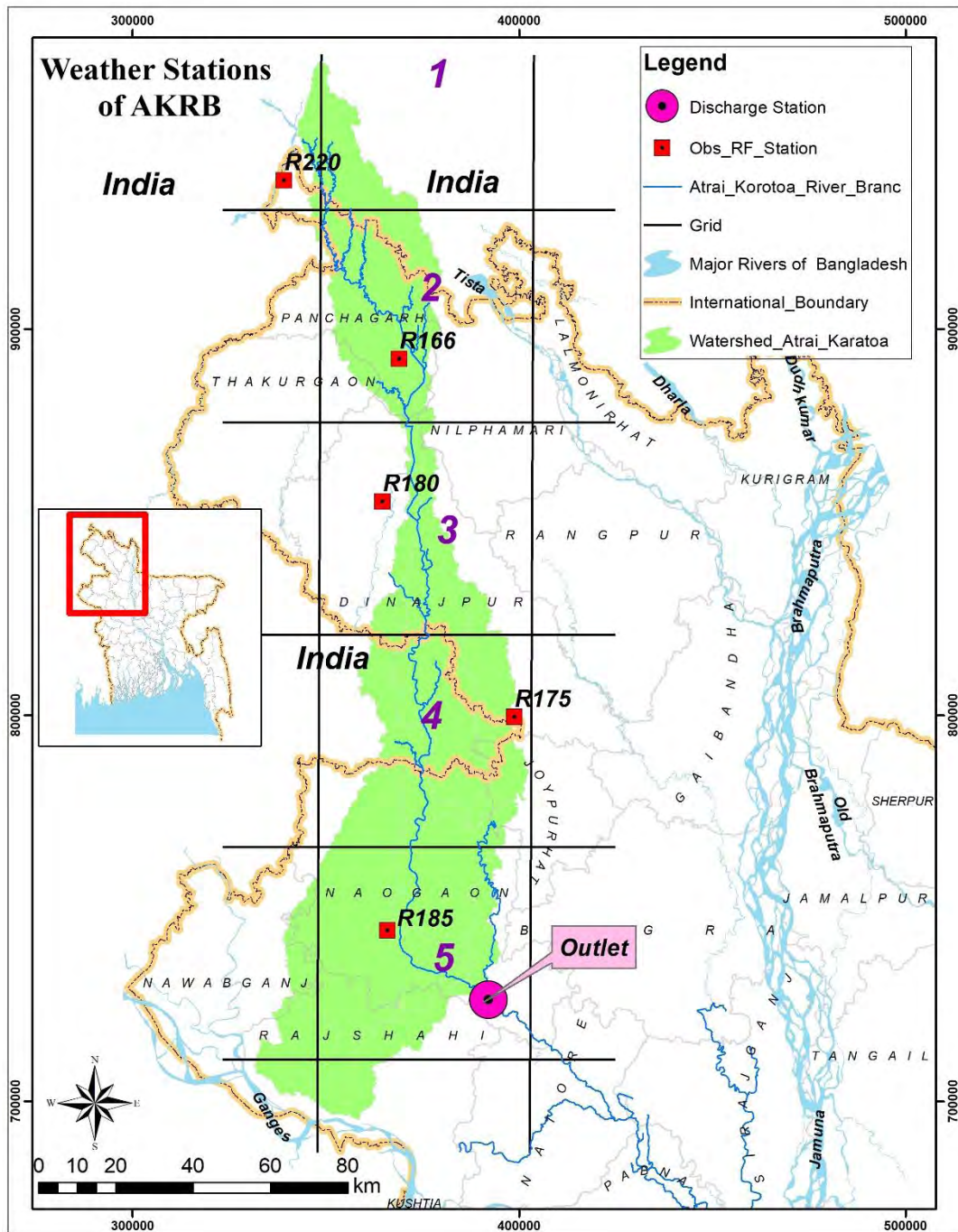
Figure 3. 2: Available weather stations on Atrai-Karatoa River Basin

Precipitation

In the Atrai-Karatoa River Basin maximum annual total precipitation occurs at the upstream of the catchment. The precipitation gradually decreases as we move downstream. Minimum annual total precipitation occurs at the extreme downstream of the catchment. It has been found that that the maximum annual precipitation occurs at the Panchagar district and minimum annual precipitation occurs at Rajshahi district.

Temperature

In the Atrai-Karatoa River Basin the maximum annual average temperature occurs at the downstream of the catchment. The average temperature gradually descreases as we move upstream. At the extreme upstream of the catchment, the average temperature is minimum. From the data analysis, it has been observed that the maximum average temperature occurs at the Rajshahi district and minimum average temperature occurs at Panchagar district.

Relative Humidity

In the Atrai-Karatoa River Basin the maximum annual average relative humidity occurs at the downstream of the catchment. Average relative humidity gradually decreases as we move upstream. At the extreme upstream of the catchment, the average relative humidity is minimum. Satellite data analysis identified that the minimum average relative humidity occurs at or near Panchagar district and inside the Indian Boundary and maximum average relative humidity occurs at Rajshahi district. This pattern complies with the analysis we have made in the Precipitation and Temperature segment, which is the maximum precipitation and minimum temperature is occurring where minimum relative humidity exists and minimum precipitation and maximum temperature is occurring where maximum relative humidity exists.

3.2.4 Land Use and Soil Use Classes

Land use is a description of how people utilize the land and socio-economic activity. Land use is the physical material at the surface of the earth. Land covers include grass, asphalt, trees, bare ground, water, etc. This basin holds a variety of land use classes. A major part of the basin is covered with agriculture. The states falling under Atrai-Karatoa River Basin are extensively cultivated.

In regards of physiography and soil, the 2,577 km^2 Karatoa-Bangali Floodplain is quite similar to the Teesta Meander Floodplain and is built up of a combination of Teesta and Brahmaputra deposits. The majority of places have almost level basins and smooth, wide floodplain ridges. On hills, the soils are grey or dark grey clays, and in basins, silty clay loams. There are 5 distinct varieties of general soil in the area, although non-calcareous grey floodplain and non-calcareous dark grey floodplain soils are the most common. All over the earth is slightly acidic. In general, the cultivated layer of ridge soils contains little organic matter, while basins have a reasonable amount. The fertility rate is average. This

zone includes the majority of Sirajganj and the eastern half of Bogra districts (Agroecological Zone - Banglapedia, 2018).

Lower Atrai Basin, an area of 851 km^2, is made up of the low-lying land between the Barindra Trac and the Ganges River floodplain. It encompasses the Chalon Beel region. The predominant soil type in this flat, low-lying basin region is smooth, thick, dark-grey clay. In the area, there are seven main types of soil. Organic matter and other critical nutrient status are in a medium state, although potassium availability is at a high level. The fertility level of soils is average (Agroecological Zone - Banglapedia, 2019).

The Atrai-Karatoa river basin covers an area of about 772408 Ha, of which 72348 Ha is in India. The average slope of the basin is about 10% according to the digital elevation model. The main tributaries are the Little Jmauna, Boral Upper, Bernai river and the main distributaries are Fakirny and Shib River.

The Globcover Land Cover data identified the area as having 85.20% Agricultural areas, 0.28% Mixed Forest area, 0.01% Deciduous Forest area, 0.13% Evergreen Forest Land, 0.14% Grass Land, 8.75% Urban and Industry Land, 0.02% Burned Land and 5.48% Water Body in the Atrai-Karatoa river Basin (Figure: 3.5) with Farming being the main occupation of the local inhabitant.

The soil characterization in the Atrai-Karatoa river basin contain 8 different types of soil which is mainly Grey Terrace Soils silt over clay sub layer (37.54%), Grey Floodplain Soil Silt, Loam & clay (21.71%), Black terai soils (18.05%), Calcareous dark grey floodplain soils with lime kankar (10.11%), Grey Floodplain Soil and non-calc. brown floodplain soil silt, loam, clay (7.67%), Non-calcareous brown floodplain soils and grey floodplain (2.58%), Calc. dark grey and calc. brown floodplain soil grey clay (2.16%) and Black terai clay soils (0.18%). The Atrai-Karatoa River Basin annually receives on an average about 1200 mm precipitation. The distribution of the average June through September precipitation climatology (mm/month) shows a band of average accumulated high precipitation over 300 mm/month.

3.3 Methodology

Simulation of runoff of any river basin using hydrological model involves several steps. Steps followed in the present study can be described as following:

Step 1: Data collection: This includes Digital Elevation Model (DEM), land use pattern, soil distribution, climate data, and flow time series data collection.

Step 2: Surface runoff model setup: Surface runoff model setup which includes watershed delineation, weather data file processing and selection of calculation methods

Step 3: Calibration and validation of surface runoff model: Calibration and validation of the model and evaluation of the model performance.

Step 4: Model Performance Evaluation: Based on the statistical parameters best suited model for this basin will be recommended. The flow chart of the methodology is shown below:
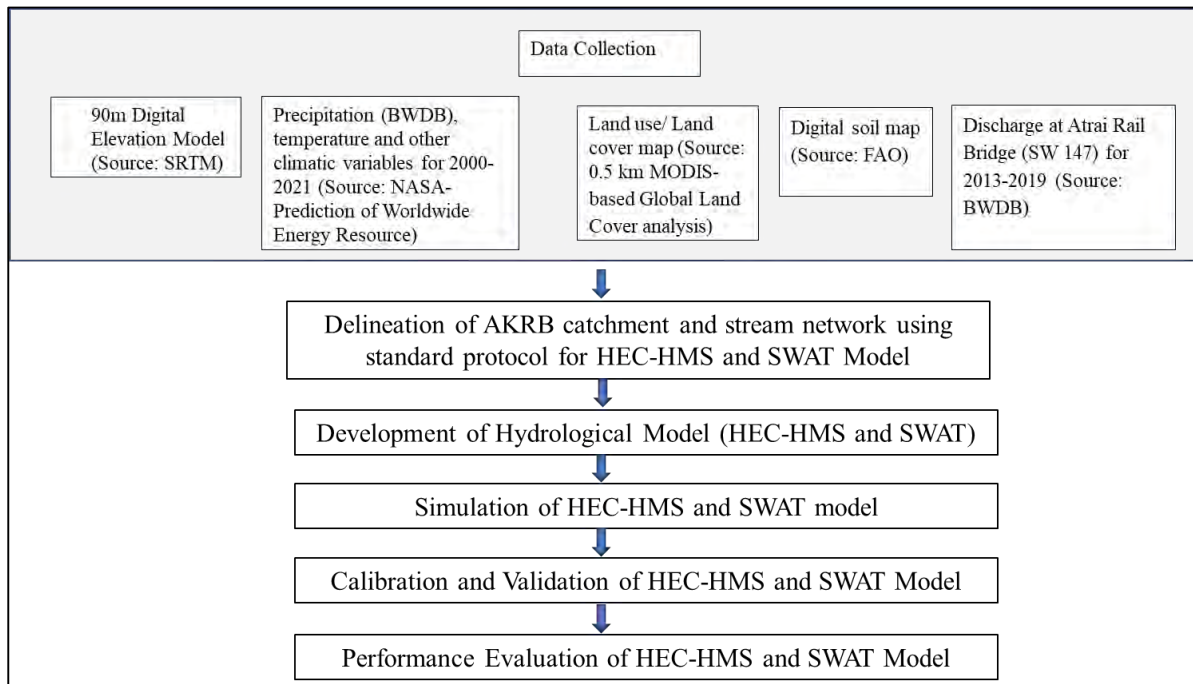

Figure 3. 3: Methodology of the Study

3.3.1 Data Collection

Digital Elevation Model (DEM) Map

Digital Elevation Model (DEM) data of 90m resolution (Figure 3.4) has been collected from Shuttle Radar Topography Mission (SRTM) website (http://srtm.csi.cgiar.org). The SRTM DEM was found to contain more surface detail and roughness than the TOPO DEM. It has been produced using radar images gathered from NASA's shuttle.
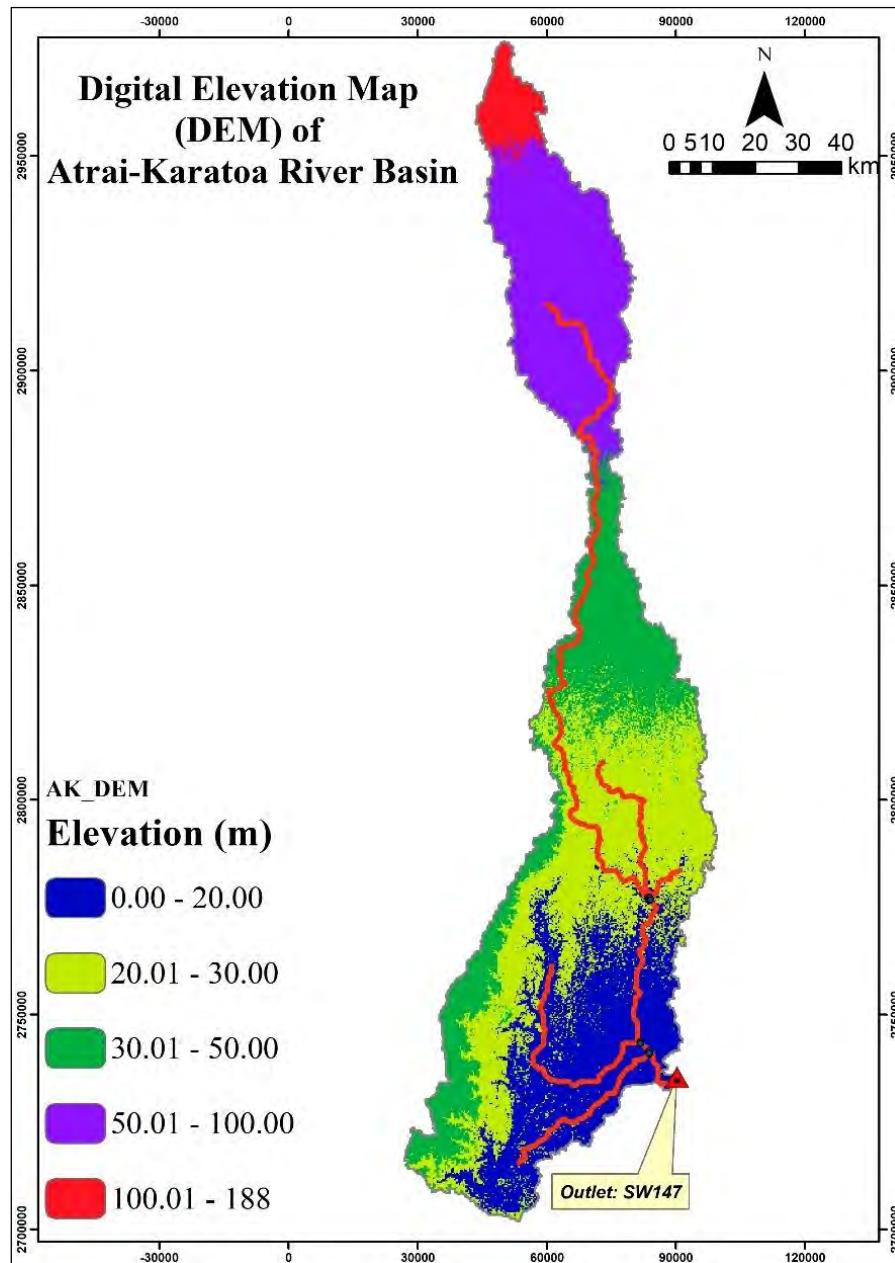
Figure 3. 4: Digital Elevation Model (DEM) of Atrai-Karatoa River Basin (AKRB)

Land use Map

Land cover is one of the most important factors that affect surface erosion, runoff, and evapotranspiration in a watershed. Land cover map of 400 m resolution has been collected from Globcover. Eight (8) land cover classes have been found in the AKRB basin which are shown in Figure 3.5.
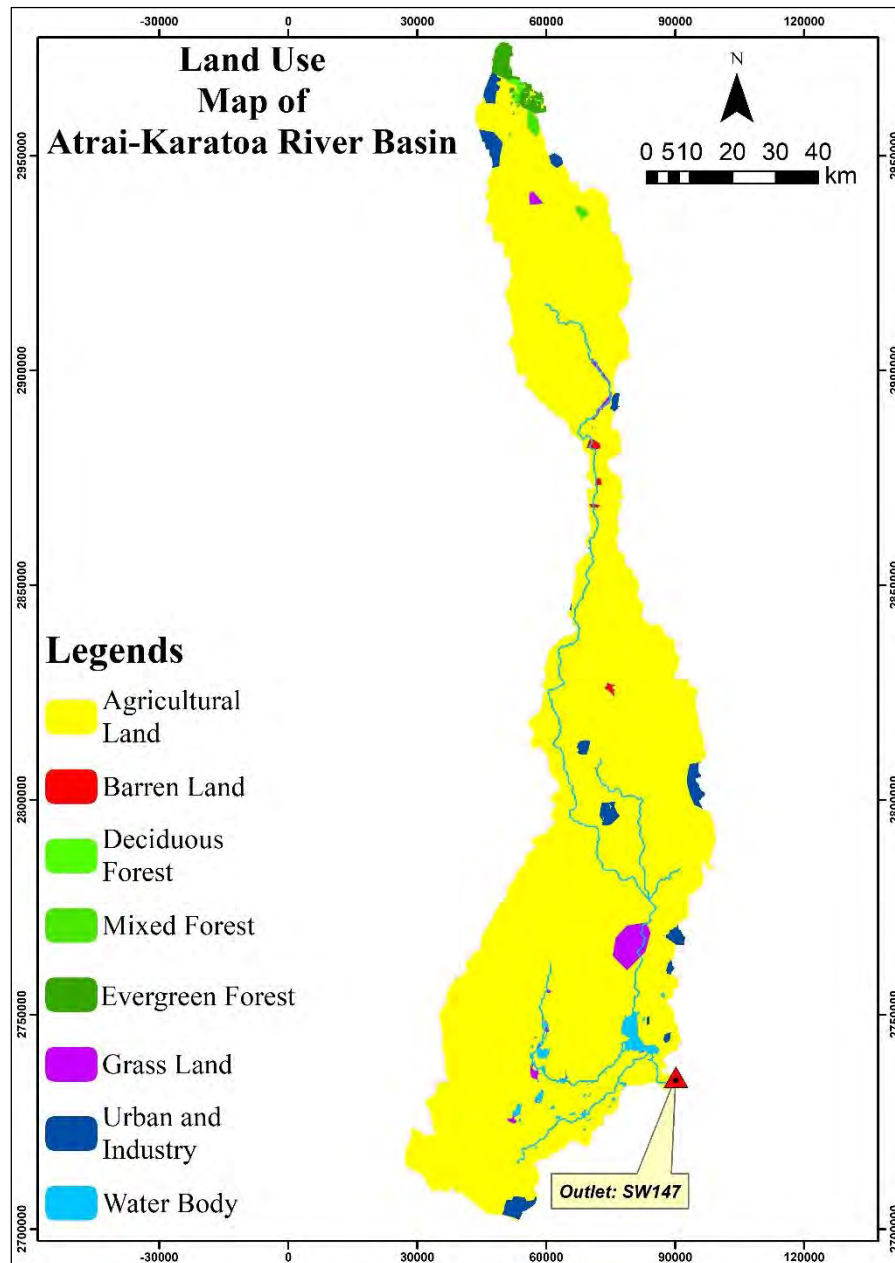
Figure 3. 5: Land Cover Map of AKRB

Soil Cover Map

Digital soil map (1:5,000,000) from FAO is used. The FAO/UNESCO Legend for the Soil Map of the World 1974 is used as an international correlation system to indicate the dominant soil unit in each cell. It refers to the soil characteristics of the Digital Soil Map of the world but can be used as a reference for the dominant soil characteristics, as well. Dominant soil types for AKRB are shown in Figure 3.6.
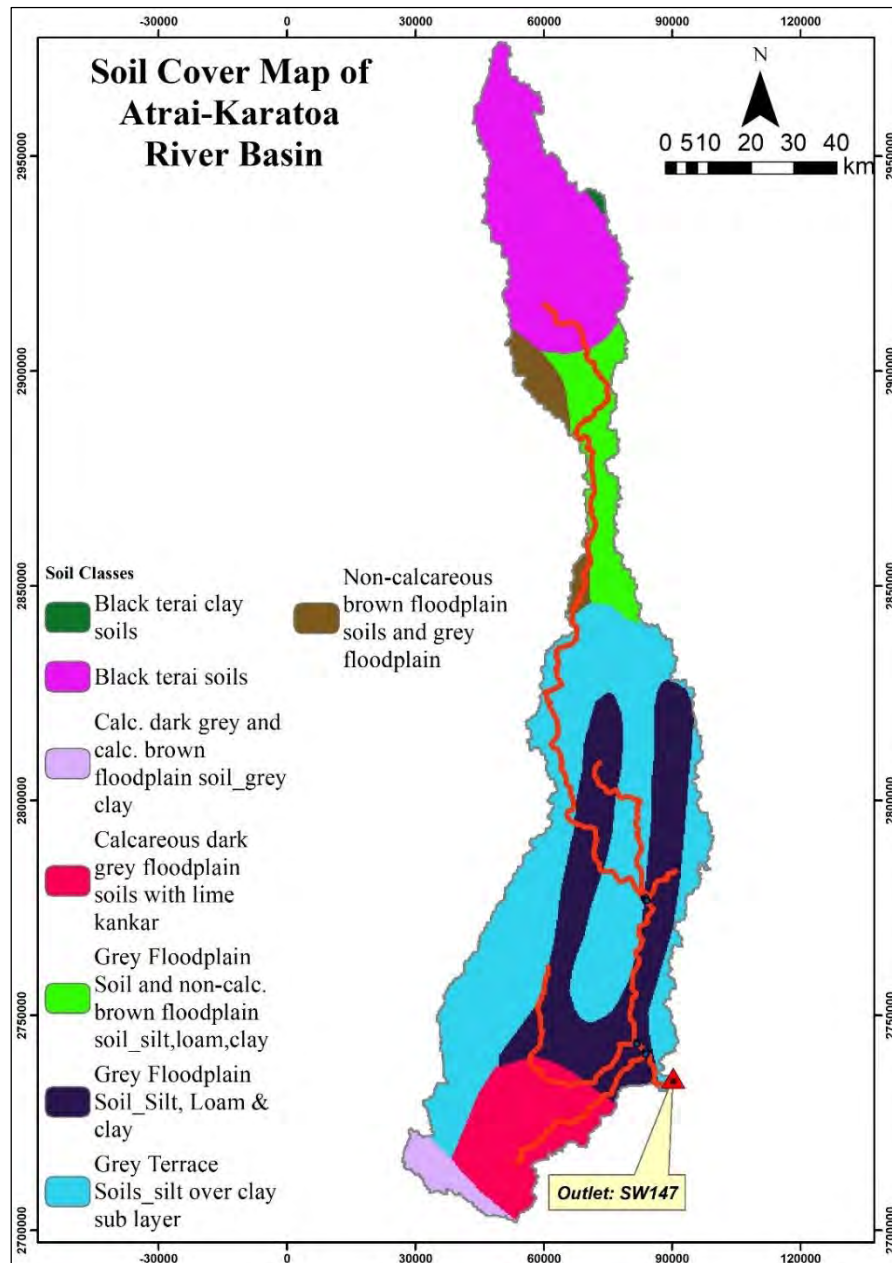
Figure 3. 6: Soil Cover Map of AKRB

Discharge and Weather Data

The HEC-HMS and SWAT model requires daily values of precipitation, evaporation, average temperature, solar radiation, relative humidity and wind speed. For this study, meteorological data for the AKRB have been collected from the NASA-Prediction of Worldwide Energy Resource (NASA-POWER) (http://power.larc.nasa.gov) for the climate normal period (2000 to 2021). It is to be noted that all the weather data collected from NASA-POWER is bias corrected and this bias is corrected based on observed ground station data.

Discharge at Atrai Rail Bridge (SW 147) for the year of 2013-2019 have been collected from Bangladesh Water Development Board (BWDB). In case of missing discharge data interpolation, rating curve have been generated from water level. Observed Evaporation and observed Rainfall data at AKRB have been collected from BWDB. Figure 3.7 and Table 3.1 shows basic data used in this study including their source, resolution, and time period.
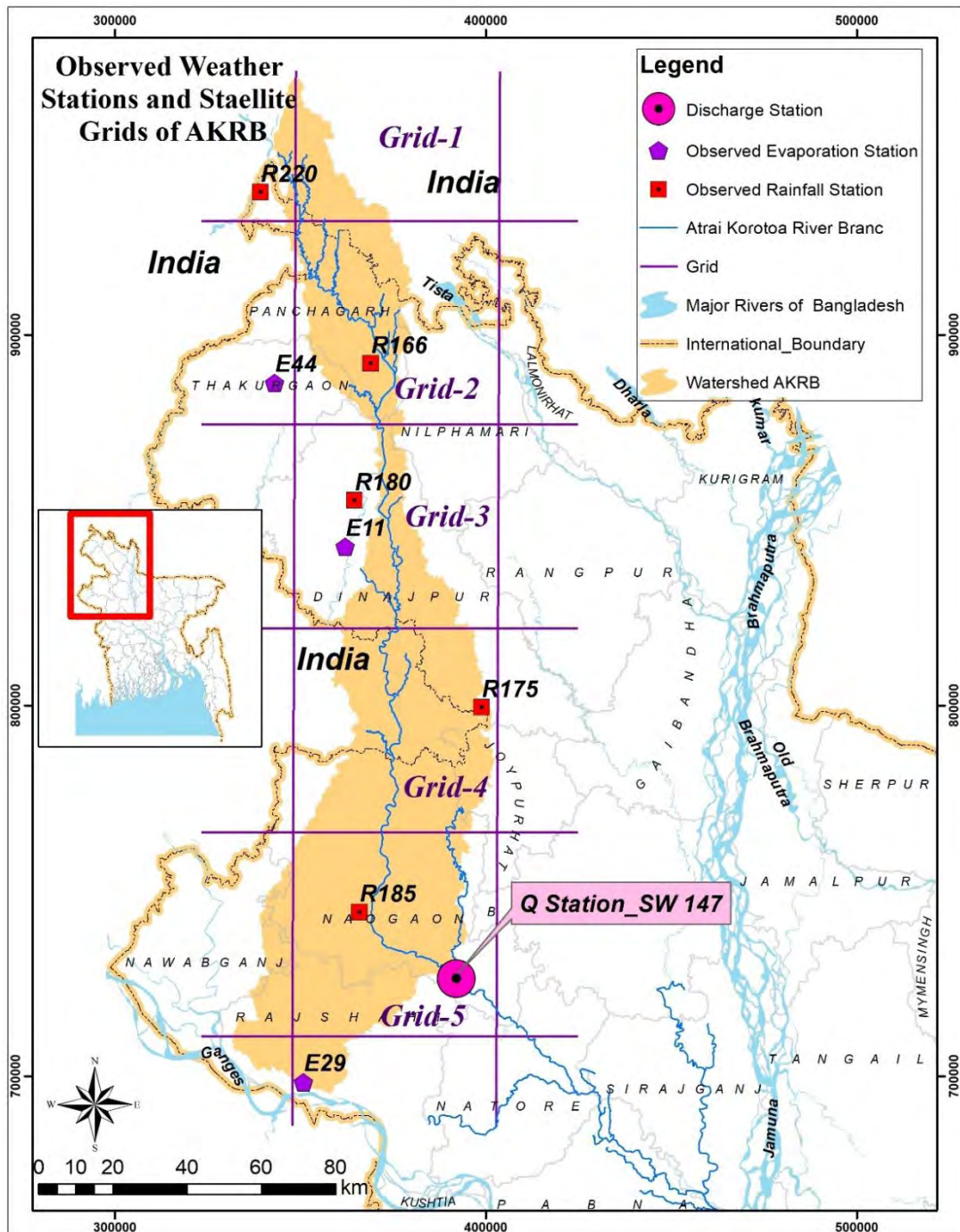

Figure 3. 7: Observed Weather Stations and Satellite Grids of AKRB

Table 3.1: Basic input data used in this study

River Name	Station Name and ID	Data Type	Duration/ Resolution	Data Source
Atrai-Karatoa River	Atrai Rail Bridge, (SW 147)	Discharge	2013-2019	BWDB
	Tentulia, Debiganj, Kantanagar, Hilli (Hakimpur), Manda	Rainfall	2000-2021	BWDB
	Dinajpur (E-11), Rajshahi (E-29), Thakurgaon (E-44)	Evaporation	2000-2019	BWDB
Atrai-Karatoa River		Temperature, Relative Humidity, Solar Radiation and Wind Speed	2000-2021	(NASA-POWER, Source: https://power.larc.nasa.gov/data-access-viewer)
		DEM	90 m	SRTM (https://www2.jpl.nasa.gov/srtm)
		Land Cover Map	2017/400m	Globcover (https://swat.tamu.edu/media/116401/ea_landuse_newres.zip)
		Digital Soil Map	2007/ 1:50000000	FAO (http://www.fao.org/home/en /)

3.3.2 Surface Runoff Model Setup

HEC-HMS Model Setup

The following steps have been taken to setup the surface runoff model for estimating surface runoff for AKRB at Atrai Rail Bridge (SW 147) station. In this study, HEC-HMS 4.8 was used. Figure 3.8 represents the Flow chart of HEC-HMS model setup:

- Delineation of watershed and stream network using GIS tool of HEC-HMS model (version 4.8).
- Processing of necessary input data.
- Development of HEC-HMS surface runoff model using HEC-HMS model.
- Editing HEC-HMS surface runoff model inputs and simulation and
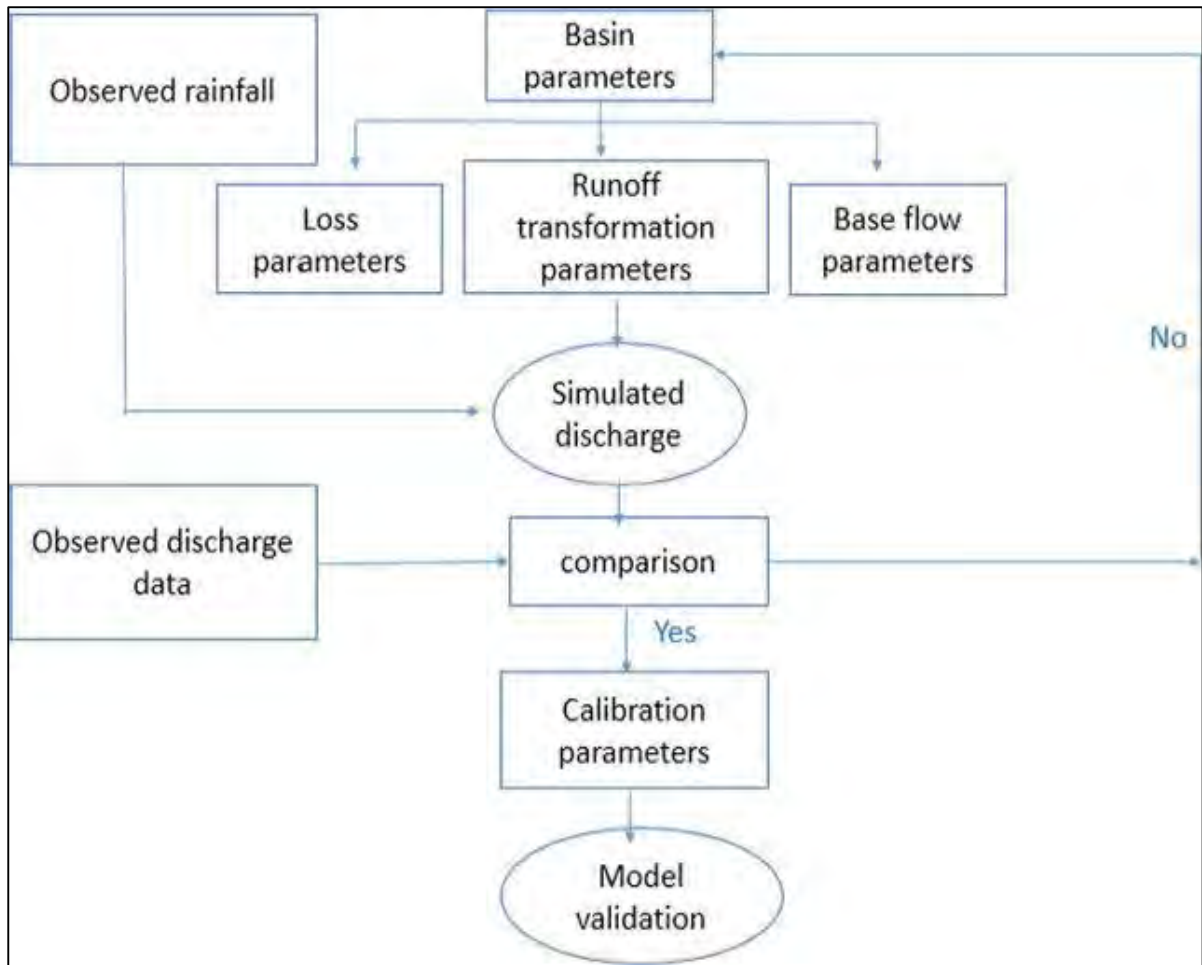- Surface runoff model calibration and validation.

Figure 3. 8: Flow Chart of Model Setup in HEC-HMS (Gaurav et al., 2021)

SWAT Model Setup

Five sequential steps have been followed to set up the SWAT (ArcSWAT version 2012.10_4.21) model, which are

- watershed delineation,
- HRU Analysis
- Weather data definition,
- Write inputs table, and
- Streamflow simulation at different points which are basically outflow of different sub-catchments.

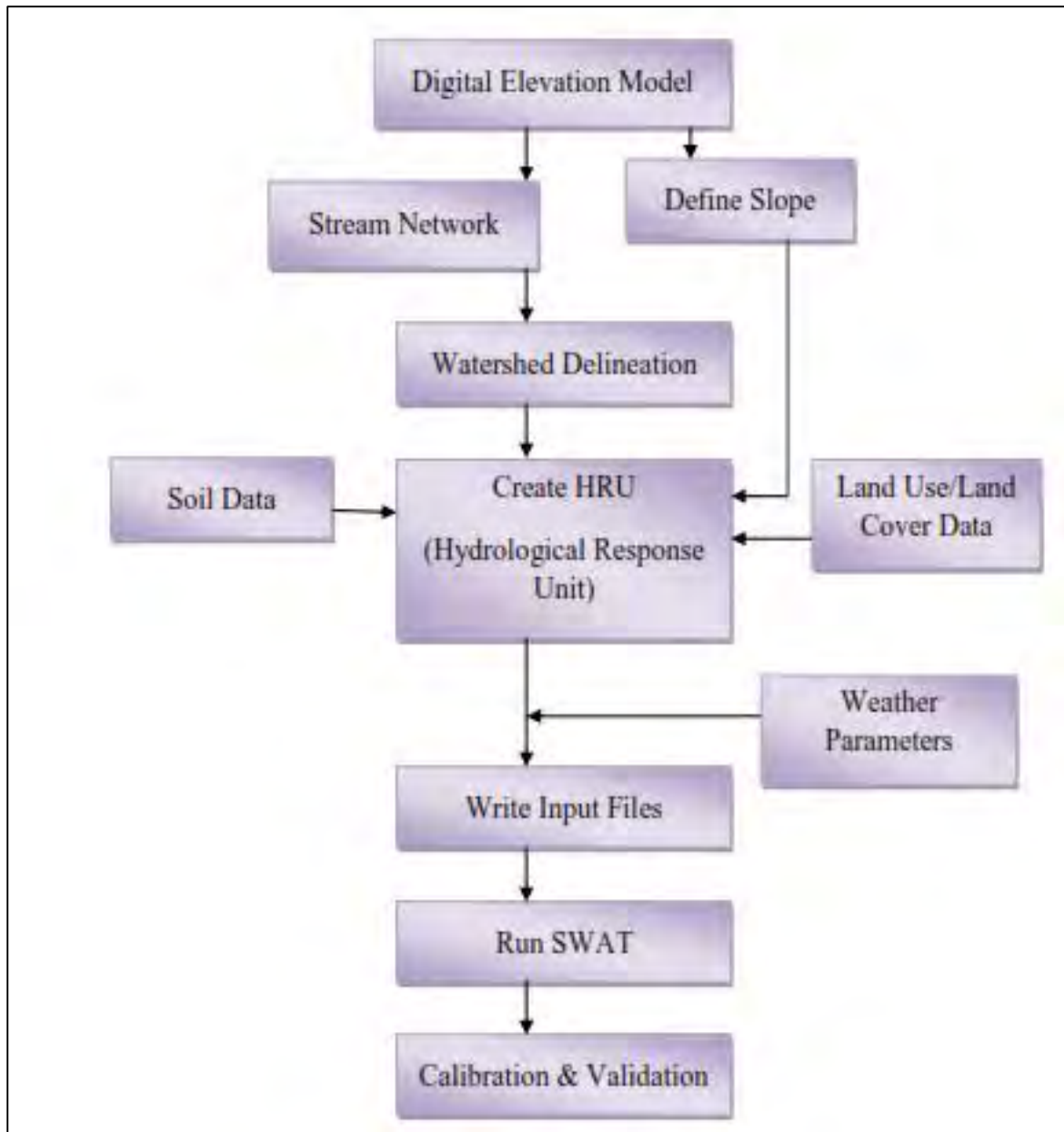Here Figure 3.9 shows the flow chart of model setup in SWAT.

Figure 3. 9: Flow Chart of Model Setup in SWAT

3.3.3 Model Calibration and Validation

Calibration

Calibration means adjustment of the model parameters so that simulated and observed data will match within the desired accuracy. Model parameters may require adjustment due to a number of reasons. There are numerous parameters in hydrological models which can be classified as physical parameters (i.e. parameters that can be physically measurable from the properties of watershed) and process parameters (i.e., parameters represent properties which are not directly measurable) (Gupta et al., 1999; Neitsch et al., 2011). In reality, all

models require some degree of calibration to fine tune the predictive ability of the model. After some test simulations it was clear that four parameters had greater influence on the shape and magnitude of the output hydrographs. They are:

SCS Curve Number Calculation

SCS (Soil Conservation Service) Curve Number (CN) is an empirical parameter used or predicting direct runoff or infiltration from rainfall excess. There are actually two ways that the program can calculate the surface runoff, one is the SCS Curve number method (1972) and the other is the Green & Ampt infiltration method (Neitsch et al., 2011). However, the Green & Ampt infiltration method requires sub daily in precipitation data which is very hard to get. That is why SCS curve number method of surface runoff calculation was used. The main parameter for the curve number calculation is CN2 which is the initial SCS runoff curve number for moisture condition II. The SCS CN is function of the soil's permeability, land use and antecedent soil water condition. The CN has a range from 30 to 100. Lower numbers indicate low runoff potential while larger numbers are for increasing runoff potential. So, the lower the curve number, the more permeable the soil is. It is worth mentioning that the CN2 parameter is highly sensitive. With the slightest change of this parameter the SWAT model completely changes the simulated runoff magnitude. Initially the SWAT model assigns a CN2 value based on the soil data and land use pattern but more often than not a user needs to change this value for better calibration. The default value of CN2 is 60-95, so only minor changes from the initial value of CN2 was required for model calibration.

Ground Water Delay

The ground water delay time parameter of the SWAT model actually represents the lag time between the times that the water exits the soil profile and enters the shallow aquifer. This parameter cannot be directly measured but will mainly depend on the depth of the water table and the hydraulic properties of the geologic formation in the vadose (region of aeration above the water table) and ground water zones. These terms of model behavior, increasing the ground water delay time actually increases the base flow of the model and generates more flow in the dry periods, damping out the hydrograph a lot. While the default value is 31 days, during the calibration process, the value of Ground Water Delay time was chosen as 50 Days.

Base Flow Recession Constant

The base flow recession constant is a direct index of ground water flow response to change in charge (Smedema and Rycroft, 1983; Neitsch et al., 2011). The value may vary from 0.1 to 0.3 with slow response to recharge and from 0.9-1 for land with rapid response. Although the base flow recession constant may be calculated, it requires a lot of data on base flow contribution into the main channel as well as data of recharge rate of shallow aquifer and storage of the shallow aquifer. Thus, it will be a very hard job to calculate the base flow recession constant. In the SWAT model environment, the baseflow recession constant has a significant effect on the shape of the hydrograph. The default value of the parameter was set to 0.048 which represent a very slow responding soil. Increasing the base flow recession constant will make the slope of the hydrograph a lot steeper, meaning that peaks will be reached faster, and the recession limb of the hydrograph will also be a lot steeper, hence meaning quicker drainage.

Ground Water Revap

Water may move from the shallow aquifer into the overlying unsaturated zone. In periods when the material overlying the aquifer is dry, water in the capillary fringe that separate the saturated and unsaturated zone will evaporate and diffuse upward. As this water gets removed, more water from the underlying aquifer will replace the evaporated one. This process is modeled by SWAT using the "GW_REVAP" parameter. The default value of GW_REVAP is 0.02 was taken during calibration.

Validation

Validation is the process of determining the degree to which a model or simulation is an accurate representation of the real world from the perspective of the intended uses of the model or simulation. Once the model parameters have been finalized during calibration process, the model is simulated with that set of parameters for a different time frame to see the model's performance. If the model performs well in predicting the output for the different timeframe it can be said to be validated. Calibration is generally done with the latest available data series. But it is not necessary to calibrate the model with latest data. After finalizing the parameters, the model was simulated for the entire time frame and simulation period was chosen as the validation period for the model. In calibration and validation stage of the model, the performance of the model is evaluated both statistically as well as graphically. The model generated mean daily discharge and observed mean daily discharge at the desire outlet.

3.3.4 Model Performance Evaluation

Statistically the performance of the model has been evaluated using the Nash-Sutcliffe Efficiency value (NSE), the coefficient of determination (proportion of the variance in the observations explained by the model, R^2), percent bias (PBIAS) and the ration of the root mean square error between the simulated and the observed values to the standard deviation of the observations (RSR) (Moriasi et al., 2007)

R^2 (Coefficient of determination)

R^2 estimates the combined dispersion against the single dispersion of the observed and predicted series and provides the relationship strength between observed and simulated values. Its value ranges from 0 to 1; a value close to 0 means very low correlation whereas a value close to 1 represents high correlation between observed and simulated discharge (Alam, 2015).

$$R^2 = \frac{[\sum_{i=1}^{n}(Q_i - \bar{Q}_i)(Q'_i - \bar{Q}'_i)^2]}{\sum_{i=1}^{n}((Q'_i - \bar{Q}'_i)^2)\sum_{i=1}^{n}(Q'_i - \bar{Q}'_i)^2} \qquad 3.1$$

where,

Q_i = observed discharge and

Q'_i = simulated discharge

NSE (Nash–Sutcliffe Efficiency)

NSE determines the relative magnitude of the residual variance compared to that of the measured data (Moriasi et al., 2007) and is one of the most widely used statistical indicators for hydrological model performance (Neitsch et al., 2011; Shrestha et al., 2013). Its value ranges from 0.4 to 1, where 1 indicates a perfect model and a value of less than 0 indicates that the mean value of the observed time series would have been a better predictor than the model.

$$NSE = 1 - \frac{\sum_{i=1}^{n}(Q_i - Q'_i)^2}{\sum_{i=1}^{n}(Q_i - \bar{Q}'_i)^2} \qquad 3.2$$

where,

Q_i = observed discharge and

Q'_i = simulated discharge

PBIAS (Percentage bias)

PBIAS indicates the average tendency of the simulated results to be greater or larger than their observed data. It measures the difference between the simulated and observed quantity and its optimum value is 0. The positive value of the model represents underestimation whereas negative value represents overestimation (Alam, 2015).

$$PBIAS = \frac{\sum_{i=1}^{n}(Q_i - Q'_i)}{\sum_{i=1}^{n} Q_i} * 100 \qquad \text{3.3}$$

where,

Q_i = observed discharge and

Q'_i = simulated discharge

RSR (RMSE-observation standard deviation ratio)

The lower value of RMSE (root mean square error) is commonly acceptable and one of the widely used error parameters. However, the satisfactory threshold of RMSE is case specific. Therefore, RSR is chosen as a complementary indicator to RMSE. The optimum value of RSR is 0 and higher value indicates lower model performance (Alam, 2015).

$$RSR = \frac{RMSE}{STDEV_{obs}} = \frac{\sqrt{\sum_{i=1}^{n}(Q_i - Q'_i)^2/n}}{\sqrt{\sum_{i=1}^{n}(Q_i - \bar{Q}'_i)^2/n}} \qquad \text{3.4}$$

where,

Q_i = observed discharge and

Q'_i = simulated discharge

The threshold value of goodness-of-fit for all models was based on Moriasi et al., (2007), as shown in Table 3.2.

Table 3.2: Model Performance Rating

Performance Rating	NSE	PBIAS	RSR
Very Good	0.75	$<\pm10$	0 to 0.5
Good	0.65-0.75	± 10 to ± 15	0.5 to 0.6
Acceptable	0.5 to 0.65	15 to ± 25	0.6 to 0.7
Unsatisfactory	<0.5	$>\pm 25$	> 0.7

Source: (Moriasi et al., 2007)

CHAPTER 4

DATA ANALYSIS AND MODEL DEVELOPMENT

4.1 General

In this chapter, the detailed analysis of the collected data and the parameter required to simulate the models are estimated. This chapter also include the detail model setup with calibration and validation processes. The detail analysis is described in the following sections of this chapter.

4.2 Delineation of Watershed and Stream Network

Delineation of watershed boundary and streams is necessary prior to the management of study area as a watershed. It is the initial step of any hydrologic modeling to get some basic watershed properties area, slope, flow length, stream network density, etc. Figure 4.1 is the delineated watershed with stream network of the study area. To delineate the watershed, stream network and some watershed characteristics of the study area, Watershed Delineator tools (of ArcSWAT version 2012.10_4.21) is used for SWAT model and GIS tool of HEC-HMS (version 4.8) is used for HEC-HMS.
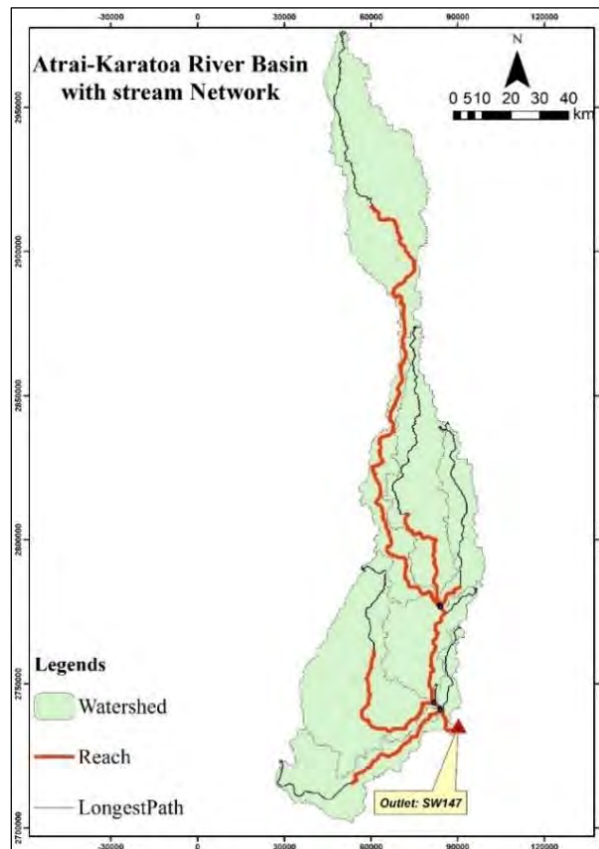
Figure 4. 1: Atrai-Karatoa River Basin with Stream Network

Furthermore, Delineated watershed was checked with the HydroBasin watershed (**HydroBasins** represents a series of vectorized polygon layers that depict sub-basin boundaries at a global scale) of Atrai-Karatoa River, where the delineated area of AKRB using HEC-HMS and SWAT is 7725 km^2 (considering watershed outlet at SW 147, study area outlet) and HydroBasin area of the watershed is 7982 km^2 (Considering watershed outlet at SW 147, study area outlet). The variations were about 3.22%, so the watershed delineation as used in this study was found satisfactory. The whole watershed area (HydroBasin) of AKRB (considering outlet at the offtake of Jamuna River) is 17713 km^2. The delineated and HydroBasin watershed of AKRB is shown in **Appendix-B**.

4.3 Processing of Necessary Input Data

4.3.1 Hydrological Data Analysis

Climate change is no longer something to happen in the future but rather an ongoing phenomenon. It is now unequivocally established that climate change is reality, and the adversities of climate transformations pose of the greatest challenges facing humanity today (IUCN, 2011). The Inter-Governmental Panel on Climate Change (IPCC) defines climate change as "a change in the state of the climate that can be identified (e.g., using statistical tests) by changes in the mean and/or the variability of its properties and that persists for an extended period, typically decades or longer".

Bangladesh is one of the top most nations vulnerable to climate change (Harmeling, 2008). IPCC also recognizes Bangladesh as one of the most vulnerable countries in the world to the negative impacts of climate change. The main impact of climate change or the phenomena of climate change can be seen on the hydrological (precipitation) and weather (Temperature and Relative Humidity) data.

For the analysis, hydrological and weather data pattern have been assessed in three segments annually, monthly and seasonally. The seasonal analysis is accomplished considering four seasons i.e., pre-Monsoon (March-May), Monsoon (June-September), post-Monsoon (October-November) and winter (December-February) for the period 2000 to 2021 (Basak et al., 2013). Though the analysis was put together separately for each observe and satellite stations only a single representing station is described here for each climatic parameter (Precipitation, Temperature and Relative Humidity) and rest of the stations are reported in **Appendix-A**.

Precipitation

There are five observed precipitation station in and around the study area, this observed station are from BWDB namely Tentulia (R220), Debiganj (R166), Kantanagar (R180), Hilli (R175) and Manda (R185) which were shown previously in Figure 3.7. The analysis was conducted on the observed precipitation data from 2000 to 2021. The detail analysis of a representing precipitation station Debiganj (R166) is described in the following section.

Debiganj (R166):

Debiganj (R166) is situated at Panchagar district inside the Bangladesh boundary. This station is placed at the upstream of the catchment. Figure 4.2 (a) shows the annual precipitation trend in the last two decades where it reflects that during 2000 to 2009 the annual precipitation trend was rising and then falling, then from 2010 to 2013 the trend was more of less flat but the annual total precipitation was about 850 mm to 900 mm but from 20014 to 2020 the trend was flat but the annual total precipitation falls drastically to about 400 mm which was a real concern for the framers. This drastic change in annual total precipitation might be one of the results of recent climate change. Figure 4.2 (b) shows the annual precipitation trend in the last two decades where it reflects that during 2000 to 2021 the annual precipitation trend was falling rapidly but during last two years the precipitation trend is rising again. Overall trend line of the chart shows that the annual precipitation is falling, and the maximum annual precipitation occur in the year of 2005 and minimum annual precipitation occur in the year of 2011 at that station.

(a) Annual monthly precipitation

(b) Total Annual precipitation
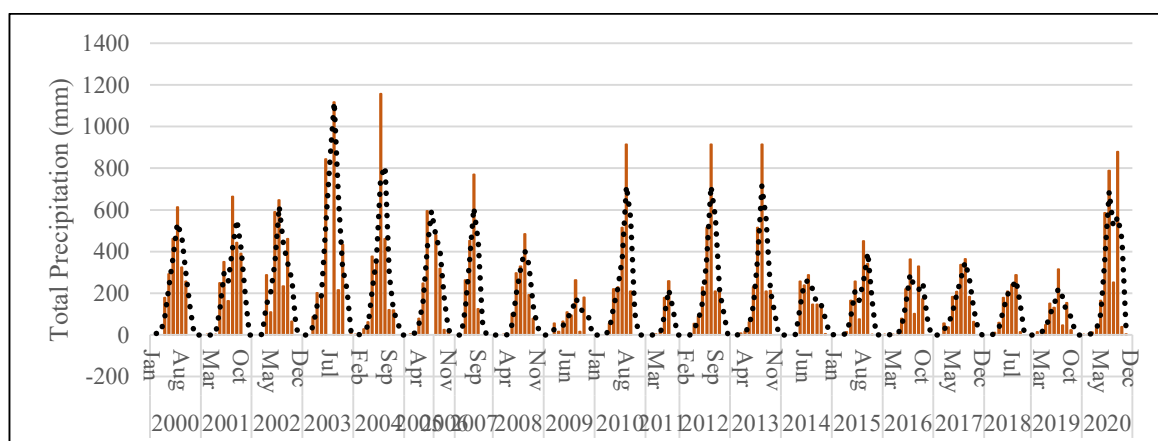
(c) Average monthly precipitation
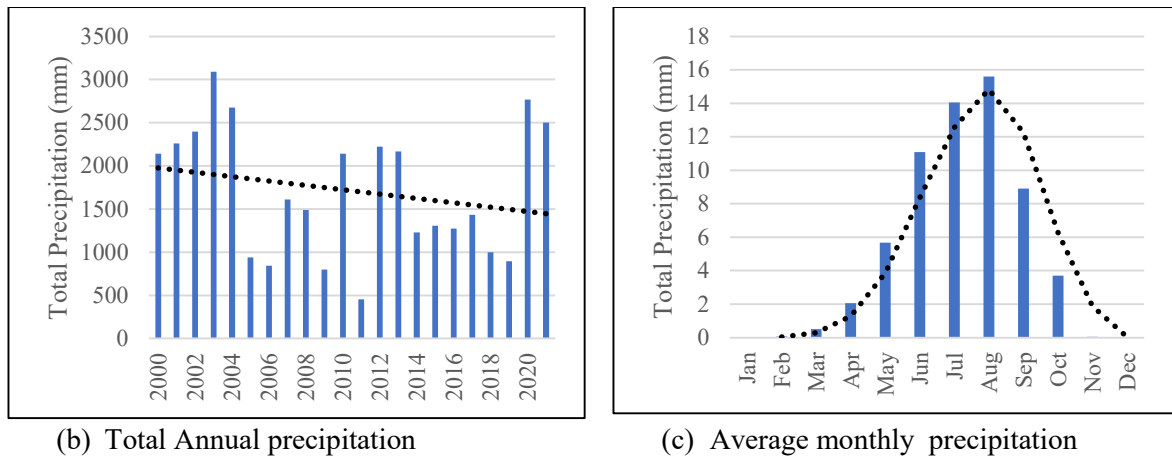
Figure 4. 2: Annual and Monthly precipitation analysis at Debiganj (R166) station

Figure 4.2 (c) shows the average monthly chart which reflects that during April to October the major portion of the yearly precipitation occur and in the month of August the maximum average monthly precipitation occurs and during November to January the minimum precipitation occurs at that station, the maximum monthly average precipitation varies from 10 mm to 15 mm at that station.

Figure 4.3 (a) shows the annual seasonal precipitation at Debiganj (R166) station which reflects that during Pre-Monsoon (Mar-May) and Monsoon (June-September) much of the precipitation occurs, during the monsoon maximum precipitation occurs which is about 1400 mm/yr. at that station.

In Figure 4.3 (b) the annual Pre-Monsoon precipitation at Debiganj (R166) station are presented which shows that during the last 21 years the pre-monsoon precipitation follows a steep decreasing trend line which reflects that during last 21 years the pre-monsoon precipitation reduced rapidly. In that period maximum precipitation occurred in year 2000 and minimum precipitation occurred in year 2003.
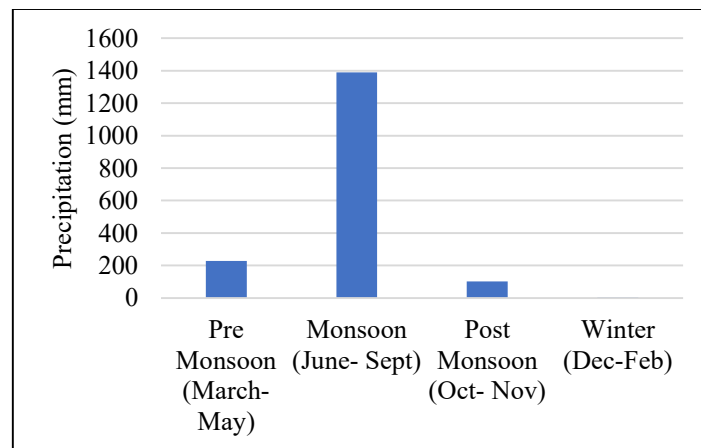
(a) Annual Seasonal Precipitation chart
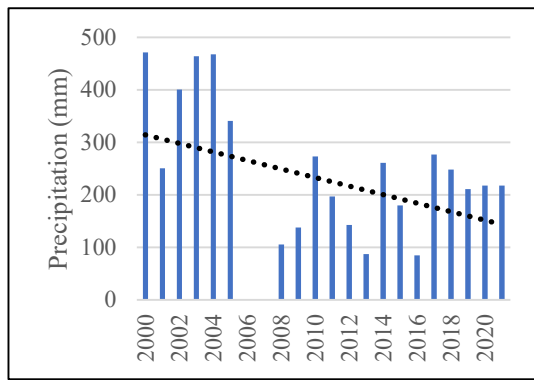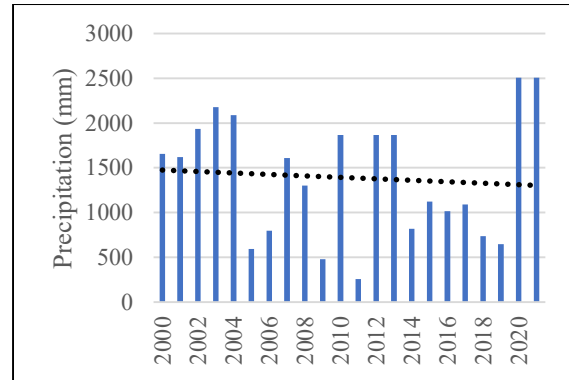
44

(b) Annual Pre-Monsoon
Precipitation chart

(c) Annual Monsoon Precipitation chart
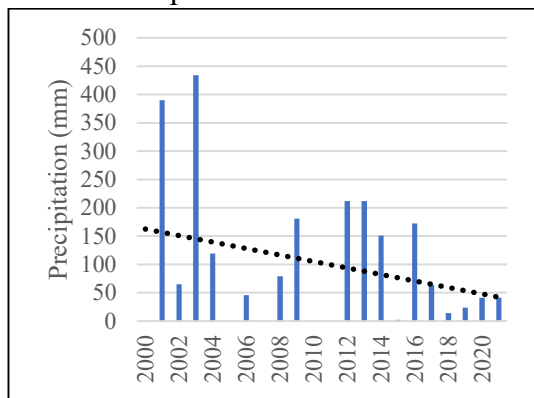
(d) Annual Post-Monsoon
Precipitation chart
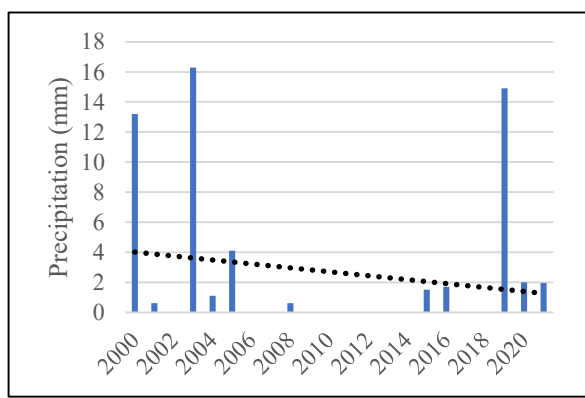
(e) Annual Winter Precipitation chart

Figure 4. 3: Seasonal precipitation analysis at Debiganj (R166) station from 2000 to 2021

Figure 4.3 (c) shows the annual Monsoon precipitation at Debiganj (R166) station which shows that during the last 21 years the monsoon precipitation follows a falling trend line which reflects that during last 21 years the monsoon precipitation reduced relatively. In that period maximum precipitation occurred in 2021 and minimum precipitation occurred in 2011. Figure 4.3 (d) shows the annual post-Monsoon precipitation at Debiganj (R166) station which shows that during the last 21 years the post-monsoon precipitation follows a steeply falling trend line which reflects that during last 21 years the post-monsoon precipitation reduces rapidly which caused lake of irrigation for crop land and insufficient flow to the major rivers which resulted in deposition of sediment and drying of Rivers. This phenomenon might be a cause of recent climate change.

Figure 4.3 (e) shows the annual winter precipitation at Debiganj (R166) station which shows that during the last 21 years the winter precipitation follows a falling trend line which reflects that during last 21 years the winter precipitation reduces. Again, from year 2000 to 2005 there was some precipitation recorded during winter but after 2005 to 2018 there was

hardly any precipitation recorded until 2019. This abrupt behavior of precipitation might be a cause of recent climate change.

Temperature

There are five satellite weather Grid station in and around the study area, this satellite Grid stations are from NASA-POWER which were shown in Figure 3.7. The analysis was conducted on the satellite weather Grid stations for temperature data from 2000 to 2021. The detail analysis of a representing Grid is described below.

Grid-2

Satellite grid station of Grid-2 weather station is situated in Panchagar district inside the Bangladesh boundary. This station is placed at the upstream of the Catchment.

Figure 4.4 (a) shows the annual temperature trend in the last two decades where it reflects that during 2000 to 2011 the annual temperature trend was quite flat and then from 2012 to 2016 the trend is rising and from 2016 to 2021 the trend is falling. During the last 20 years it has been observed that the first half (2000-2010) temperature remain normal and follows flat pattern but during the second half (2011-2021) it is rising and then falling though the change in temperature is not significant, but the pattern is abrupt in that phase, this abrupt behavior during the last decade may be the result of possible climate change. Overall trend line of the chart shows that the annual temperature is flat, and the maximum annual temperature occurs in the year of 2016 and minimum annual temperature occurs in the year 2011 at that station. Figure 4.4 (b) shows the average monthly chart which reflects that during April to June average maximum temperature occurs in that station. Maximum monthly average temperature varies from 25 ^{0}C to 30 ^{0}C at that station.
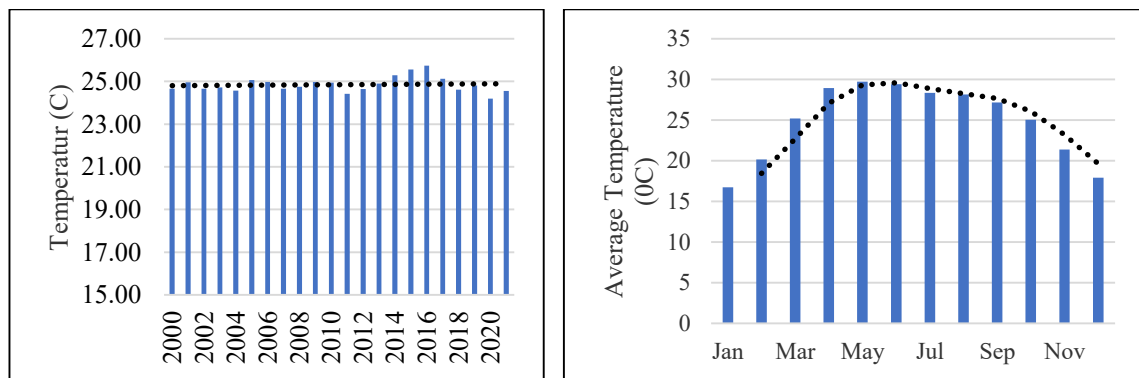
(a) Average Annual Temperature   (b) Average monthly Temperature

Figure 4. 4: Annual and Monthly Temperature analysis at Grid-2 from 2000 to 2021

Figure 4.5 (a) shows the annual seasonal temperature at Grid-2 which reflects that during Pre-Monsoon (March-May) and Monsoon (June-September) maximum temperature occurs which is about 27 ^{0}C at that station. Figure 4.5 (b) shows the annual Pre-Monsoon temperature at Grid-2 which shows that during the last 21 years the pre-monsoon temperature follows a declining trend line which reflects that during last 21 years the pre-monsoon temperature is decreasing. In that period maximum temperature occurred in 2016 and minimum temperature occurred in 2020.
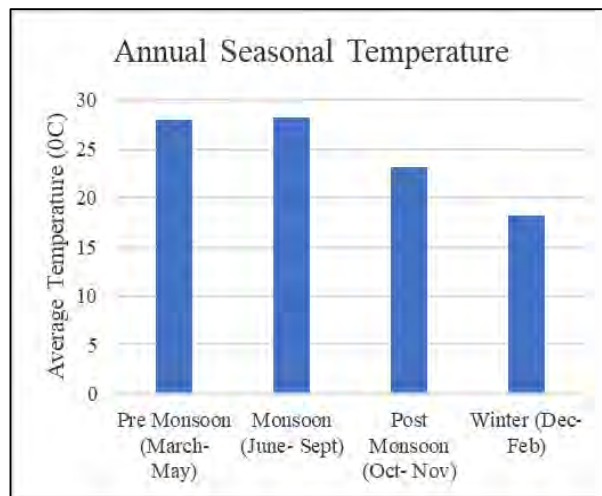
(a) Annual Seasonal Temperature chart
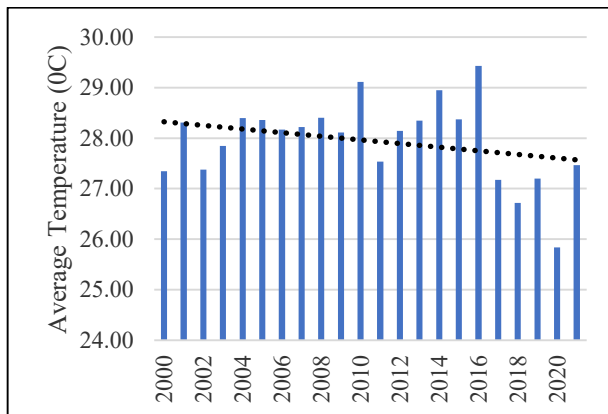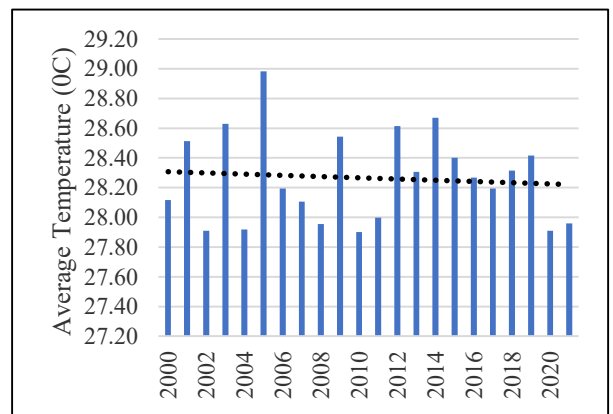
(b) Annual Pre-Monsoon Temperature chart

(c) Annual Monsoon Temperature chart
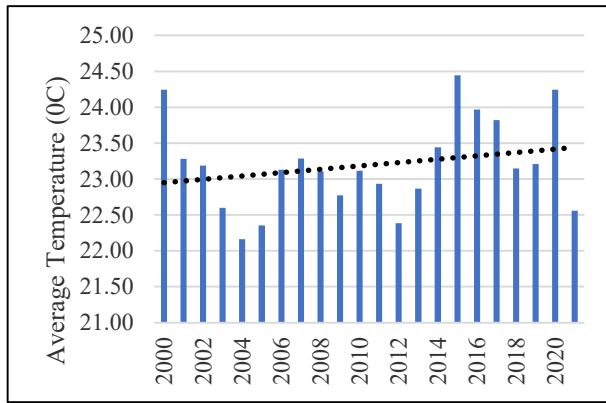
(d) Annual Post-Monsoon Temperature chart
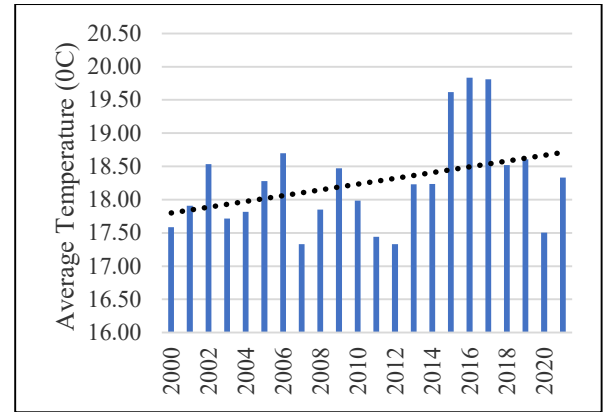
(e) Annual Winter Temperature chart

Figure 4. 5: Seasonal Temperature analysis at Grid-2 from 2000 to 2021

Figure 4.5 (c) shows the annual Monsoon temperature at Grid-2 which shows that during the last 21 years the monsoon temperature follows a mildly falling trend line which reflects that during last 21 years the monsoon temperature reduces partially. In that period maximum temperature occurred in 2005 and minimum temperature occurred in 2010. Figure 4.5 (d) shows the annual post-Monsoon temperature at Grid-2 which shows that during the last 21 years the post-monsoon temperature follows a rising trend line which reflects that during last 21 years the post-monsoon temperature increased. Specially during the last 10 years' temperature fluctuation is more relative to the previous 10 years. This phenomenon might be a cause of recent climate change. Figure 4.5 (e) shows the annual winter temperature at Grid-2 which shows that during the last 21 years the winter temperature follows a rapidly rising trend line which reflects that during last 21 years the winter temperature is rising rapidly. This rising temperature trend during winter season might be a cause of recent climate change. From the above discussion we can also see that the pre-Monsoon temperature is decreasing gradually in the last decade which is unusual to the seasonal characteristics. It reflects that during the last 2 decades the impact of climate change is visible.

Relative Humidity

There are five satellite weather Grid station in and around the study area, this satellite grid stations are from NASA-POWER which are shown previously in Figure 3.7. The analysis was conducted on the satellite weather grid station for Relative Humidity data from year

2000 to 2021. The detail analysis of a representing Weather Station for Grid-2 is described below.

Grid-2

Weather station of Grid-2 is situated in Panchagar district inside the Bangladesh boundary. This station is placed at the upstream of the Catchment. Figure 4.6 (a) shows the annual relative humidity trend in the last two decades where it reflects that during 2000 to 2021 the annual relative humidity trend was rising. The maximum annual relative humidity occurs in the year 2020 and minimum annual relative humidity occurs in the year 2012 at that station. Figure 4.6 (b) shows the average monthly chart which reflects that during May to September average maximum relative humidity occurs in that station. Maximum monthly average relative humidity varies from 40% to 85% at that station.
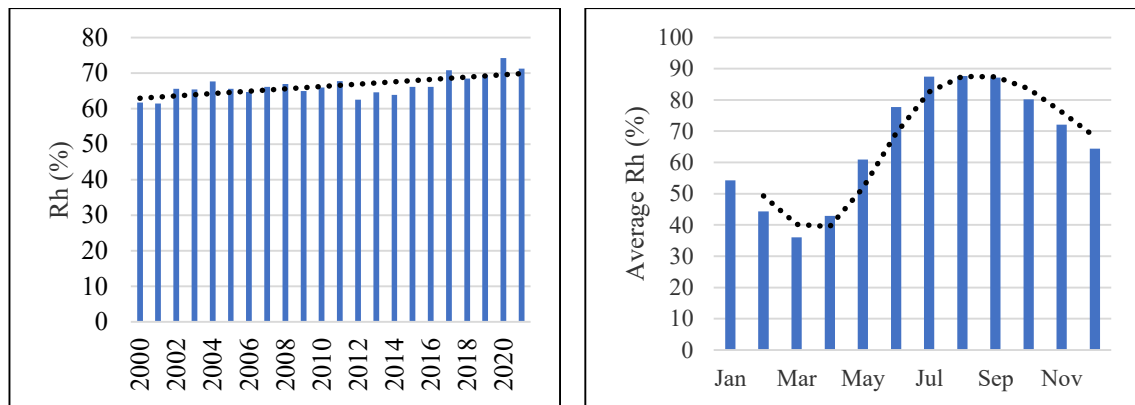
(a) Average Annual Relative Humidity   (b) Average monthly Relative Humidity

Figure 4. 6: Annual and Monthly Relative Humidity analysis at Grid-2 from 2000 to 2021

Figure 4.7 (a) shows the annual seasonal relative humidity at Grid-2 which reflects that during Monsoon (June-September) and Post-Monsoon (October-November) maximum relative humidity occurs which is about 82% at that station. Figure 4.7 (b) shows the annual Pre-Monsoon relative humidity at Grid-2 which shows that during the last 21 years the pre-monsoon relative humidity follows a rising trend line which reflects that during last 21 years the pre-monsoon relative humidity is increasing. Specially from 2015 to 2021 it shows a very steeply rising trend which might be a cause of possible climate change. In that period maximum relative humidity occurred in 2020 and minimum relative humidity occurred in 2014.
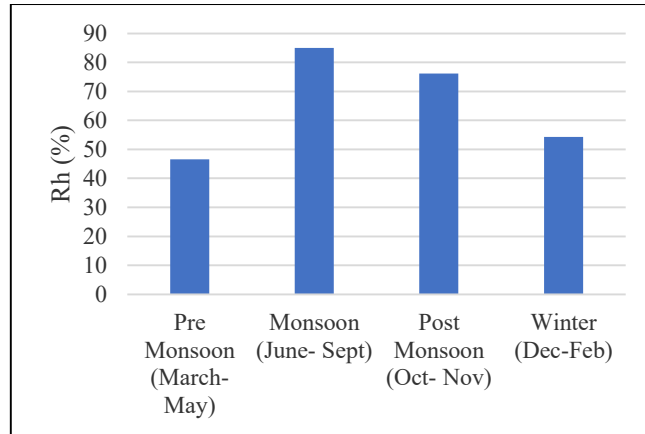
(a) Annual Seasonal Relative Humidity chart
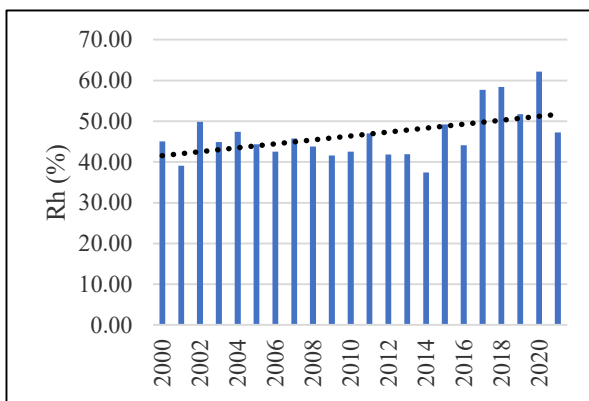
(b) Annual Pre-Monsoon Relative
Humidity chart
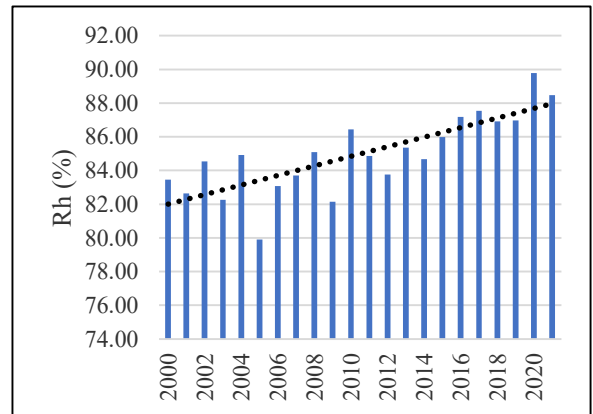
(c) Annual Monsoon Relative Humidity
chart
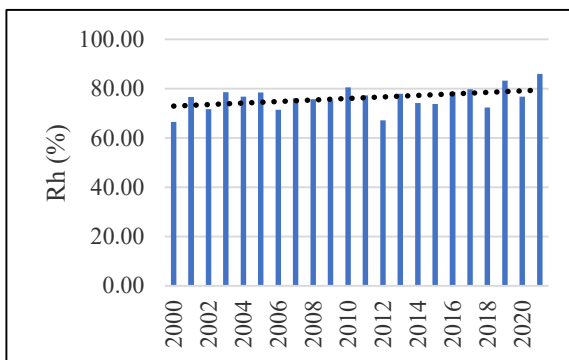
(d) Annual Post-Monsoon Relative
Humidity chart
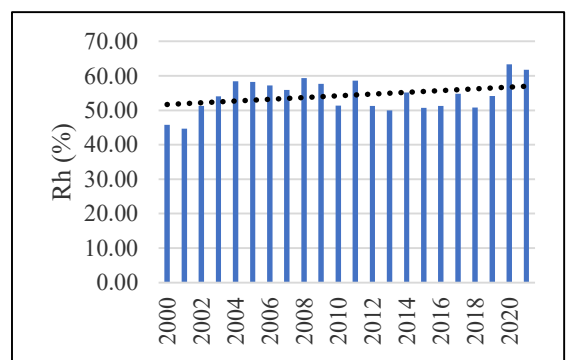
(e) Annual Winter Relative Humidity
chart

Figure 4. 7: Seasonal Relative Humidity analysis at Grid-2 from 2000 to 2021

Figure 4.7 (c) shows the annual Monsoon relative humidity at Grid-2 which shows that
during last 21 years the monsoon relative humidity follows rising trend line which reflects

that during last 21 years the monsoon relative humidity increased significantly. This phenomenon might be the cause of possible climate change. In that period maximum relative humidity occurred in 2020 and minimum relative humidity occurred in 2005. Figure 4.7 (d) shows the annual post-Monsoon relative humidity at Grid-2 which shows that during the last 21 years' post-monsoon relative humidity follows a rising trend line which reflects that during last 21 years the post-monsoon relative humidity increased. This phenomenon might be a cause of recent climate change.

Figure 4.7 (e) shows the annual winter relative humidity at Grid-2 which shows that during last 21 years winter relative humidity follows a rising trend line which reflects that during last 21 years the winter relative humidity is rising rapidly. Specially during the last 10 years the fluctuation of relative humidity is more significant than the previous 10 years. This rising relative humidity trend during winter season might be a cause of recent climate change.

Stage-Discharge Relationship for Observed Flow:

A rating curve is an important tool for a hydrologist to predict discharge from the observations of water level (Bhattacharya and Solomatine, 2005). In early 19th century, discharge was estimated at suitable sections using current-meters and other methods (IWM, 2017). Flood management, hydraulic design, and many other water resources projects in the field of surface hydrology, hydraulics is depending on the quality in discharge prediction. A discharge hydrograph can be developed using a water level hydrograph with the help of a rating curve (Bhattacharya and Solomatine, 2005). A rating curve for Atrai-Karatoa river is developed using the observed water level and discharge data from 1998 to 2019 at the Atrai Rail Bridge (SW 147) station which is shown in Figure 4.8.
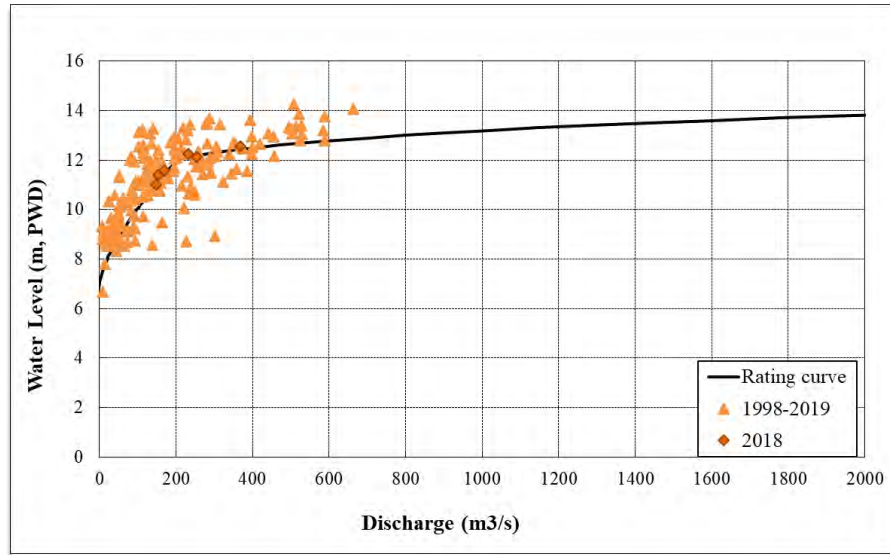
Figure 4. 8: An illustrative rating curve (at Atrai Ryl Bridge, SW-147 station on Atrai River)

A rating curve is an encapsulation of the relationship between water level and discharge of a river at a particular location. The rating curve is expressed in the following form:

$$Q(h) = \alpha(H - h_0)^\beta \qquad\qquad 4.1$$

Where, Q is the estimated discharge, H is the water level, h_o is the level at the zero discharge, and $\alpha \ and \ \beta$ are the rating curve parameters.

Using equation 4.1 the rating curve equation for Atrai River at Atrai Rail Bridge, SW-147 station is developed, which is shown in equation 4.2:

$$Q = 18.05(H - 8.0)^2 \qquad\qquad 4.2$$

where, $\alpha = 18.05 \ and \ \beta = 2$

Using equation 4.2, observed flow for Atrai-Karatoa River is generated and the generated flow hydrograph is presented in Figure 4.9.
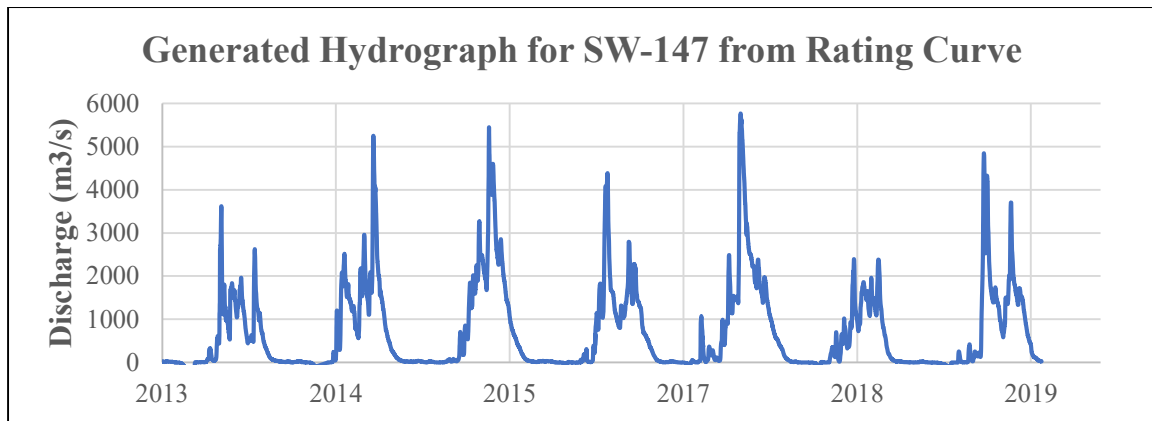
Figure 4. 9: Generated Hydrograph (at Atrai Ryl Bridge, SW-147 station on Atrai River) from the Rating Curve

4.3.2 Determination of Gage Weighting Factors

It is necessary to use interpolation methods to achieve accurate estimation of the spatial distribution of the rainfall. Thiessen polygons are an exact method of interpolation that assumes that the values of un-sampled locations are equal to the value of the nearest sampled point. To establish the area of influence of each precipitation gage Thiessen polygons method are used. Thiessen polygons are created by subdividing lines joining nearest neighbor points, drawing perpendicular bisectors through these lines, and then using these bisectors to assemble polygon edges. If observed data points are irregularly spaced a surface of irregular polygons will be produced. Intersections of Thiessen polygons with the sub-basin polygons are shown in Figure 4.10. It introduces a new set of smaller polygons such that each Thiessen polygon is related to one Thiessen polygon and one sub-basin polygon. For calculating the average precipitation over an area in Thiessen polygon method weightage is given to the various stations on a rational basis.
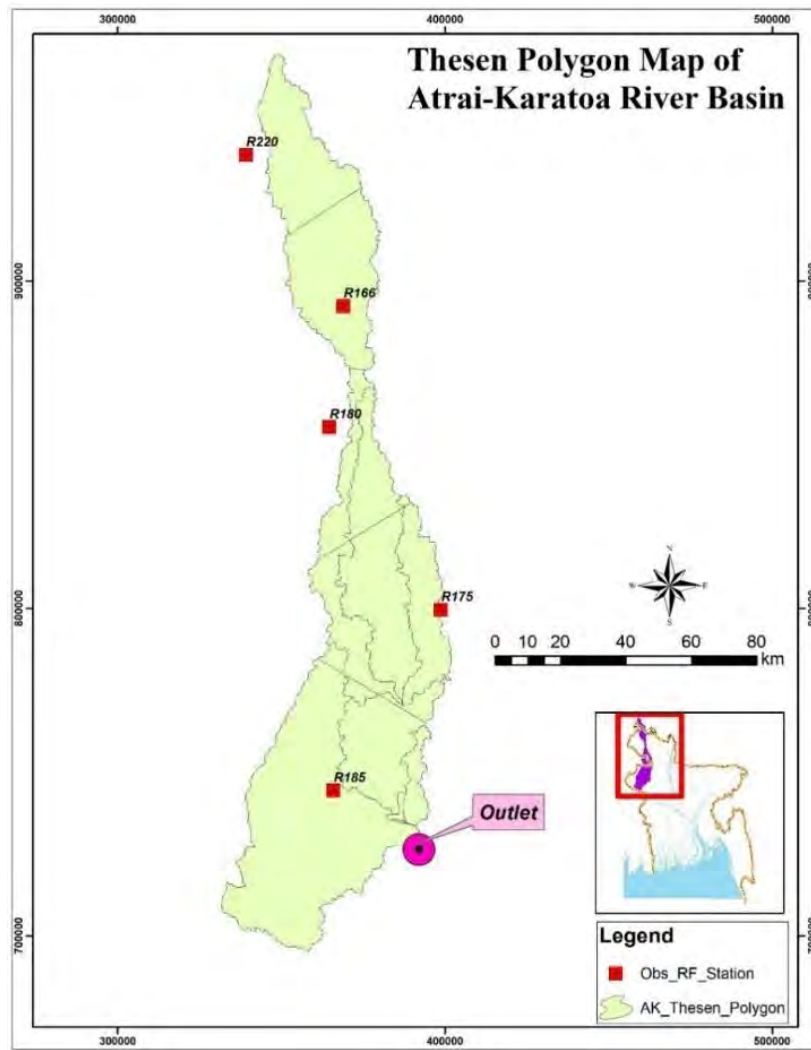
Figure 4. 10: Thiessen polygons map of Atrai-Karatoa River Basin

The weightage factor is defined as the ratio of area of a Thiessen polygon to the area of its corresponding sub-basin polygon and can be expressed as:

$$W_{ij} = \frac{A_{ij}}{S_j} \qquad\qquad\qquad 4.3$$

where

A_{ij} = area of the polygon generated by the intersection of sub-basin j with Thiessen polygon of gage i.

S_j = area of sub-basin j.

W_{ij} = weightage factor of gage i for sub-basin j.

The sum of depth weights of a sub-basin should equal to unity. Table 4.1 represents intersected sub-basin polygon with Thiessen polygon for a selected area. Gage information including gage name, ID and sub-basin information consisting of name, name of each gage

with corresponding weight is recorded after calculating the weightage based on sub-basin and Thiessen polygon data sets.

Table 4. 1: Estimated weightage factors for sub-basins considering different BWDB Station

Sub-basin ID	Station ID	Station Name	Sub-basin Aria_S_j (m^2)	Polygon Area_S_{ij} (m^2)	Weightage factor of gage i for sub-basin j	Total weightage factor
S_1	R166	Debiganj	256410.00	1058816719.8	0.41	
S_1	R175	Hilli (Hakimpur)	256410.00	384388778.01	0.15	
S_1	R180	Kantanagar	256410.00	269138260.60	0.10	1.00
S_1	R185	Manda	256410.00	44808910.17	0.10	
S_1	R220	Tentulia	256410.00	605374438.64	0.24	
S_2	R175	Hilli (Hakimpur)	117207.00	793682748.46	0.68	1.00
S_2	R180	Kantanagar	117207.00	378387251.54	0.32	
S_3	R175	Hilli (Hakimpur)	18.00	180000.00	1.00	1.00
S_4	R175	Hilli (Hakimpur)	54990.00	539233209.16	0.98	1.00
S_4	R180	Kantanagar	54990.00	9626999.40	0.02	
S_5	R175	Hilli (Hakimpur)	71127.00	88946612.96	0.13	1.00
S_5	R185	Manda	71127.00	622323387.04	0.87	
S_6	R185	Manda	1971.00	19710000.00	1.00	1.00
S_7	R175	Hilli (Hakimpur)	171531.00	44549256.47	0.34	1.00
S_7	R185	Manda	171531.00	1130690774.1	0.66	
S_8	R185	Manda	20637.00	150750829.12	1.00	1.00
S_9	R185	Manda	78624.00	3794022.26	1.00	1.00

4.3.3 Estimation of Impervious Area

Land cover map based on 0.5 km MODIS-based Global Land Cover analysis provides the information of different land cover types in Atrai-Karatoa River Basin (AKRB). HEC-HMS model needs the percentage of impervious area for each sub-basin. Considering artificial surface area for each sub-basin and validate it in Google Earth Pro, percentage of impervious area for each sub-basin of AKRB has been estimated and the values are within 0 to 10%. Table 4.2 shows the Initial Absorption, Curve Number and Impervious Layer percentages of AKRB.

Table 4. 2: Initial Absorption, Curve Number, and Impervious Layer of AKRB

Sub-basin No.	Initial Absorption (mm)	Curve Number	Impervious Layer (%)
S_1	55	52	5
S_2	59	50	5
S_3	45	64	7
S_4	40	75	8
S_5	39	68	7.5
S_6	59	50	5
S_7	52	48	5
S_8	58	50	5
S_9	59	50	5

4.3.4 Estimation of Lag Time (T_L) and Time of Concentration (T_C)

The peak discharge resulting from runoff-producing rainfall depends on how quickly the runoff reaches the watershed outlet. Hydrologic methods for calculation of peak discharge require some measure of the watershed's response time as an input. The two most common measures of hydrologic response time are time of concentration (T_C) and lag time (T_L). Lag time is needed for flood hydrograph calculations, and the time of concentration is needed to calculate peak flows by the rational method. The Natural Resources Conservation Service (NRCS) defines lag time as the time interval between the occurrence of a sudden burst of runoff-producing rainfall over the basin and the resulting peak at the basin outlet. Time of concentration (T_L) is defined as the time required for runoff to travel from the most remote point in the basin to the basin outlet (NRCS, 2010). Equation used to calculate the Lag time and Time of Concentration is given below:

$$T_L = \frac{L^{0.8}(S + 1)^{0.7}}{1900Y^{0.5}} \qquad \text{4. 4}$$

And

$$S = \frac{1000}{CN} - 10 \qquad \text{4. 5}$$

where,

T_L = Lag Time

L = Longest flow path (ft).

S = Potential maximum retention (in).

Y= average watershed slope (%) and

CN = Curve Number

A watershed's lag time and time of concentration are closely related to the length, slope, and roughness of the longest flow path. Urban watersheds have much shorter lag times and times of concentration than rural watersheds due to the lower frictional resistance of the urban infrastructure (curb and gutter streets, storm sewers, etc.). The lag time of a gaged watershed can be determined from an analysis of precipitation and water-level records if the time intervals between data values are sufficiently short. However, time of concentration cannot be determined from gaging data or measured in the field. Time of concentration can be estimated with hydraulic calculations, but the estimate may be unreliable due to idealized representation of irregular field conditions and large uncertainties in Manning roughness coefficients and other inputs. Alternatively, T_C can be estimated from lag time. According to the NRCS, in an average natural watershed with an approximately uniform distribution of runoff, lag time and time of concentration are related by:

$$T_c = 0.06 T_L \qquad\qquad 4.6$$

Although its origin is not well documented and its generality is uncertain, this relationship has been widely accepted in engineering practice for several decades. In this study, we assume Equation 4.6 is valid as a reasonable approximation and apply this relationship to estimate time of concentration from lag time. List of T_C and T_L of each sub-basin is given in Table 4.3.

Table 4. 3: Estimated Lag Time and Time of Concentration of AKRB

Sub-basin No.	Lag Time, T_L (hr)	Time of Concentration, T_C (hr)
S_1	47.20	2.83
S_2	45.64	2.74
S_3	41.57	2.49
S_4	40.80	2.45
S_5	27.89	1.67
S_6	43.60	2.62
S_7	31.35	1.88
S_8	37.70	2.26
S_9	45.98	2.76

4.3.5 Estimation of Base Flow

Base flow (also called drought flow, groundwater recession flow, low flow, low-water flow, low-water discharge and sustained or fair-weather runoff) is the portion of the

streamflow that is sustained between precipitation events, fed to streams by delayed pathways. It should not be confused with groundwater flow. Again, base flow can be defined as a portion of streamflow that is not directly generated from the excess rainfall during a storm event. In other words, this is the flow that would exist in the stream without the contribution of direct runoff from the rainfall.

Base flow can be estimated in several ways which are included below
1. Straight Line method
2. Varying Slope Method and
3. Fixed Base Method

In that study base flow is calculated using the straight-line separation method. Value of Base flow for the AKRB varies from 5 to 20 m^3/s. Figure 4.11 (a) shows the method used for base flow separation and Figure 4.11 (b) shows the base flow separation technique used for Atrai-Karatoa River Basin and Table 4.4 shows the estimated base flow for Atrai-Karatoa River Basin.
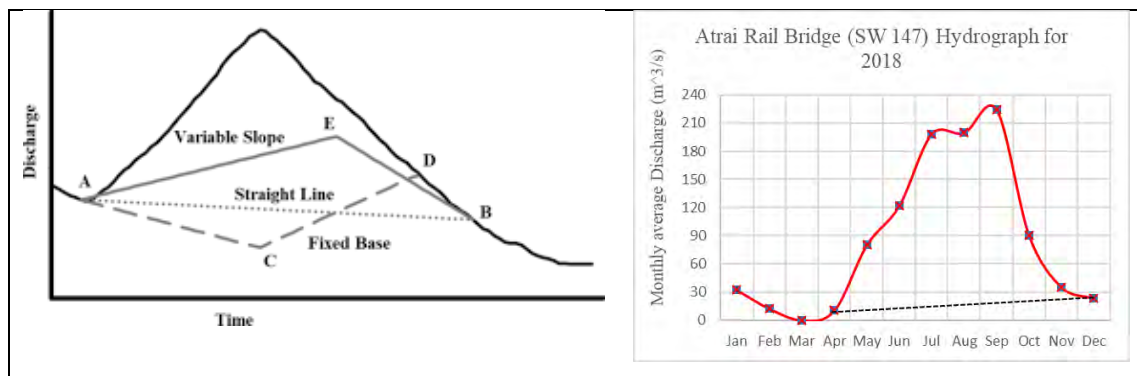
(a) Methods of Base flow Separation   (b) Base flow Seperation of Atrai Karatoa River

Figure 4. 11: Base Flow Separation Method of AKRB

Table 4. 4: Estimated Base flow for AKRB

Sub Basin No.	Base Flow (m³/s)											
	Jan	Feb	Mar	Apr	May	Jun	Jul	Aug	Sep	Oct	Nov	Dec
S_1	6	5	5	5	11	14	15	15	17	16	8.5	7
S_2	6	5	5	5	11	14	15	15	17	16	8.5	7
S_3	6	5	5	5	11	14	15	15	17	16	8.5	7
S_4	6	5	5	5	11	14	15	15	17	16	8.5	7
S_5	6	5	5	5	11	14	15	15	17	16	8.5	7
S_6	6	5	5	5	11	14	15	12	17	16	8.5	7
S_7	6	5	5	5	11	14	15	15	17	16	8.5	7
S_8	6	5	5	5	11	14	15	15	17	16	8.5	7
S_9	6	5	5	5	11	14	15	12	17	16	8.5	7

4.4 Model Development in HEC-HMS

4.4.1 Initial Model Set-up

First of all, basin model is created after a project is open in HEC-HMS (version 4.8) software. The terrain data of the study area is incorporated with the basin model after being projected the terrain data. Then using the GIS tool of HEC HMS, the watershed is delineated providing the outlet of the catchment. The automated watershed delineator subdivides the whole watershed into 9 sub-basins. After the watershed delineation required input data is incorporated to the model (Hydrologic Engineering Center, 2000). In HEC-HMS window, the meteorological data set of weather stations have been generated using HEC-DSSVue. It is a data storage system where data for precipitation and temperature for present and future timeline has been stored.

A base run with all necessary input data, hydrological models and meteorological model has been simulated to check the connections among the sub-basins and junctions. Initially, Nash Sutcliffe Co-efficient for model run was 0.19 and it was in unsatisfactory stage. The rest of the parameters which were not estimated in this study using secondary data or literature are decided to be calibrated in that stage.

4.4.2 Sensitivity Parameters Selection

HEC-HMS has the capabilities to process automated calibration to minimize a specific objective function, such as sum of the absolute error, sum of the squared error, percent error in peak, and peak-weighted root mean square error. However, in many cases, the resulting

automated parameters are not reasonable and practical. In this study, manual calibrated method was adopted to determine a practical range of the parameter values preserving the hydrograph shape, minimum error in peak discharges and volumes. To identify the most sensitive parameter, which is needed to calibrate first, multiple simulation was performed by changing different parameters within the recommended range to identify the sensitivity of the parameters. From these simulations it was observed that curve number (CN) and Muskingum K and X were the most sensitive parameters among all the parameters. The value of CN varies from 50 to 75 in the study area, Muskingum K varies from 45 to 65 hr. and Muskingum X varies from 0.02 to 0.09. The sensitive parameters and its adopted value & standard range is listed in Table 4.5.

Table 4. 5: Sensitive parameters and values used for calibration in HEC-HMS model

Parameter Name	Final Value	Standard Range	Source
Curve Number (CN)	50 to 75	30 to 100	Technical
Muskingum K (hr)	45 to 65	--	Manual of
Muskingum X	0.02 to 0.09	0 to 0.5	HEC-HMS

4.5 Model Development in SWAT

4.5.1 Initial Model Set-up

The first step in the model setup involves a delineation of the basin and sub-basin boundaries. This is accomplished using the automatic watershed delineation tool of ArcSWAT (version 2012.10_4.21) employing a 90 m DEM for AKRB. The Bangladesh Transverse Mercator (BTM) projection has been used for the DEM and all other GIS layers. All the watershed delineation steps such as filling sink, defining flow direction and accumulation have been done automatically through the user interface. After watershed delineation, AKRB have been divided into 9 watersheds based on the threshold area of 1600 ha. After delineation, the basin was divided into 9 sub-basins as shown in Figure 4.12. Soil and land use maps were loaded into SWAT to extract the land use and soil information of the AKRB. The land use, soil layer and slope class were overlaid to define the HRUs of the AKRB. A total of 25 HRUs were produced and included in the simulation. The discretization of basin into HRUs allows a detailed simulation of the hydrological processes.
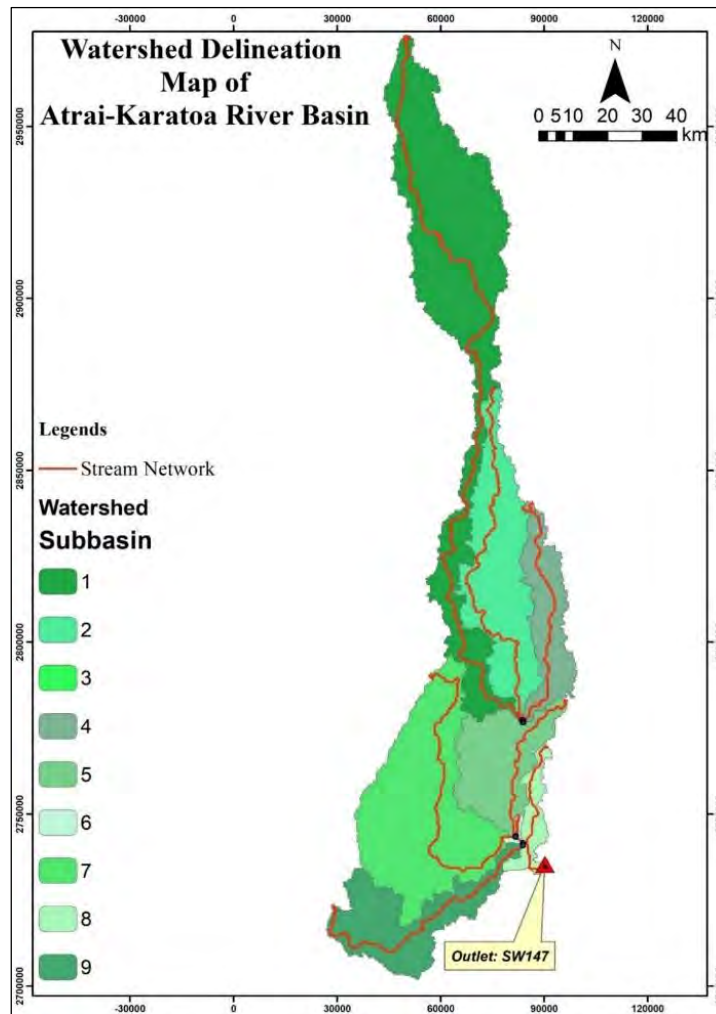
Figure 4.12: Sub Basins and Delineated River Network of AKRB

The climate of a watershed provides the moisture and energy inputs that control the water balance and determine the relative importance of the different components of the hydrologic cycle. The climatic variables required by SWAT consist of daily precipitation, maximum/minimum air temperature, solar radiation, wind speed and relative humidity. The model allows values for daily precipitation, maximum/minimum air temperatures, solar radiation, wind speed and relative humidity to be input from records of observed or generated data using weather generator tools (WXGEN) (Arnold et al., 1998).

The weather data for the AKRB have been used from NASA-POWER only the Precipitation data were collected from BWDB. The data includes daily weather data (minimum and maximum temperature, wind speed, relative humidity) starting from 2000 to 2021 which is used for SWAT modeling. The SWAT model has been simulated for the period of 2010 to 2019 based on the availability of discharge data. To describe the

61

distribution of rainfall, SWAT provides two options: a skewed normal distribution and a mixed exponential distribution. In the simulation for the present study, the skewed normal probability distribution function of SWAT model is used to define the rate and velocity of flow. Water is routed through the channel network using the variable storage routing method or the Muskingum River routing method. In this simulation the Muskingum River routing method has been used for channel routing. For estimating runoff, the SCS curve number method has been used. The Hargreaves method has been used to calculate potential evapotranspiration (PET) as it requires less weather parameter. The skewed normal distribution method has been used for rainfall distribution. Note that, the model was applied for 2010 to 2019 with a daily time step to facilitate the 3 years' warm-up period where 2010-2013 was taken same as the year 2013.

4.5.2 Parameter Selection

Model users are often faced with the different task of determining which parameters to calibrate so that the model response mimics the actual field, subsurface, and channel conditions as closely as possible. When the number of parameters in a model is substantial as a result of either a large number of sub-processes being considered or because of the model structure itself, the calibration process becomes complex and computationally extensive (Rossi et al., 2008). In such cases determination of sensitivity of parameters is necessary.

In this study sensitivity of different parameters have been inspected by changing the values manually and doing simulation run. After several simulations it was observed that the most sensitive parameter among all the parameters Alpha factor for groundwater recession, ALPHA_BF_D (standard range = 0.1-1 days^{-1}, Final Value = 0.1 days^{-1}), Ground Water Delay, GW_Delay (standard range = 1-500 days, Final Value = 50 days), Ground Water" revap" coefficient, GW_Revap (standard range = 0.02-0.2, Final Value = 0.135) and Curve Number, CN (standard range = 1-100, Final Value = 50-75) is most sensitive parameters. The sensitive parameters and its adopted value & standard range is listed in Table 4.6.

Table 4. 6: Sensitive parameters and values used for calibration in SWAT model

Parameter Name	Final Value	Standard Range	Source
Alpha factor for groundwater recession, ALPHA_BF_D (days^{-1})	0.1	0.1 to 1	Technical Manual of SWAT
Ground Water Delay, (GW_Delay) (days)	50	1 to 500	
Ground Water" revap" coefficient, GW_Revap	0.135	0.02 to 0.2	
Curve Number (CN)	50 to 75	30 to 100	

4.6 Calibration and validation

Calibration is the process whereby selected parameters and variables of the model are adjusted to make the model output match observations. There are numerous parameters in hydrological models which can be classified as physical parameters (i.e., parameters that can be physically measurable from the properties of watershed) and process parameters (i.e., parameters represents properties which are not directly measurable) (Yilmaz et al., 2010). A sensitivity parameter selection process was carried out to identify the sensitive parameters.

The calibration is carried out manually. To make this process faster, only a few of sensible model parameters, which affect significantly the hydrographs, are used (Vo et al., 2018). It was found that, out of 27 selected parameters, the Alpha factor for groundwater recession, Ground water revap co-efficient, curve number and groundwater delay time parameters to which the flow has sensitivity. However, the curve number (CN) was found to be the main sensitive parameter for all outlets for both the models. Table 4.7, Table 4.8, and Table 4.9 shows the final estimated values of parameters in HEC-HMS and SWAT model respectively.

Table 4. 7: Final estimated values of parameters in HEC-HMS model

Subbasin No.	Lag Time, T_L (hr)	Time of Concentration, Tc (hrs)	Initial Absorption (mm)	Curve Number	Impervious Layer (%)	Base Flow (m^3/s)											
						Jan	Feb	Mar	Apr	May	Jun	Jul	Aug	Sep	Oct	Nov	Dec
S_1	47.20	2.83	55	52	5	6	5	5	5	11	14	15	15	17	16	8.5	7
S_2	45.64	2.74	59	50	5	6	5	5	5	11	14	15	15	17	16	8.5	7
S_3	41.57	2.49	45	64	7	6	5	5	5	11	14	15	15	17	16	8.5	7
S_4	40.80	2.45	40	75	8	6	5	5	5	11	14	15	15	17	16	8.5	7
S_5	27.89	1.67	39	68	7.5	6	5	5	5	11	14	15	15	17	16	8.5	7
S_6	43.60	2.62	59	50	5	6	5	5	5	11	14	15	12	17	16	8.5	7
S_7	31.35	1.88	52	48	5	6	5	5	5	11	14	15	15	17	16	8.5	7
S_8	37.70	2.26	58	50	5	6	5	5	5	11	14	15	15	17	16	8.5	7
S_9	45.98	2.76	59	50	5	6	5	5	5	11	14	15	12	17	16	8.5	7

Table 4. 8: Final estimated values of channel parameters in HEC-HMS model

Parameters		Value
Manning's Roughness coefficient (Overland Flow)		0.018, 0.025, 0.035
Effective river width		120 m - 500 m
Length		455 km
Bed Slope		0.0004
Manning's n (Channel Flow)		0.025 – 0.04
Loss/Gain	Flow Rate	12.6 m³/s
	Fraction	0.2

Table 4. 9: Default estimated values of parameters in SWAT model

Parameters	Value
Initial depth of water in the shallow aquifer [mm]	1000
Initial depth of water in the deep aquifer [mm]	2000
Groundwater delay [days]	50
Threshold depth of water in the shallow aquifer required for return flow to occur [mm]	500
Threshold depth of water in the shallow aquifer for "revap" to occur [mm]	350
Deep aquifer percolation fraction	0.4
Initial groundwater height [m]	1
CN2: Initial SCS CN II value	75
Average slope length [m]	110
Average slope steepness [m/m]	0.01
Manning's "n" value for overland flow	0.14
Maximum canopy storage [mm]	10
Soil evaporation compensation factor	0.57
Plant uptake compensation factor	0.65
Pothole evaporation coefficient	0.5
Average distance to stream [m]	35
Decomposition response to soil temperature and moisture	1
Maximum humification rate	1
Undisturbed soil turnover rate under optimum soil water and temperature	0.055
Nitrogen uptake reduction factor not currently used	300
Lag coefficient	0.3
Surface runoff lag time in the HRU (days)	2
Curve number retention parameter adjustment factor to adjust surface runoff for flat slopes	1

For calibration and validation, the models were simulated for a period of 2017 to 2019 and 2013 to 2016 respectively at Atrai Rail Bridge (SW 147) station against discharge. Figure 4.13 shows the model calibration and validation location. In calibration and validation stage, model performance is evaluated based on statistically and graphically.
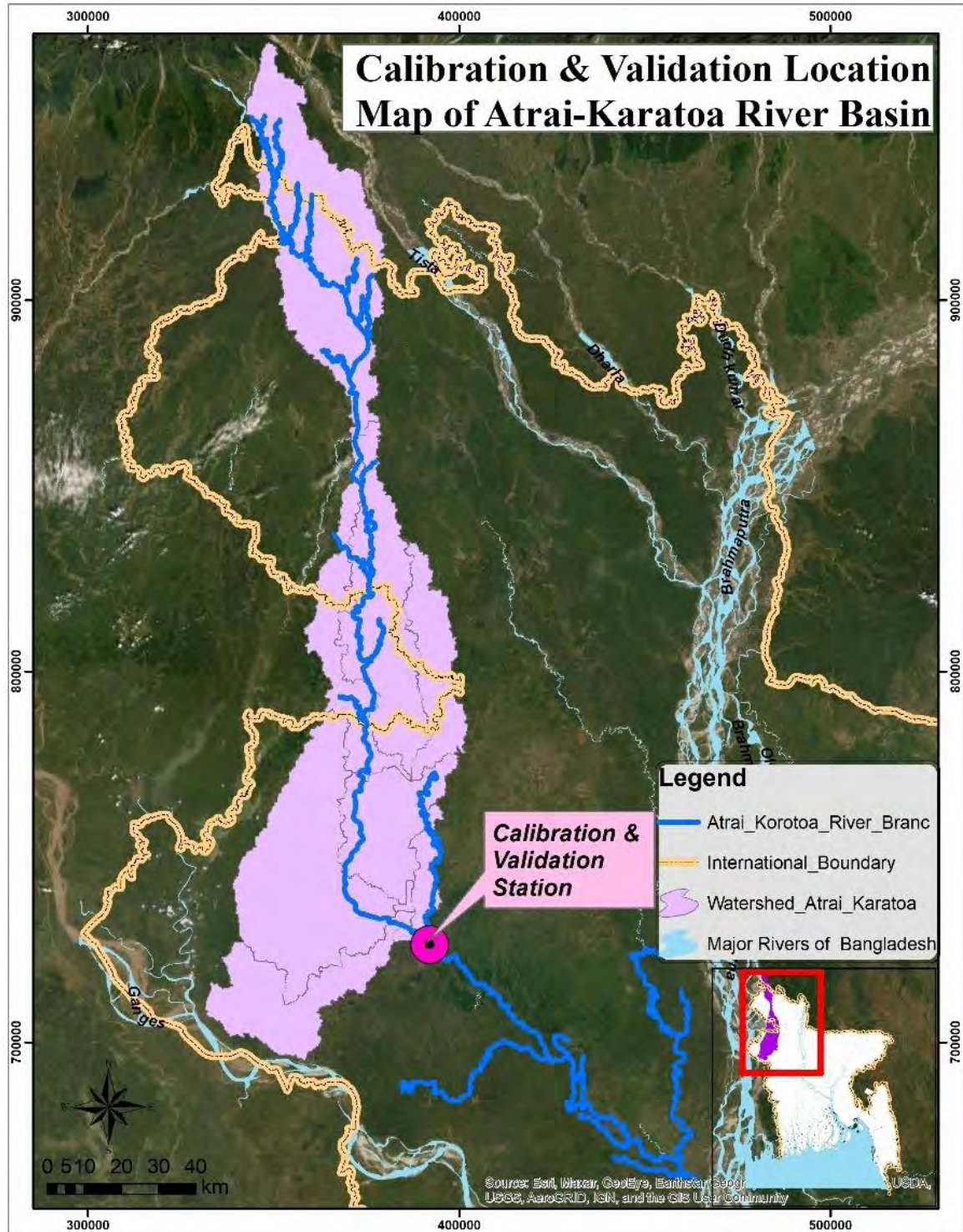
Figure 4. 13: Calibration and Validation Location of AKRB

CHAPTER 5

RESULTS AND DISCUSSION

5.1 General

In this chapter the calibration, validation, and performances of HEC-HMS and SWAT model are discussed. For performance analysis, statistical parameters have been calculated which are also included in this chapter. The future scenario analysis and the model performance using future scenario are also included in that chapter.

5.2 Calibration and Validation of Model

5.2.1 Calibration and Validation of HEC-HMS and SWAT Model

The main purpose of calibration and validation is to obtain an economical and reproducible method of identifying a parameter set for a particular catchment under particular conditions, which gives the best possible fit between the simulated and observed discharge for a particular calibration i.e., the calibrated parameter set aims at minimizing the difference between simulated and observed discharge. This process is considered to be necessary because there may be uncertainties in the model input and because of that, models give only simplified representations of the catchment's physical processes. In calibration and validation stage, model performance is evaluated based on statistically and graphically.

Figure 5.1 shows the graphical representation of daily observed and simulated flow for calibration and Figure 5.2 shows the graphical representation of daily observed and simulated flow for validation period for HEC-HMS model. It was found that the simulated flow is in great compliance with the observed flow for both monsoon and dry season. For calibration period the simulated flow slightly over-estimated the peak discharge and for validation period the simulated flow slightly under-estimated the peak discharge. However, HEC-HMS model slightly over-estimated the dry season flow during validation stage.
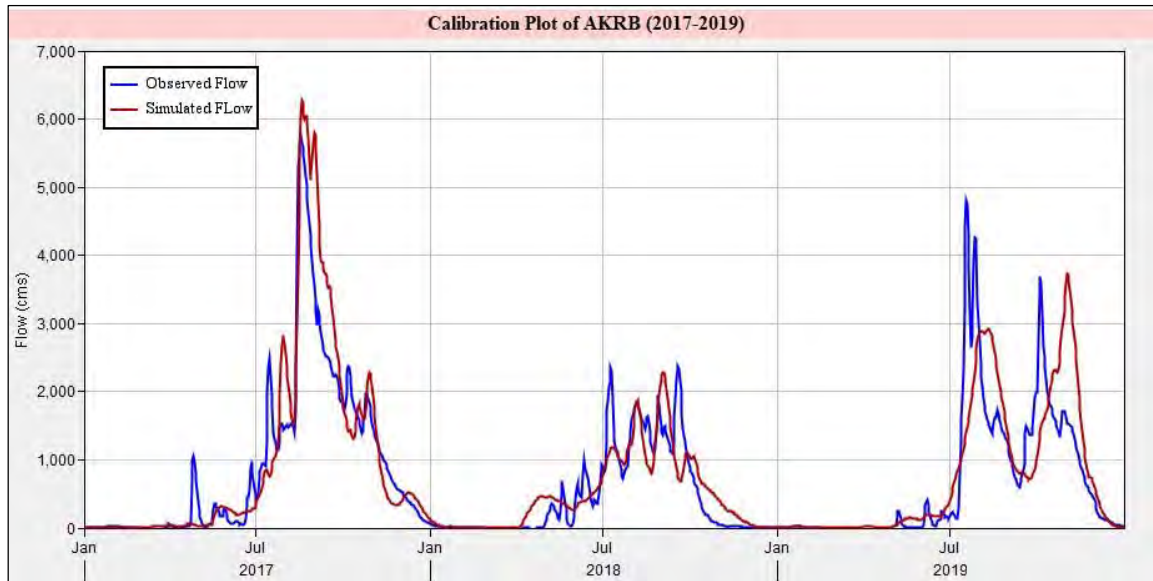
Figure 5. 1: HEC-HMS daily observed and simulated flows for the calibration period (2017-2019)
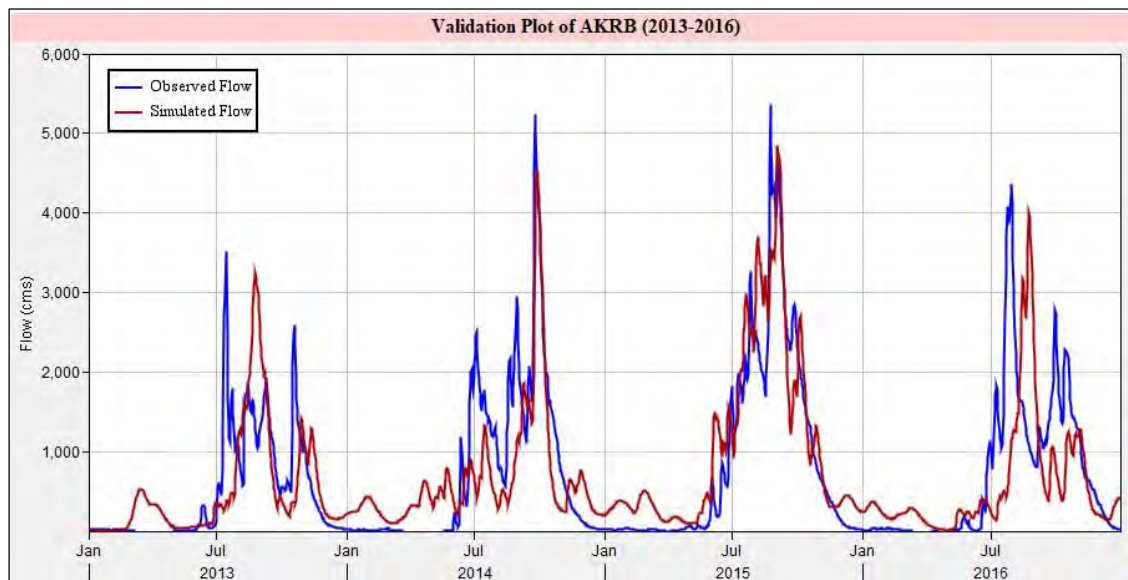
Figure 5. 2: HEC-HMS daily observed and simulated flows for the validation period (2013-2016)

Figure 5.3 shows the graphical representation of daily observed and simulated flow for calibration and Figure 5.4 shows the graphical representation of daily observed and simulated flow for validation period for SWAT model. It was found that the simulated flow is in great compliance with the observed flow for both monsoon and dry season. For calibration period the simulated flow and observed flow peak almost matches to each other but for validation period the simulated flow slightly overestimated the peak discharge.
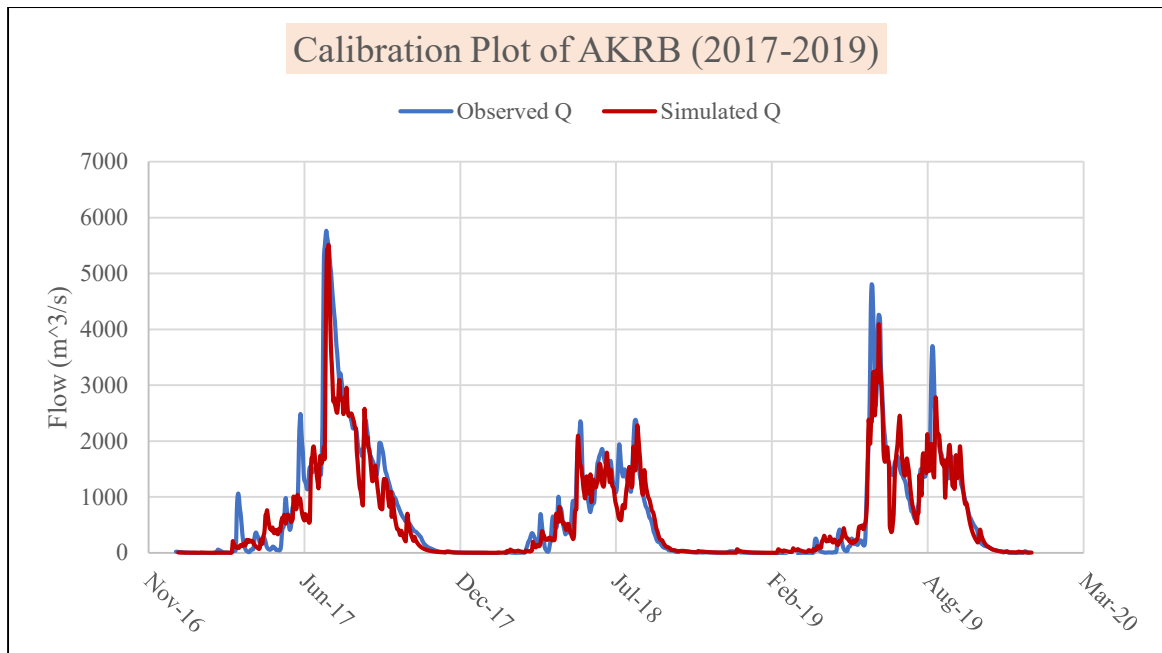
Figure 5. 3: SWAT daily observed and simulated flows for the calibration period (2017-2019)
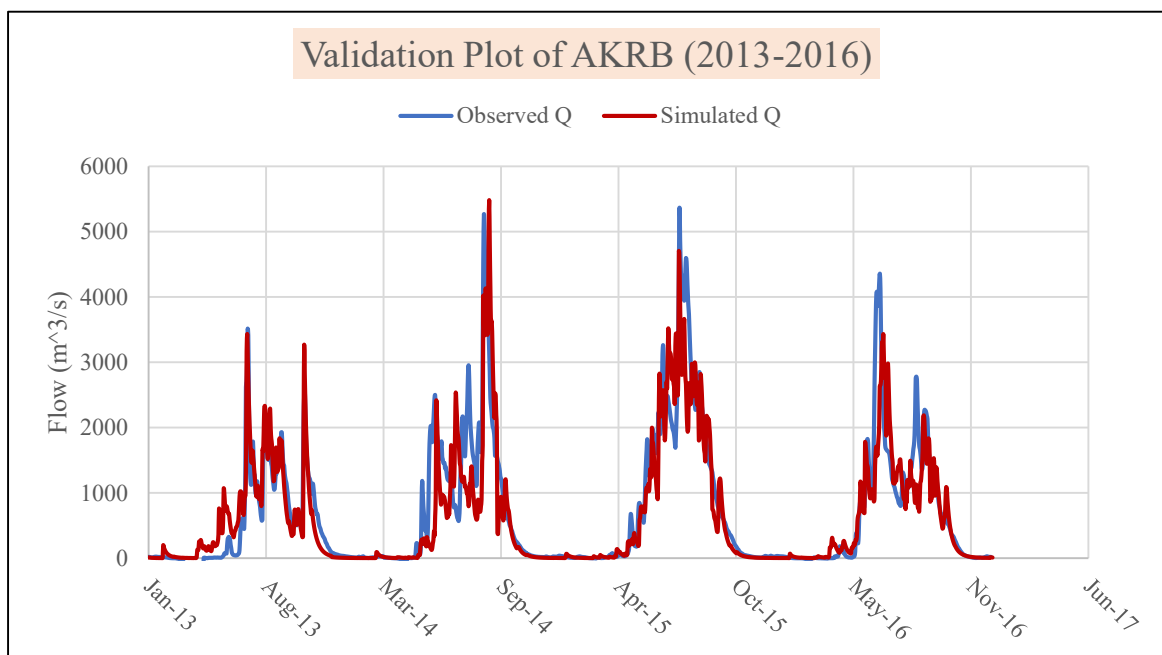
Figure 5. 4: SWAT daily observed and simulated flows for the validation period (2013-2016)

5.2.2 Model Performance Evaluation

Statistically the performance of the model has been evaluated using the NSE, PBIAS, RSR and R^2 values. The statistical model performance is given in Table 5.1. General reported rating of NSE, PBIAS, RSR and R^2 are given in Table 3.2.

Table 5. 1: Model performance statistics for calibration (2017-2019) and validation (2013-2016) period of the AKRB

Model	Type	Observed Mean (m³/s)	Simulated Mean (m³/s)	Model Performance			
				NSE	PBIAS	RSR	R^2
HEC-HMS	Calibration	691.12	755.34	0.68	8.19	0.61	0.70
	Validation	717.72	703.40	0.55	-2.67	0.68	0.56
SWAT	Calibration	691.12	611.75	0.84	11.48	0.47	0.86
	Validation	717.72	634.40	0.75	8.45	0.55	0.75

For HEC-HMS model the NSE values are 0.68 and 0.55 for calibration and validation period, respectively. The PBIAS and RSR values are found to be 8.19 and 0.61 in calibration stage and -2.67 and 0.68 in validation stage, respectively. The R^2 values are 0.70 and 0.56 for calibration and validation stage, respectively. These statistics demonstrate that HEC-HMS model generally performed well in both calibration and validation stages based on historical measured data for AKRB (Moriasi et al., 2007). For SWAT model the NSE values are 0.84 and 0.75 for calibration and validation period, respectively. The PBIAS and RSR values are found to be 11.48 and 0.47 in calibration stage and 8.45 and 0.55 in validation stage, respectively. The R^2 values are 0.86 and 0.75 for calibration and validation stage, respectively. These statistics demonstrate that SWAT model generally performed well in both calibration and validation stages based on historical measured data for AKRB (Moriasi et al., 2007).

Based on the above statistical parameters and visual representation of both models, it can be assumed that both models perform satisfactorily for both calibration and validation periods, although for the AKRB, SWAT model performs better than HEC-HMS model.

5.3 Future Scenario Analysis

Future scenario analysis is done considering different return periods of rainfall event scenario, where present land use is considered. The detail method and analysis are discussed in the following sections.

5.3.1 Determination of Design Discharge

Frequency analysis of hydrological and hydrometric data is carried out to find the extreme rainfall events and discharge for different return periods. Statistical analysis of observed discharge is carried out. Yearly maximum discharge data at Atrai Rail Bridge (SW 147) is

considered for frequency analysis and design flood levels for 10, 25, 50 and 100 years return periods are identified using Extreme Value Analysis (EVA) tool in MIKE Zero software with 21 years (1998 to 2019) observed discharge. Three statistical distribution methods have been considered for determining the discharge for different return period. Gumbel (GUM), Log Pearson Type III (LP3) and Log Normal Distribution (LN2) statistical distribution methods have been tested to fit the observed discharge data. Methods of Moment (MOM) has been used as an estimation method and Monte Carlo method has been used for uncertainty calculations. Goodness of fit has been tested with Chi-Square and K-S Test method. The Log Normal distribution method poses the smallest value for Chi-Square among the three methods which is adopted for the future analysis. Goodness of fit test for discharge is presented in Table 5.2 and frequency analysis for different return period is presented in Table 5.3. Figure 5.5 shows the log normal distribution of observed discharge at Atrai Rail Bridge of Atrai River.

Table 5. 2: Goodness of Fit Test for Identifying Design Discharge for Atrai-Karatoa River

Test	Log-Normal Distribution	Log-Pearson-III Distribution	Gumbel EV1 Distribution
Chi Square Test	3.60	5.20	4.00
K-S Test	0.17	0.17	0.21

Table 5. 3: Observed Discharge at Atrai-Karatoa Rail Bridge (estimated from frequency analysis) in Atrai River

Probability Distribution	Return Period in years			
	10	25	50	100
Gumbel (EV1)	597.527	733.148	833.759	933.627
Log Pearson-III	592.676	677.359	731.84	780.692
Log Normal	719.46	987.582	1211.829	1456.723
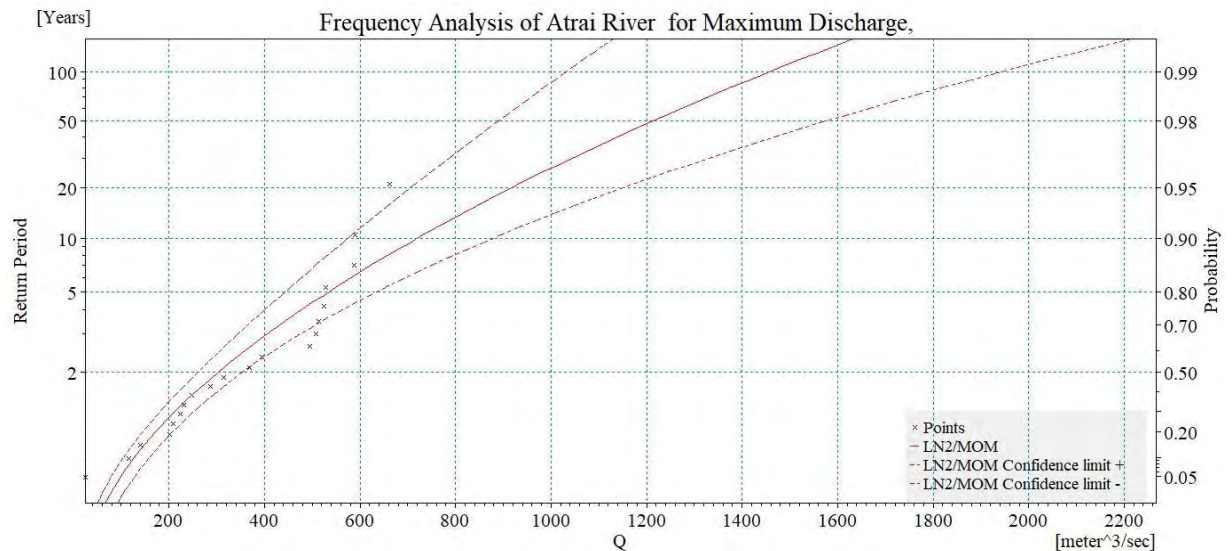
Figure 5. 5: Log normal distribution of Discharge at Atrai Rail Bridge of Atrai River

5.3.2 Determination of Design Rainfall Event

Different design rainfall events have been calculated using the rainfall stations information situated in the study area. Different rainfall events have been analyzed from the daily rainfall data to understand the consecutive rainfall effects in the study area. Yearly maximum rainfall data for 50 years (1970-2020) has been carried out for determining 1day cumulative rainfall events to prepare the future simulation plan. Table 5.4 shows the yearly maximum rainfall event for the last 50 years at Debiganj.

Table 5. 4: Yearly maximum rainfall of Debiganj for 1-day cumulative rainfall event

Year	1-day Cumulative rainfall (mm)	Year	1-day Cumulative rainfall (mm)
1970	286	1985	166.4
1971	196.7	1986	206.8
1972	180.6	1987	201.9
1973	181.6	1988	166.1
1974	162.6	1989	219.6
1975	119.4	1990	227.8
1976	208.3	1991	226.5
1977	114.3	1992	167
1978	139.7	1993	189
1979	132.3	1994	106.7
1980	134.1	1995	221
1981	152.4	1996	210.7
1982	139.9	1997	202.8
1983	115.6	1998	235.7
1984	176.5	1999	138.5

Year	1-day Cumulative rainfall (mm)	Year	1-day Cumulative rainfall (mm)
2000	124.5	2011	38.3
2001	168.7	2012	180.6
2002	150	2013	180.6
2003	286	2014	40.7
2004	165.4	2015	68.6
2005	90.4	2016	58.2
2006	84.2	2017	99
2007	104.6	2018	43
2008	95.8	2019	78.7
2009	74.2	2020	196.7
2010	180.6		

These 50 years' yearly maximum rainfall data have been taken into consideration and used them to determine different return period rainfall information for Debiganj stations. This step is repeated for all the stations within the study area. Three statistical distribution methods have been considered for determining the rainfall for different return period. Gumbel (Gum), Log Pearson Type III (LP3) and Log Normal Distribution (LN2) statistical distribution methods have been tested to fit the raw rainfall data. Goodness of fit has been tested with Chi-Square method. Methods of Moment (MOM) has been used as an estimation method and Monte Carlo method has been used for uncertainty calculations. Goodness of fit has been tested with Chi-Square method. Four different return periods (10, 25, 50 and 100 years) have been considered to estimate the design rainfall. Table 5.5 presents the design rainfall for different return periods.

Table 5. 5: Design rainfall of different rainfall stations of AKRB at different return periods for different rainfall events

Station	Item	Hydrological Events	1-day rainfall (mm)		
		Return Period [years]	GUM	LP3	LN2
Debiganj	Estimated Design Rainfall of Debiganj Rainfall Station for different return periods	10	203.19	205.52	213.48
		25	250.64	251.59	278.32
		50	285.84	284.51	330.33
		100	320.78	316.28	385.37
	Goodness-of-fit statistics	CHISQ	2.81	3.19	1.67
Hilli	Estimated Design Rainfall of Hilli Rainfall Station for different return periods	10	198.55	199.61	191.47
		25	244.4	253.09	238.44
		50	278.42	292.95	274.75
		100	312.18	332.46	312.1
	Goodness-of-fit statistics	CHISQ	7.76	8.14	8.14
Kantanagar	Estimated Design Rainfall of Kantanagar Rainfall Station for different return periods	10	231.61	231.41	262.28
		25	283.95	268.13	350.06
		50	322.79	292.45	421.83
		100	361.34	314.73	498.88
	Goodness-of-fit statistics	CHISQ	0.52	0.52	0.52
Manda	Estimated Design Rainfall of Manda Rainfall Station for different return periods	10	143.85	140.78	138.76
		25	167.52	174.93	157.44
		50	185.09	201.85	170.82
		100	202.53	229.42	183.83
	Goodness-of-fit statistics	CHISQ	3.57	3.95	5.86
Tentulia	Estimated Design Rainfall of Tentulia Rainfall Station for different return periods	10	281.12	276.87	308.48
		25	328.44	301.6	371.75
		50	363.55	316.76	419.36
		100	398.4	329.88	467.38
	Goodness-of-fit statistics	CHISQ	7.76	0.91	10.05

Goodness of fit has been tested with the Chi-Squares method. It has been observed that for different stations, different distribution method provides the lower Chi-Square value during calculation of 1-day design rainfall. Considering this, the future simulation is conducted adopting the matching year's rainfall data of each station for each event.

Considering this, further simulations are carried out using the highest quantity of rainfall that corresponds to the or closest to the precipitation of the aforementioned year's (Return period) rainfall. The return period year rainfall is obtained using the statistical approach with the lowest CHISQ value. The typical return period plot for a 1-day cumulative rainfall event is shown in Figure: 5.6.
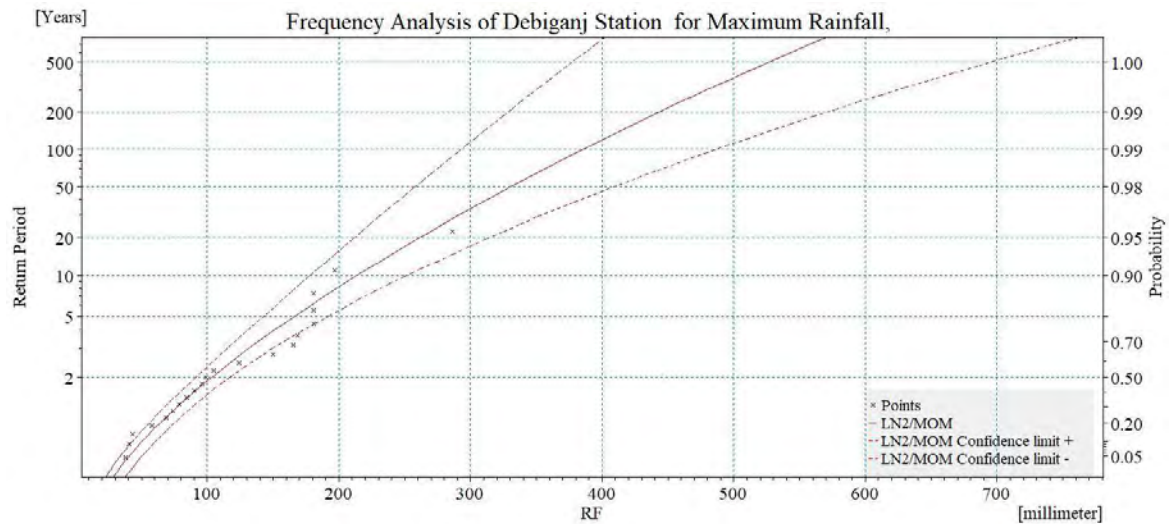
Figure 5. 6: Design rainfall of Debiganj station for 1-day cumulative rainfall by Log Normal statistical distribution method

5.3.3 Simulation of Models Considering different return periods of rainfall event

From the projected rainfall for future rainfall events both HEC-HMS and SWAT model is simulated for each event and the simulated runoff is plotted against observed runoff generated for future return period (10, 25, 50 and 100 years). Table 5.6 and Figure 5.7 shows the observed and simulated discharge at different return periods.

Table 5. 6: Observed and Simulated Discharge for different return periods considering different return periods of rainfall events

Return Period (Years)	Observed Predicted Discharge (m³/s)	HEC-HMS Simulated Discharge (m³/s)	% Variation of HEC-HMS w.r.t Observed Discharge	SWAT Simulated Discharge (m³/s)	% Variation of SWAT w.r.t Observed Discharge
10	719.46	790.3	9.85%	758.688	5.45%
25	987.582	1043.3	5.64%	1025.42	3.83%
50	1211.829	1274.5	5.17%	1255.65	3.62%
100	1456.723	1551	6.47%	1515.35	4.02%
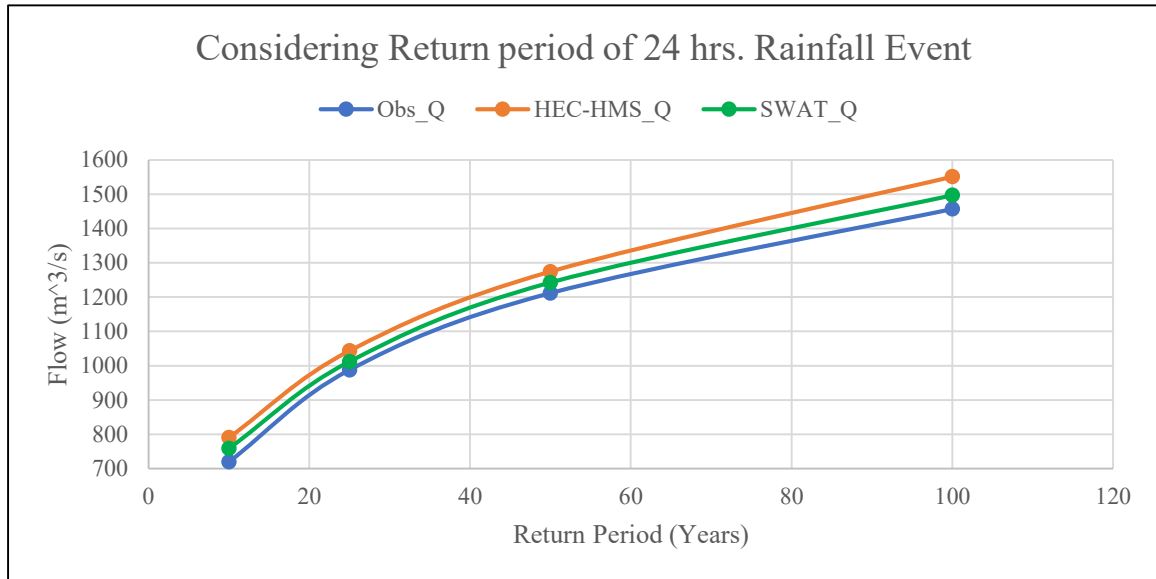
Figure 5. 7: Observed and Simulated Flow for different return periods different return periods of rainfall event

From the Table 5.6 and Figure 5.7 we can observed that both HEC-HMS and SWAT follows the same trend as observed flow but between HEC-HMS and SWAT model, HEC-HMS overestimates the flow more. Again, if we observe that both the models' predictions are quite comparable to observed flow where the variation of predicted flow with the observed flow lies in-between 5% to 10% for HEC-HMS model and 3% to 6% for SWAT model.

5.4 Discussion

For HEC-HMS model the NSE, PBIAS and RSR and R^2 values are 0.68, 8.19, 0.61, 0.70, and 0.55, -2.67, 0.68, 0.56 for calibration and validation period, respectively. These statistics has shown a satisfactory correlation between simulated and observed discharge at Atrai Rail Bridge (SW 147) of AKRB. Khoi and Nguyen (2016) have found in their study the values of NSE, PBIAS and R^2 are 0.62, -10.00 and 0.64 for calibration and 0.74, -1.00 and 0.77 for validation respectively for HEC-HMS model. Here it can be observed that HEC-HMS is performing similar to the study of Khoi and Nguyen's (2016) model for both calibration and validation stage.

For SWAT model the NSE, PBIAS, RSR and R^2 values are 0.84, 11.48, 0.47, 0.86 and 0.75, 8.45, 0.55, 0.75 for calibration and validation period respectively. These statistics has shown a satisfactory correlation between simulated and observed discharge at Atrai Rail

Bridge (SW 147) of AKRB. Khoi and Nguyen (2016), also found in their study the values of NSE, PBIAS and R^2 are 0.69, -4.00 and 0.85 for calibration and 0.77, 4.00 and 0.81 for validation respectively for SWAT model. Here it can be observed that SWAT is performing similar to the study of Khoi and Nguyen's (2016) model for both calibration and validation stage. In the study of Khoi and Nguyen (2016), they found both model performs satisfactorily in terms of flow and statistical value but between the two models SWAT model was performing better than HEC-HMS model for their watershed. Here in this study we can observed that both HEC-HMS and SWAT is performing satisfactorily like Khoi and Nguyen's (2016) study and SWAT was capturing the peak flow and dry season flow better than the HEC-HMS model. Though HEC-HMS model is capturing the medium and peak flow better but it could not capture the dry season flow properly.

Based on the above statistical parameters of both models, it can be assumed that both models perform admirably for both the calibration and validation periods, although for the AKRB, SWAT model performs better compared with HEC-HMS model.

CHAPTER 6

CONCLUSIONS AND RECOMMENDATIONS

6.1 Conclusions

Atrai-Karatoa River Basin (AKRB), like other watersheds in many parts of Bangladesh is poorly gauged or not gauged at all. Under the circumstances streamflow data are not adequately available. To overcome this obstacle a calibrated and validated model is a useful tool. This study is conducted to develop such a tool.

The calculations of this study are summarized below.

- The NSE, PBIAS, RSR and R^2 values for calibration stage in HEC-HMS model are 0.68, 8.19, 0.61 and 0.70, respectively. The NSE, PBIAS, RSR and R^2 values for validation stage in HEC-HMS model are 0.55, -2.67, 0.68 and 0.56, respectively.

- The NSE, PBIAS, RSR and R^2 values for calibration stage in SWAT model are 0.84, 11.48, 0.47 and 0.86, respectively. The NSE, PBIAS, RSR and R^2 values for validation stage in SWAT model are 0.75, 8.45, 0.55 and 0.75, respectively.

- From the study, it has been found that both models performed satisfactorily for AKRB but between the two models SWAT model performed better compared with HEC-HMS model for the AKRB.

- The event-based simulations considering return period of 24 hrs. rainfall event under existing land use condition both models provide quite comparable results for the period (10-100 years) where the variations are 5% to 10% for HEC-HMS model and 3% to 5% for SWAT model with respect to observed predicted discharge.

- HEC-HMS is both lumped and semi distributed model and SWAT is a semi distributed model, in HEC-HMS the sub-basin parameters are provided manually for each sub-basin and in SWAT each sub-basin is sub-divided into multiple hydraulic response unit (HRU). The data requirement of SWAT model is much more complex than HEC-HMS model.

6.2 Recommendations

Recommendations for future extension of the present work have been discussed in the following sections.

- Due to the lack of observed climatic parameters like relative humidity, wind speed and solar radiation, satellite grid data were used which might have some bias, thus future study can be conducted using the observed climatic data which would give more reliable results.

- In this study the climate change scenarios are considered based on available observed data analysis. Further study can be conducted considering the RCP scenarios.

- Along with climatic change, land use change can be included in the future study which will give more realistic results.

REFERENCES:

Agroecological Zone - Banglapedia (2019). Available at:
https://en.banglapedia.org/index.php/Agroecological_Zone (Accessed: 23 June 2022).

Ahmed, T., Al Hossain, B.M.T., Aktar, M.N., Fida, M., Khan, A., Islam, A.S., Yazdan, M.M.S., Noor, F. and Rahaman, A.Z. (2011). Climate Change Impacts on Water Availability in the Ganges Basin. 5th International Conference on Water & Flood Management (ICWFM-2015).

Alam, S. (2015). Impact of Climate Change on Future Flow of Brahmaputra River Basin Using Swat Model. Bangladesh University of Engineering and Technology (BUET), Dhaka.

Ali, S., Jaiswal, R.K., Bharti, B. and Kumari, C. (2019). Comparative Analysis of Conceptual Rainfall-Runoff Modeling in Chhattisgarh, India. International Journal of Advance and Innovative Research, 6(2 (X)), pp. 20–28.

Anaba, L.A., Banadda, N., Kiggundu, N., Wanyama, J., Engel, B. and Moriasi, D. (2016). Application of SWAT to Assess the Effects of Land Use Change in the Murchison Bay Catchment in Uganda. Computational Water, Energy, and Environmental Engineering, 6(1), pp. 24–40. doi: 10.4236/CWEEE.2017.61003.

Arnold, J.G., Srinivasan, R., Muttiah, R.S. and Williams, J.R. (1998). Large Area Hydrologic Modeling and Assessment Part I: Model Development. Journal of the American Water Resources Association, 34(1), pp. 73–89. doi: 10.1111/j.1752-1688.1998.tb05961.x.

Bhattacharya, B., & Solomatine, D. P. (2005). Neural networks and M5 model trees in modelling water level–discharge relationship. Neurocomputing, 63, 381-396.

Brirhet, H. and Benaabidate, L. (2016). Comparison of Two Hydrological Models (Lumped and Distributed) over a Pilot Area of the Issen Watershed in the Souss Basin, Morocco. European Scientific Journal, ESJ, 12(18), p. 347. doi: 10.19044/esj.2016.v12n18p347.

Cornelissen, T., Diekkrüger, B. and Giertz, S. (2013). A Comparison of Hydrological Models for Assessing the Impact of Land Use and Climate Change on Discharge in a Tropical Catchment. Journal of Hydrology, 498, pp.221-236.

Chow, V.T., Maidment, D.R. and Larry, W. (1988). Applied Hydrology. International edition, MacGraw-Hill', Inc, 149.

Elias, S. A. and Alderton, D. (2020). Encyclopedia of geology. 2nd edn. Academic Press. Available at: https://www.elsevier.com/books/encyclopedia-of-geology/elias/978-0-08-102908-4 (Accessed: 24 February 2022).

Gashaw, T., Tulu, T., Argaw, M. and Worqlul, A.W. (2018). Modeling the Hydrological Impacts of Land Use/Land Cover Changes in the Andassa Watershed, Blue Nile Basin, Ethiopia. Science of the Total Environment, 619, pp.1394-1408.

Gupta, H. V., Sorooshian, S. and Yapo, P. O. (1999). Status of Automatic Calibration for Hydrologic Models: Comparison with Multilevel Expert Calibration. Journal of Hydrologic Engineering, 4(2), pp. 135–143. doi: 10.1061/(ASCE)1084-0699(1999)4:2(135).

Harmeling, S. and Harmeling, S. (2008). Global Climate Risk Index 2009 Weather-Related Loss Events and Their Impacts on Countries in 2007 and in a Long-Term Comparison. Available at: http://citeseerx.ist.psu.edu/viewdoc/summary?doi=10.1.1.485.4751 (Accessed: 25 May 2022).

Hossain, M. A., Dipu, H. R. and Jhan, R. K. (2020). Spatial and Temporal Changes of Plankton Assemblages in Atrai River , Bangladesh. International Journal of Fisheries and Aquatic Studies, 8(3), pp. 15–21.

Hydrologic Engineering Center (2000). Hydrologic Modeling System Technical Reference Manual. Hydrologic Modeling System HEC-HMS Technical Reference Manual, (March), p. 148.

IUCN , Protocol for Monitoring of Impacts of Climate Change and Climate Variability in Bangladesh. Available at: https://www.iucn.org/content/protocol-monitoring-impacts-climate-change-and-climate-variability-bangladesh (Accessed: 25 May 2022).

Islam, M. R. and Mia, M. J. (2016). Length–Weight and Length–Length Relationships of Five Fish Species in the Atrai River, Dinajpur, Bangladesh. Journal of Applied Ichthyology, 32(6), pp. 1371–1373. doi: 10.1111/jai.13210.

IWM (2017). Institute of Water Modelling Data Collection and Updating of Regional Models for 2017, NWRM. (June).

Jahan, C.S., Rahaman, M., Arefin, R., Ali, S. and Mazumder, Q.H. (2018). Morphometric Analysis and Hydrological Inference for Water Resource Management in Atrai-Sib River Basin, NW Bangladesh Using Remote Sensing and GIS Technique. Journal of the Geological Society of India, 91(5), pp. 613–620. doi: 10.1007/s12594-018-0912-z.

Khoi and Nguyen, D. (2016). Comparison of the HEC-HMS and SWAT Hydrological Models in Simulating the Stream flow. Vietnam Journal of Science and Technology, 53(5), pp. 189–195.

Khaled, M., Saiful, I.A., Tarekul, I.G., Lorenzo, A., Uddin, K.M.J., Kumar, B.S. and Kumar, D.M. (2018). Future Floods in Bangladesh under 1.5° C, 2° C, and 4° C Global Warming Scenarios. American Society of Civil Engineers.

Khan, I. and Ali, M. (2019). Potential changes to the water balance of the Teesta river basin due to climate change. American Journal of Water Resources, 7(3), pp.95-105.

Kumar, N., Singh, S.K., Singh, V.G. and Dzwairo, B. (2018). Investigation of Impacts of Land Use/Land Cover Change on Water Availability of Tons River Basin, Madhya Pradesh, India. Modeling Earth Systems and Environment, 4(1), pp.295-310.

Lund, J. R., Scheierling, S. M. and Milne, G. (2010). Modeling for Watershed

Management. Journal of Natural Resource Conservation and Management, 1(1, March 25. 2020), pp. 29–34. doi: 10.51396/ANRCM.1.1.2020.29-34.

Moriasi, D.N., Arnold, J.G., Van Liew, M.W., Bingner, R.L., Harmel, R.D. and Veith, T.L. (2007). Model Evaluation Guidelines for Systematic Quantification of Accuracy in Watershed Simulations. Transactions of the ASABE, 50(3), pp. 885–900. doi: 10.13031/2013.23153.

Msrblog (2019). Report on River Morphology of Bangladesh. Available at: http://www.msrblog.com/science/report-on-river-morphology-of-bangladesh-2.html (Accessed: 23 June 2022).

NASA POWER , Docs , Data Services , Daily API - NASA POWER , Docs. Available at: https://power.larc.nasa.gov/docs/services/api/temporal/daily/ (Accessed: 15 June 2022).

NRCS (2010).National Resources Inventory Rangeland Resource Assessment. | Available at:https://www.nrcs.usda.gov/wps/portal/nrcs/detail/national/technical/?cid=stelprdb1041 620 (Accessed: 10 April 2022).

Neitsch, S.L., Arnold, J.G., Kiniry, J.R. and Williams, J.R. (2011). Soil & Water Assessment Tool Theoretical Documentation Version 2009. Texas Water Resources Institute, pp. 1–647. doi: 10.1016/j.scitotenv.2015.11.063.

Nowreen, S., Haque, P., Mondal, M.S. and Zzaman, R.U. (2020). Hydrological Assessment for the Availability of Water for Off-Stream Uses of Atrai-Karatoa River in Bangladesh. Water Policy, 22(1), pp. 70–84. doi: 10.2166/wp.2020.034.

Nishat, B. and Rahman, S.M. (2009). Water Resources Modeling of the Ganges-Brahmaputra-Meghna River Basins Using Satellite Remote Sensing Data. JAWRA Journal of the American Water Resources Association, 45(6), pp.1313-1327.

Quader, M. F. (1995). A Study on Stage-Discharge Relationship of Atrai River. Department of Water Resources Engineering, Bangladesh University of Engineering and Technology, Dhaka.

Raihan, F., Beaumont, L.J., Maina, J., Saiful Islam, A. and Harrison, S.P. (2020). Simulating Streamflow in the Upper Halda Basin of Southeastern Bangladesh Using SWAT Model. Hydrological Sciences Journal, 65(1), pp.138-151.

Rossi, C.G., Dybala, T.J., Moriasi, D.N., Arnold, J.G., Amonett, C.A.R.L. and Marek, T.O.D.D. (2008). Hydrologic Calibration and Validation of the Soil and Water Assessment Tool for the Leon River Watershed. Journal of Soil and Water Conservation, 63(6), pp.533-541.

Sorman, A.A., Emin, T.A.S. and Dogan, Y.O. (2020). Comparison of Hydrological Models in Upper Aras Basin. Pamukkale Üniversitesi Mühendislik Bilimleri Dergisi, 26(6), pp.1015-1022.

Talukdar, G., Swain, J. B. and Patra, K. C. (2021). Flood Inundation Mapping and Hazard Assessment of Baitarani River Basin Using Hydrologic and Hydraulic Model. Natural

Hazards, 109(1), pp. 389–403. doi: 10.1007/S11069-021-04841-3.

Titumir, J. K. B. R. A. M. and Chandra, D. N. (2013). Climate Change in Bangladesh: A Historical Analysis of Temperature and Rainfall Data in Rural Bangladesh View project Climate Change in Bangladesh: A Historical Analysis of Temperature and Rainfall Data. Journal of Environment, 02(January), pp. 41–46. Available at: www.scientific-journals.co.uk.

Tegegne, G., Park, D.K. and Kim, Y.O. (2017). Comparison of Hydrological Models for the Assessment of Water Resources in a Data-Scarce Region, The Upper Blue Nile River Basin. Journal of Hydrology: Regional Studies, 14, pp.49-66.

USDA-NRCS (2010). National Engineering Handbook Chapter 15, Time of Concentration. pp. 1–15.

Venkatesh, B., Chandramohan, T., Purandara, B. K., Jose, M. K., & Nayak, P. C. (2018). Modeling of a River Basin Using SWAT Model. Hydrologic Modeling (pp. 707-714). Springer, Singapore.

Vo, N. D., Nguyen, Q. B., Le, C. H., Doan, T. D., Le, V. H., & Gourbesville, P. (2018). Comparing Model Effectiveness on Simulating Catchment Hydrological Regime. Advances in Hydroinformatics (pp. 401-414). Springer, Singapore.

Watson, B. M., McKeown, R. A., Putz, G., & MacDonald, J. D. (2008). Modification of SWAT for Modelling Streamflow from Forested Watersheds on the Canadian Boreal Plain. Journal of Environmental Engineering and Science, 7(S1), 145-159. doi: 10.1139/S09-003.

Yilmaz, K. K., Vrugt, J. A., Gupta, H. V., & Sorooshian, S. (2010). Model calibration in watershed hydrology. Advances in Data-Based Approaches for Hydrologic Modeling and Forecasting, pp. 53–105. doi: 10.1142/9789814307987_0003.

APPENDIX-A
(Precipitation, Temperature and
Relative Humidity plot)

Precipitation

Tentulia (R220)
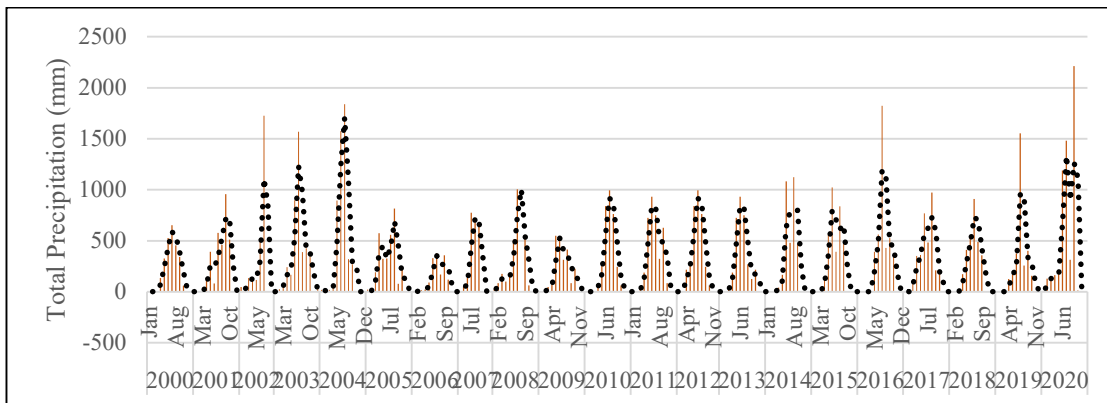
(a) Annual monthly precipitation
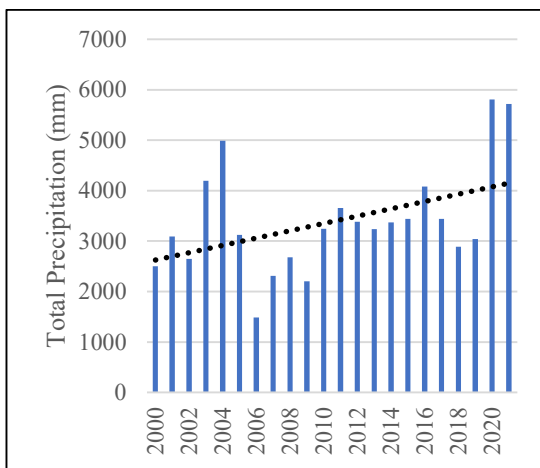
(b) Total Annual precipitation
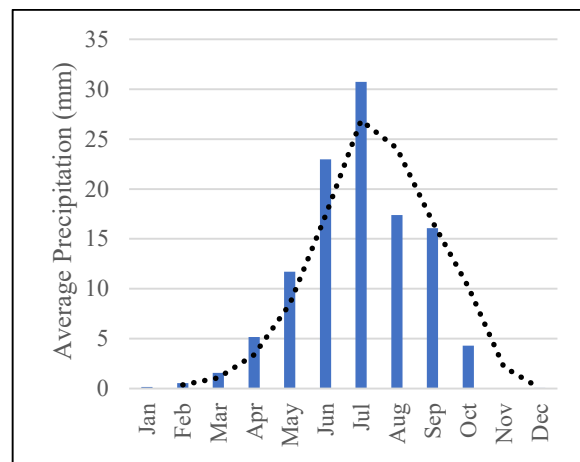
(c) Average monthly precipitation

Figure A 1: Annual and Monthly precipitation analysis at Tentulia (R220) station from 2000 to 2021
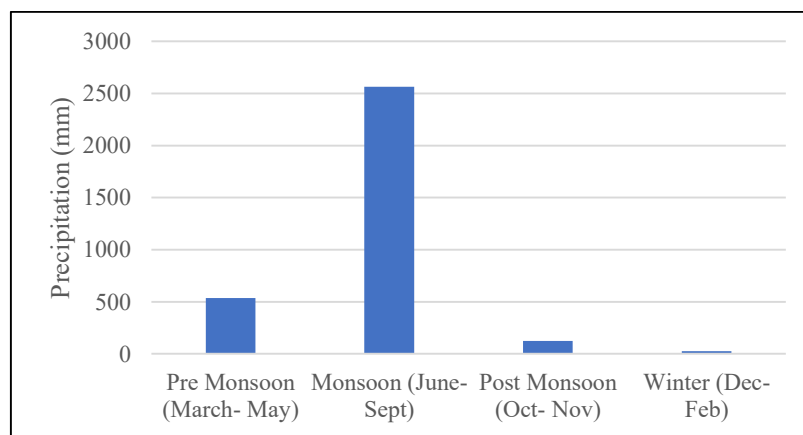
(a) Annual Seasonal Precipitation chart
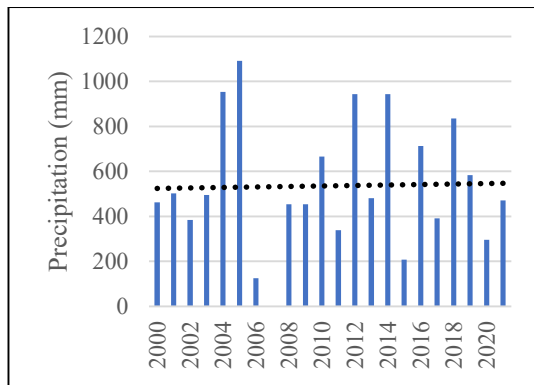
(b) Annual Pre-Monsoon
Precipitation chart
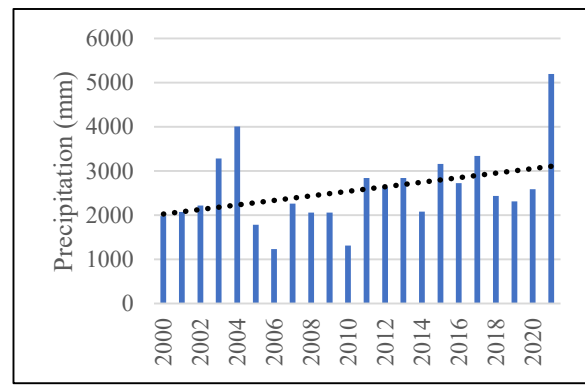
(c) Annual Monsoon Precipitation chart
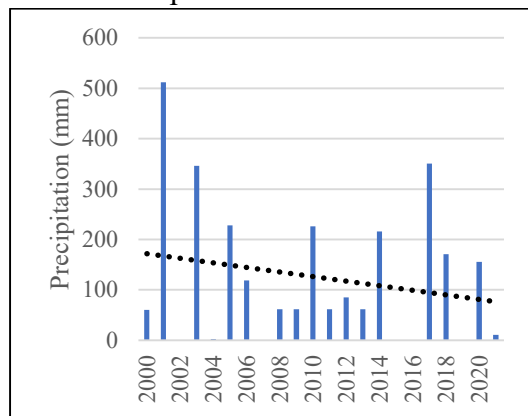
(d) Annual Post-Monsoon
Precipitation chart
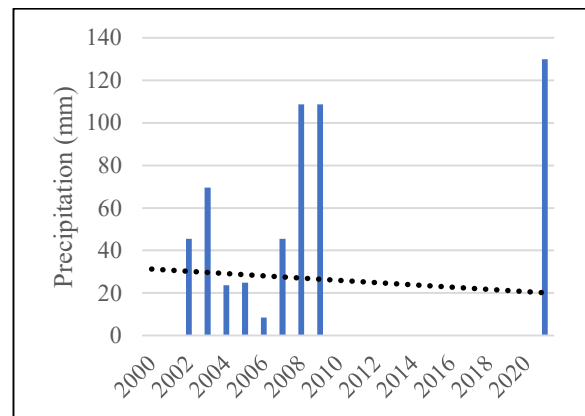
(e) Annual Winter Precipitation chart

Figure A 2: Seasonal precipitation analysis at Tentulia (R220) station from 2000 to 2021

Debiganj (R166)
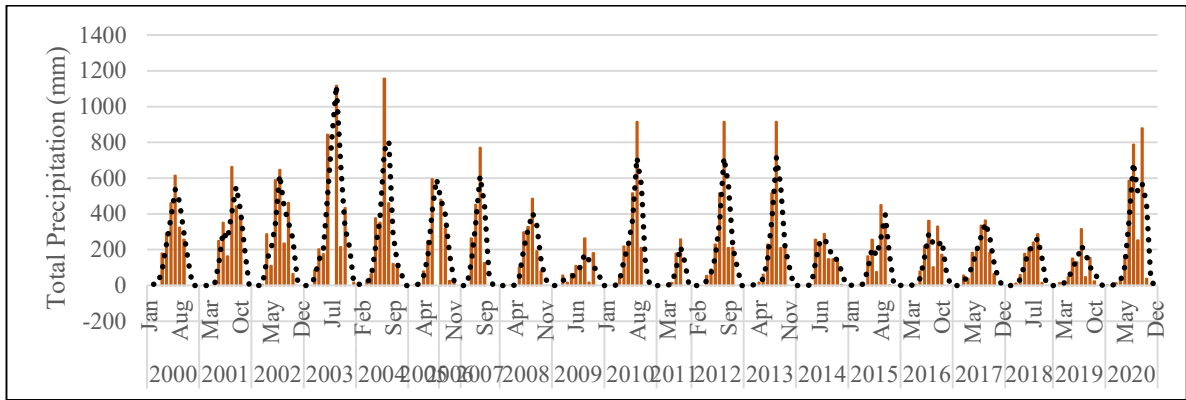
(d) Annual monthly precipitation
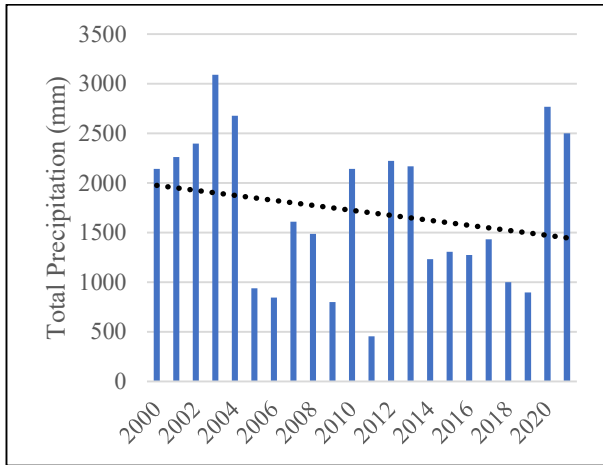
(e) Total Annual precipitation
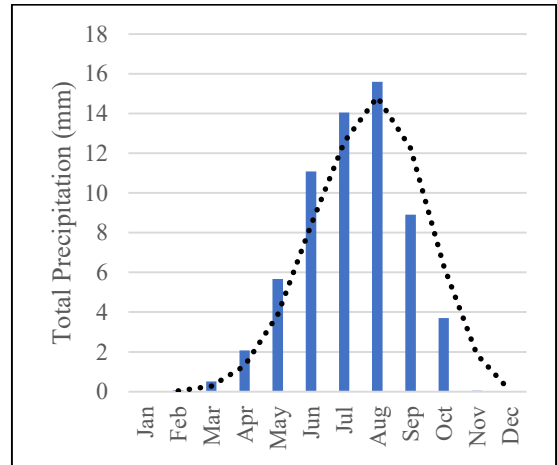
(f) Average monthly precipitation

Figure A 3: Annual and Monthly precipitation analysis at Debiganj (R166) station
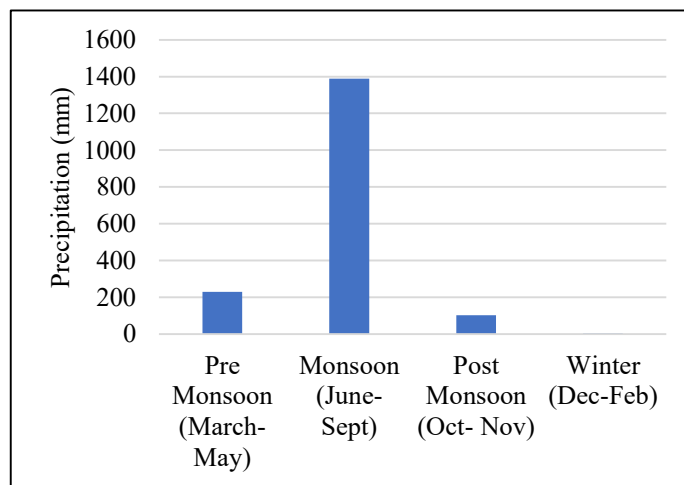
(a) Annual Seasonal Precipitation chart
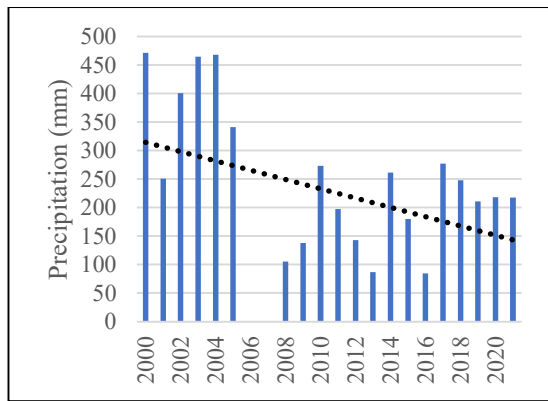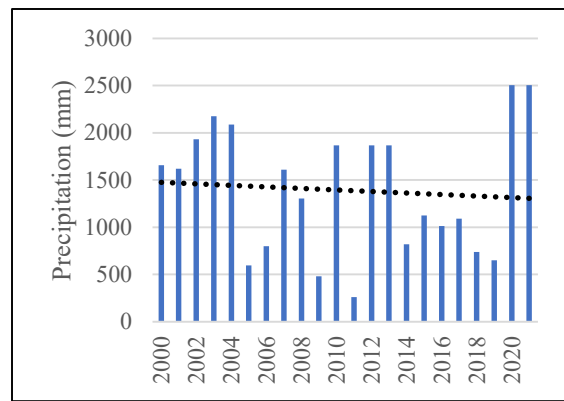
(b) Annual Pre-Monsoon
Precipitation chart

(c) Annual Monsoon Precipitation chart
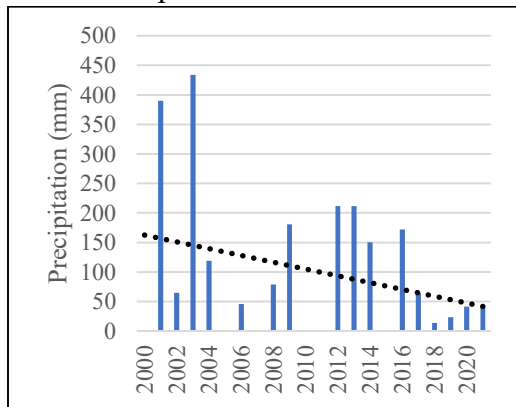
(d) Annual Post-Monsoon
Precipitation chart
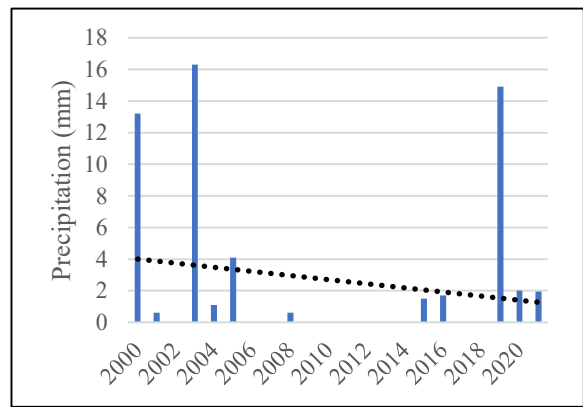
(e) Annual Winter Precipitation chart

Figure A 4: Seasonal precipitation analysis at Debiganj (R166) station from 2000 to 2021

Kantanagar (R180)
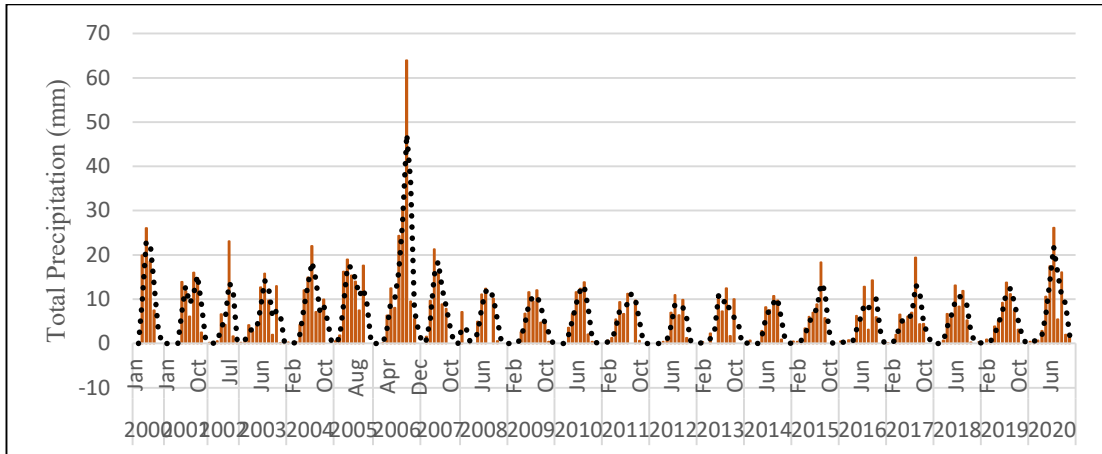
(a) Annual monthly precipitation
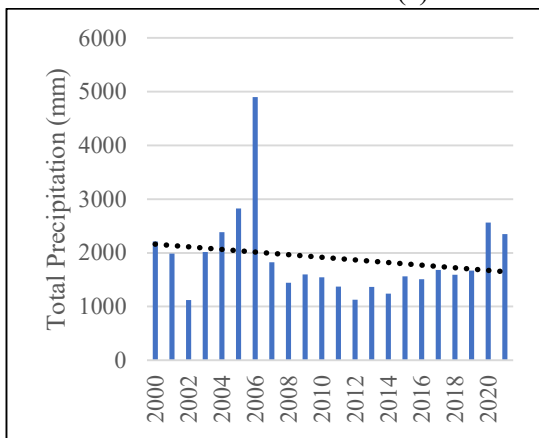
(b) Total Annual precipitation
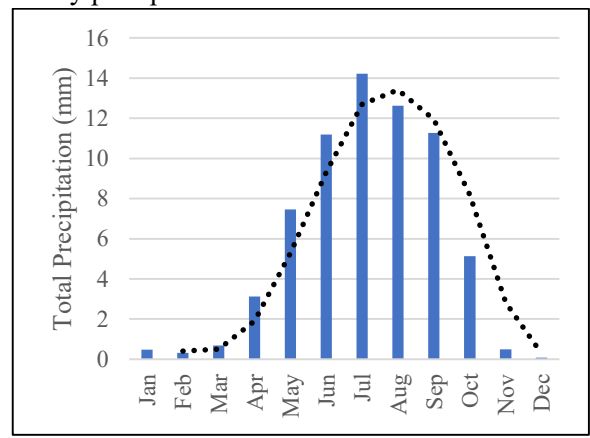
(c) Average monthly precipitation

Figure A 5: Annual and Monthly precipitation analysis at Kantanagar (R180) station from 2000 to 2021
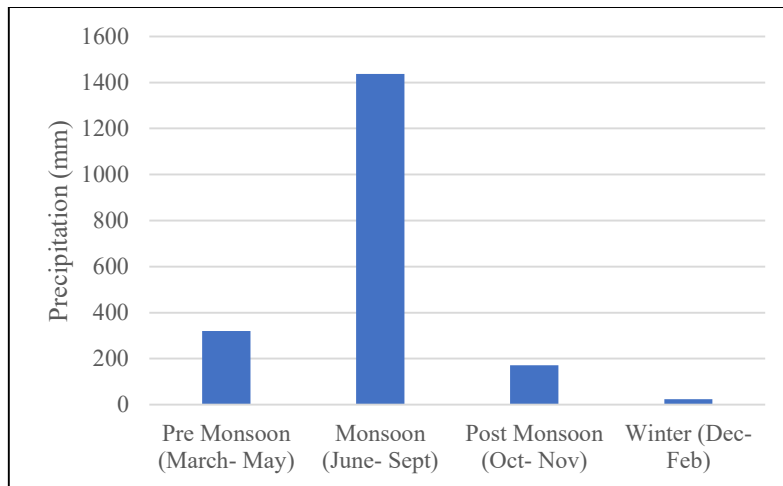
(a) Annual Seasonal Precipitation chart
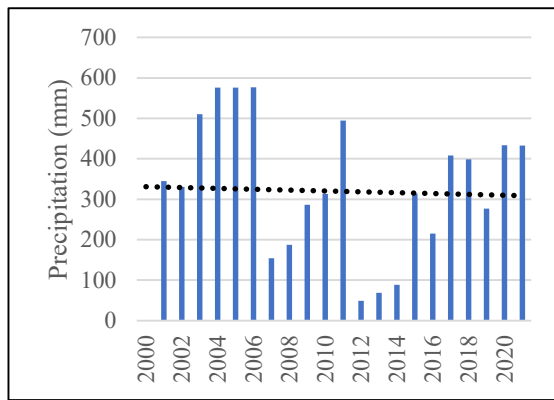
(b) Annual Pre-Monsoon
Precipitation chart
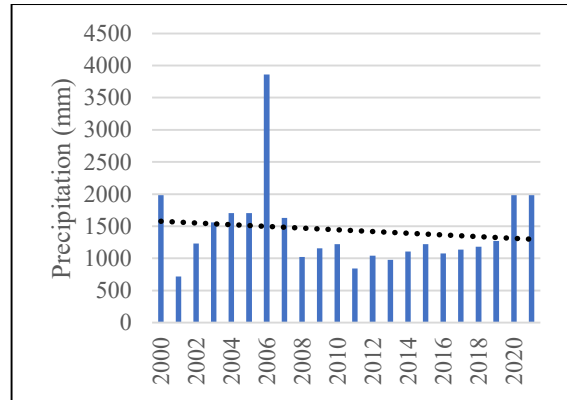
(c) Annual Monsoon Precipitation
chart
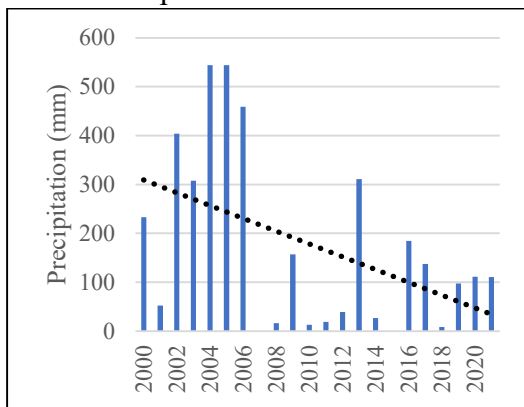
(d) Annual Post-Monsoon
Precipitation chart
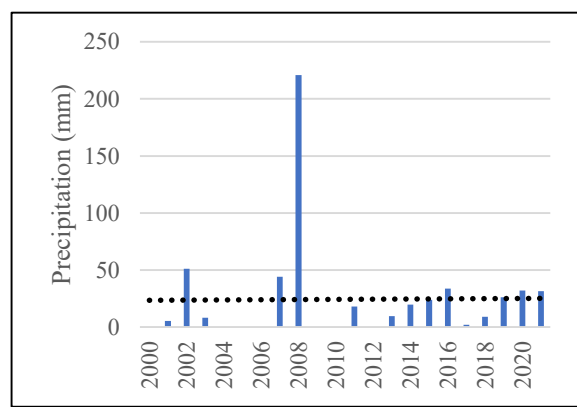
(e) Annual Winter Precipitation chart

Figure A 6: Seasonal precipitation analysis at Kantanagar (R180) station from 2000 to 2021

Hilli (R175)
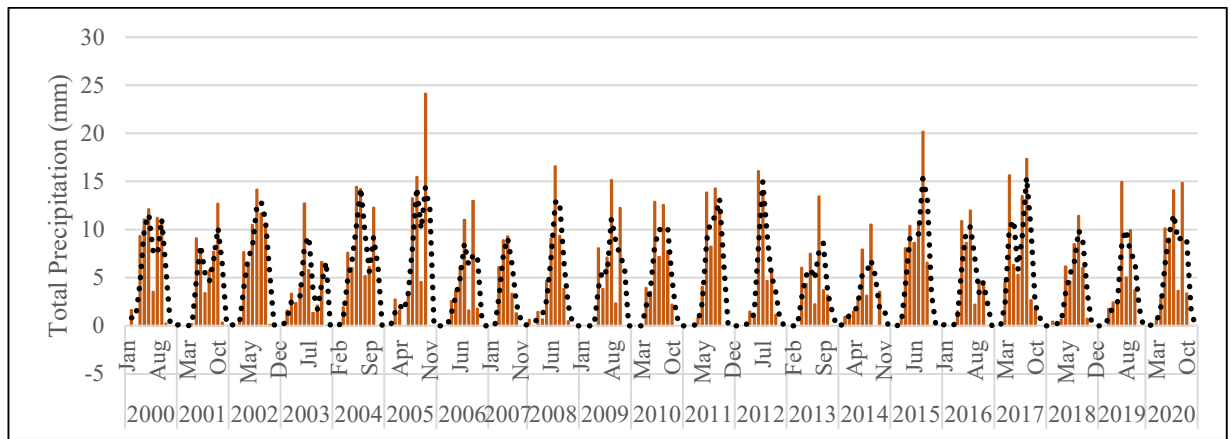
(a) Annual monthly precipitation
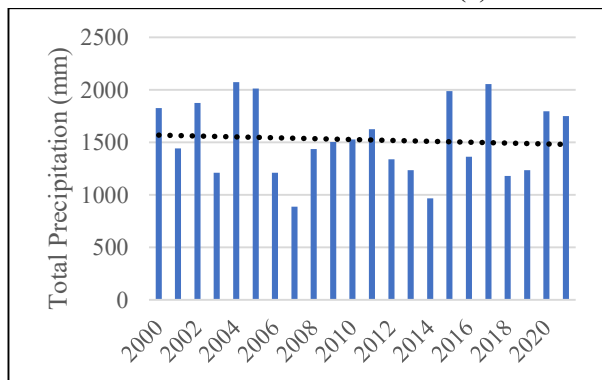
(b) Total Annual precipitation
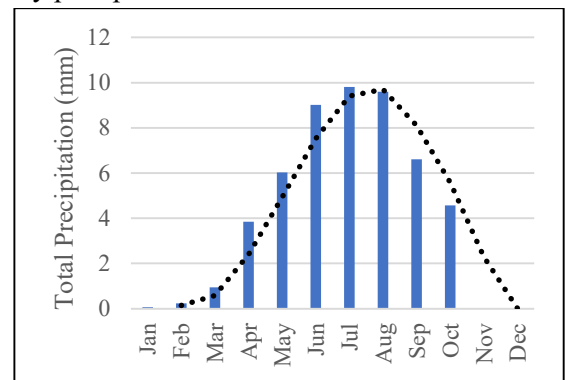
(c) Average monthly precipitation

Figure A 7: Annual and Monthly precipitation analysis at Hilli (R175) station from 2000 to 2021
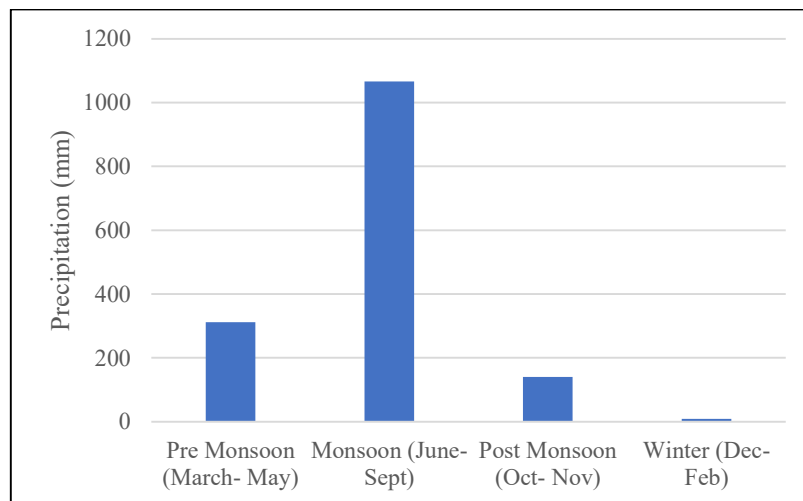
(a) Annual Seasonal Precipitation chart
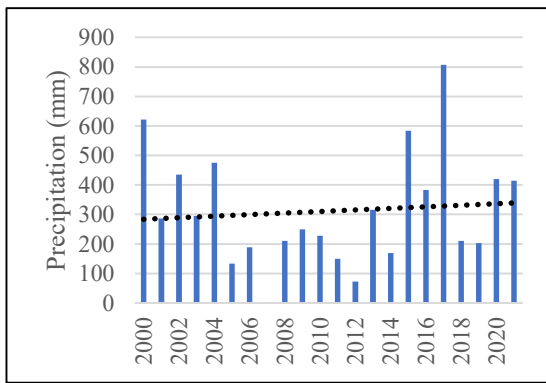
(b) Annual Pre-Monsoon
Precipitation chart
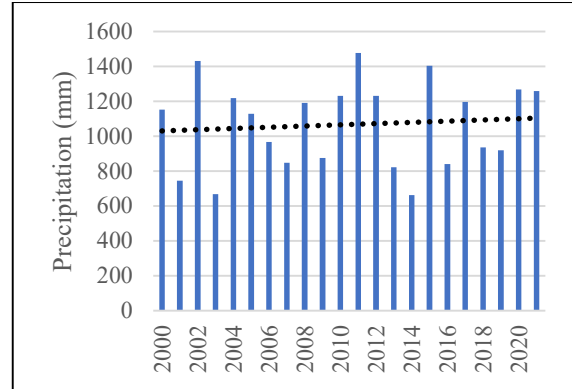
(c) Annual Monsoon Precipitation
chart
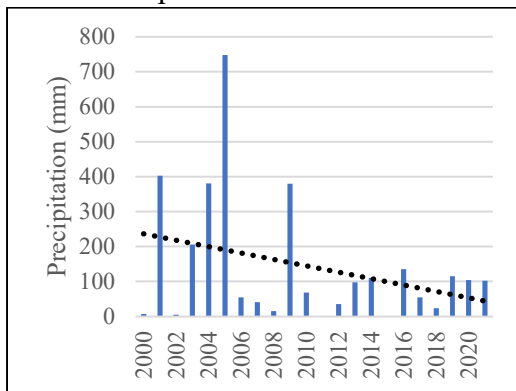
(d) Annual Post-Monsoon
Precipitation chart
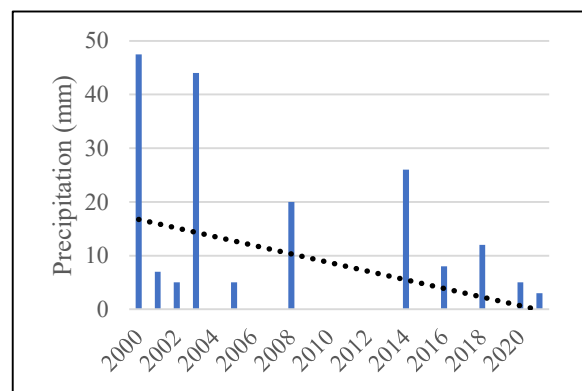
(e) Annual Winter Precipitation chart

Figure A 8: Seasonal precipitation analysis at Hilli (R175) station from 2000 to 2021

Manda (R185)
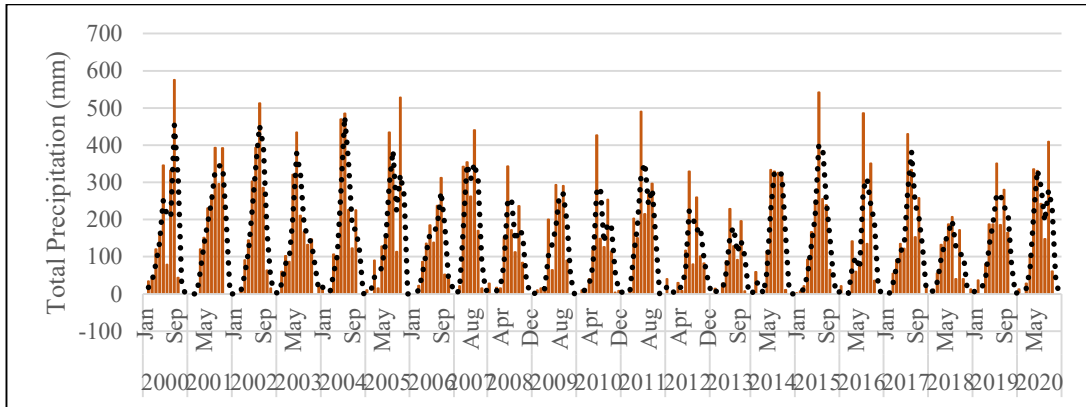
(a) Annual monthly precipitation
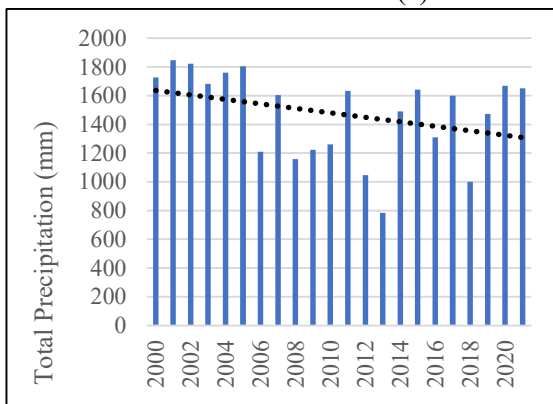
(b) Total Annual precipitation
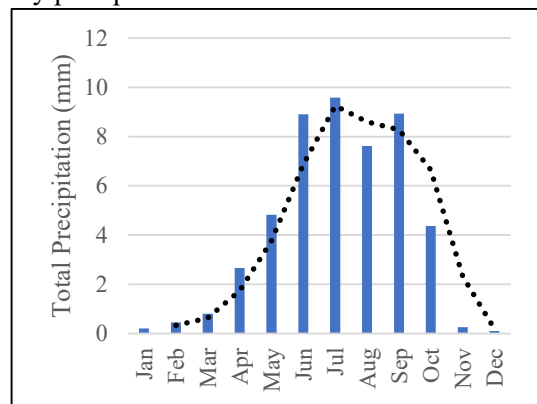
(c) Average monthly precipitation

Figure A 9: Annual and Monthly precipitation analysis at Manda (R185) station from 2000 to 2021
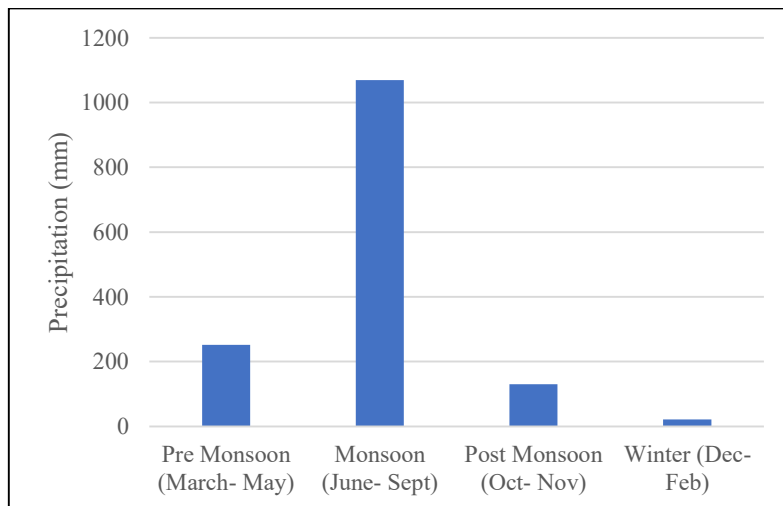
(a) Annual Seasonal Precipitation chart
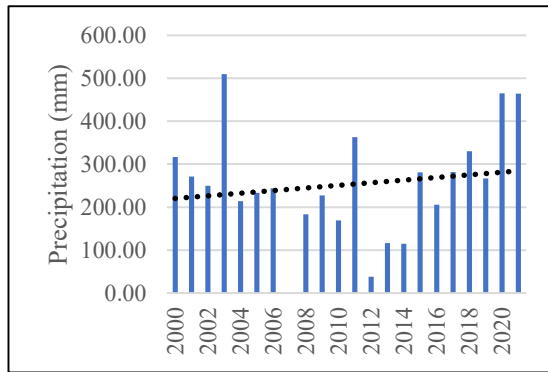
(b) Annual Pre-Monsoon
Precipitation chart
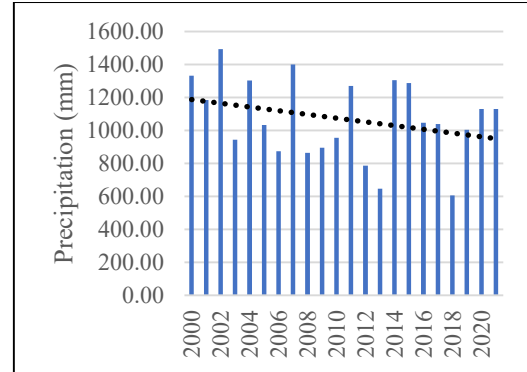
(c) Annual Monsoon Precipitation
chart
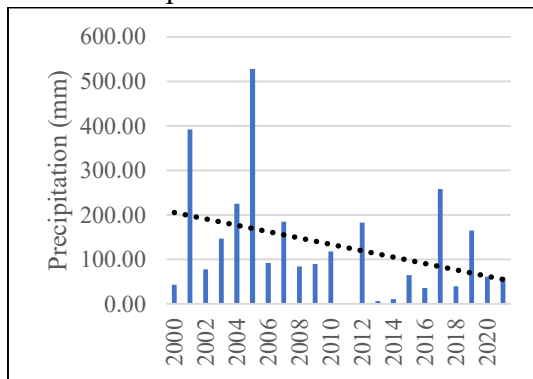
(d) Annual Post-Monsoon
Precipitation chart
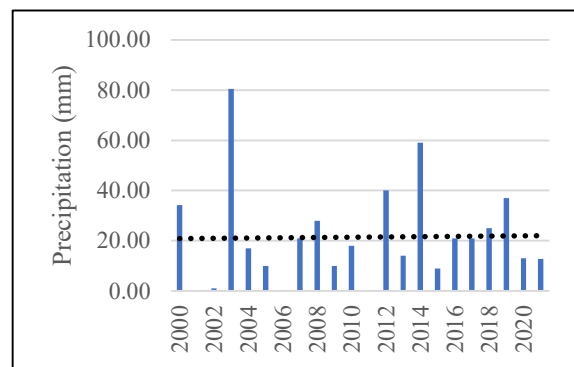
(e) Annual Winter Precipitation chart

Figure A 10: Seasonal precipitation analysis at Manda (R185) station from 2000 to 2021
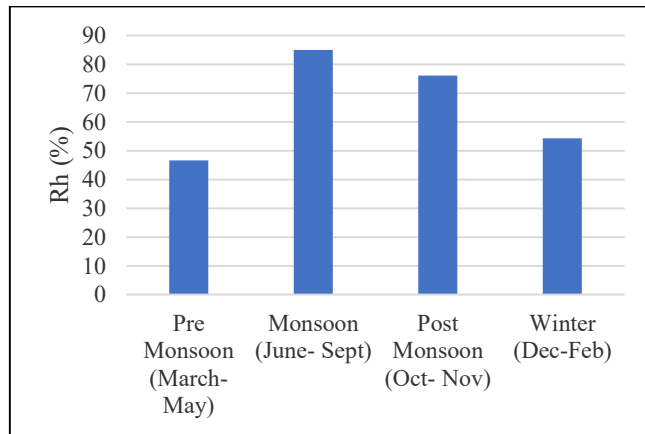
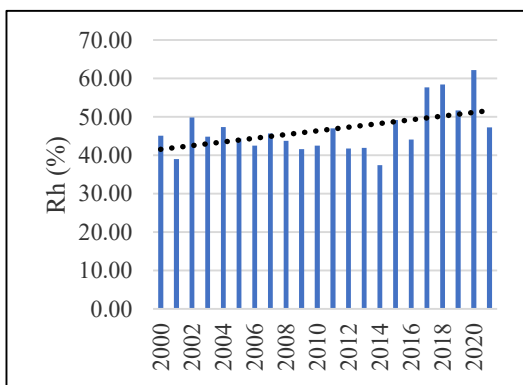# Temperature

Grid-1
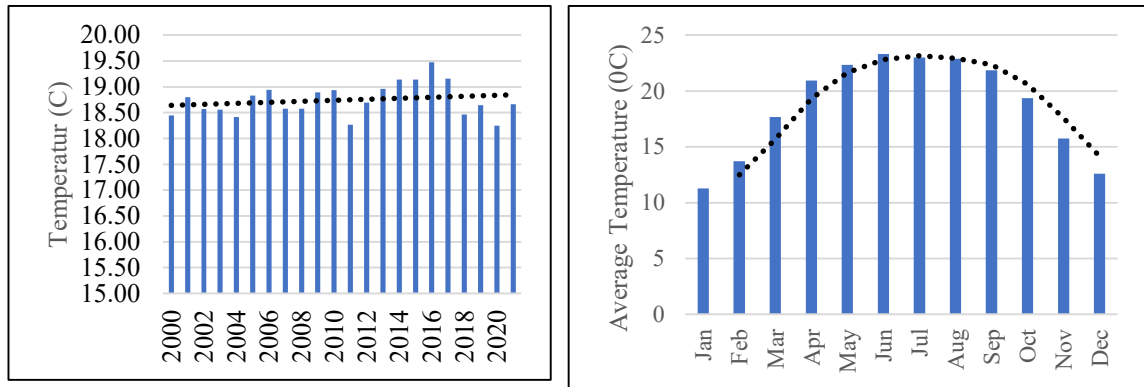
(a) Average Annual Temperature

(b) Average monthly Temperature

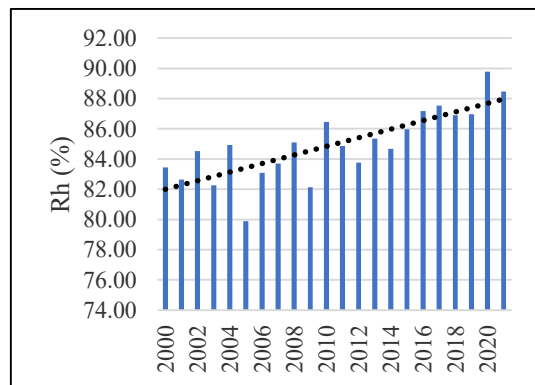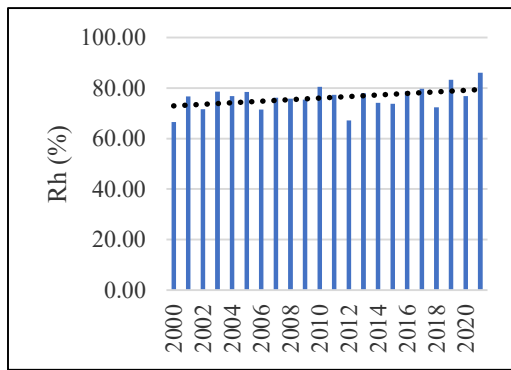**Figure A 11:** Annual and Monthly Temperature analysis at Grid-1 from 2000 to 2021
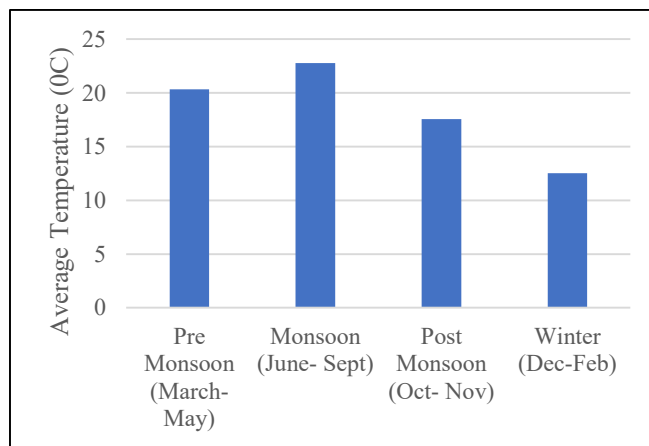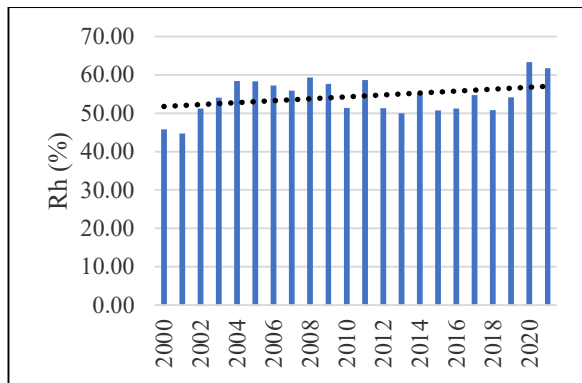

(a) Annual Seasonal Temperature chart
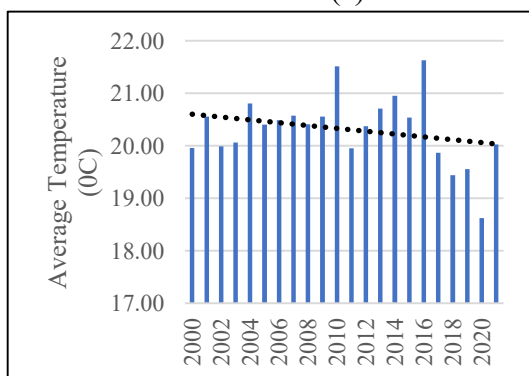
(b) Annual Pre-Monsoon Temperature chart
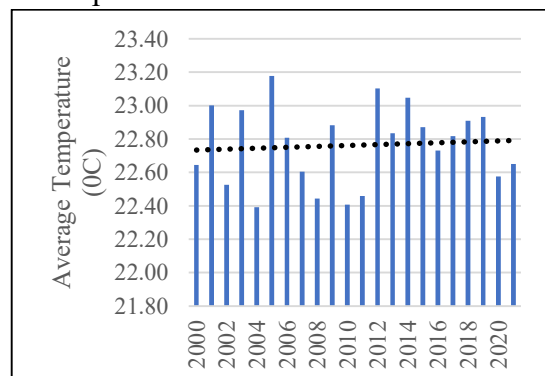
(c) Annual Monsoon Temperature chart
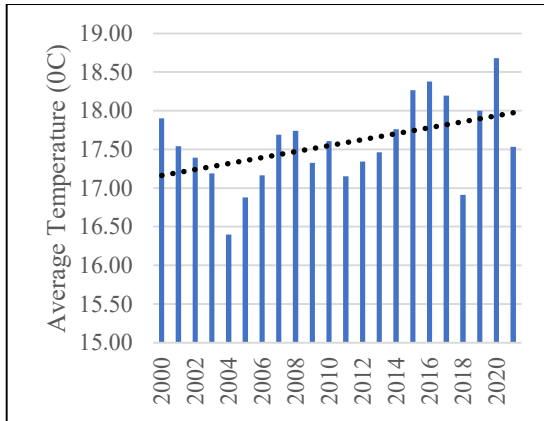
(d) Annual Post-Monsoon
Temperature chart
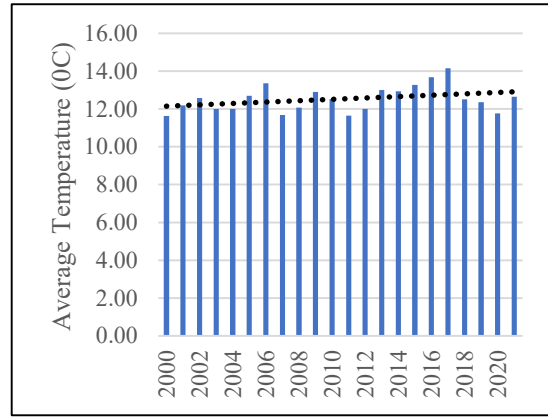
(e) Annual Winter Temperature chart

Figure A 12: Seasonal Temperature analysis at Grid-1 from 2000 to 2021
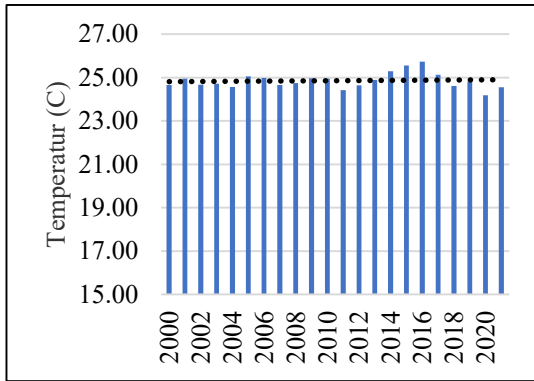
Grid-2

(a) Average Annual Temperature
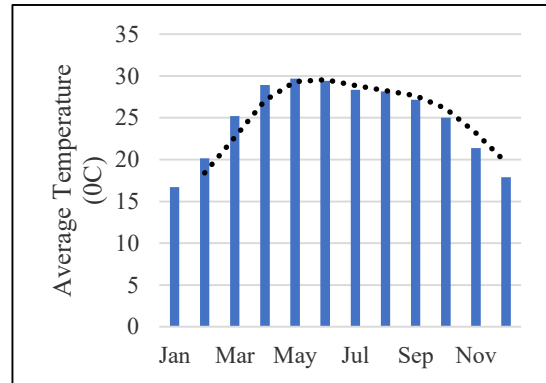
(b) Average monthly Temperature

Figure A 13: Annual and Monthly Temperature analysis at Grid-2 from 2000 to 2021
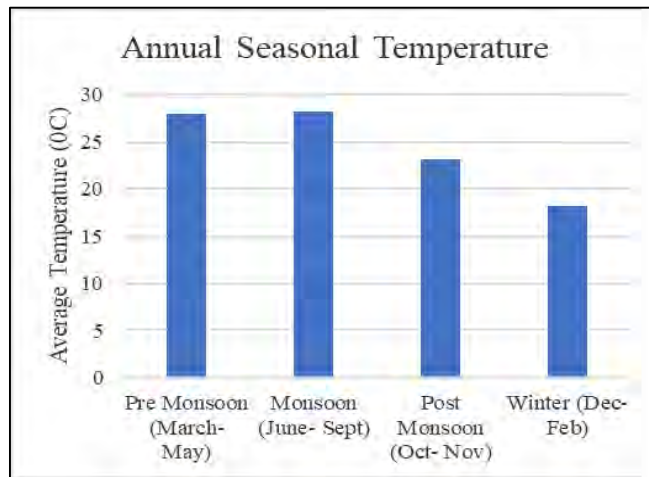
(a) Annual Seasonal Temperature chart
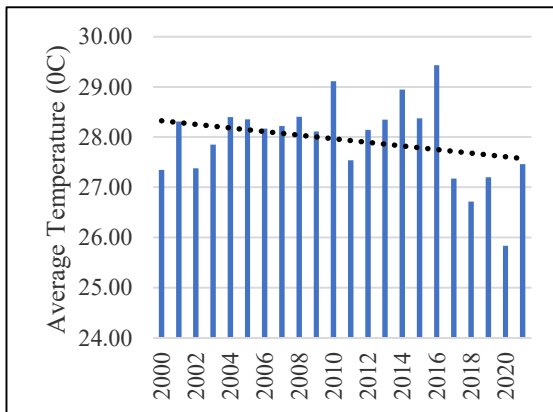
(b) Annual Pre-Monsoon Temperature chart
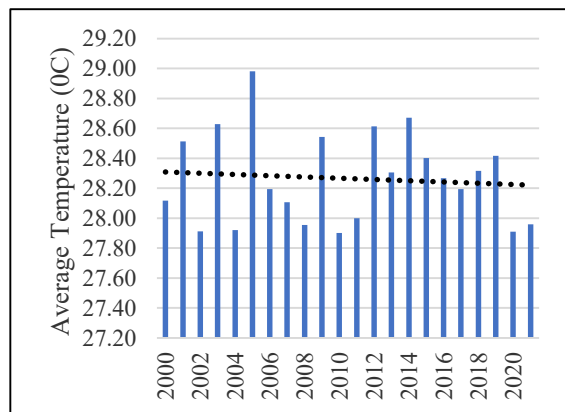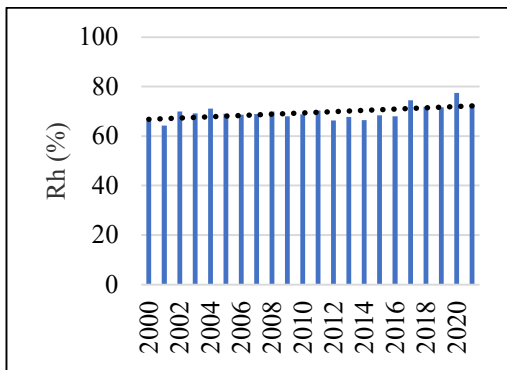

(c) Annual Monsoon Temperature chart
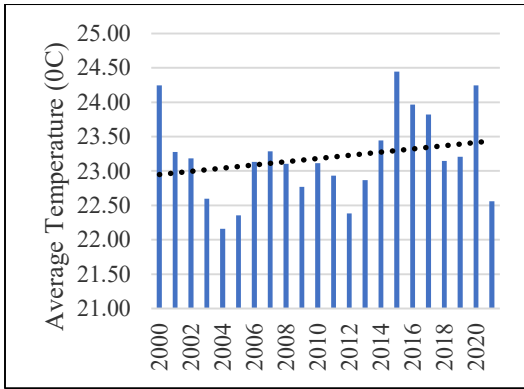
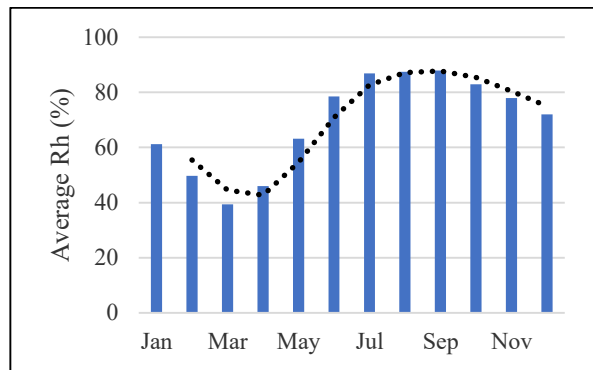(d) Annual Post-Monsoon
Temperature chart
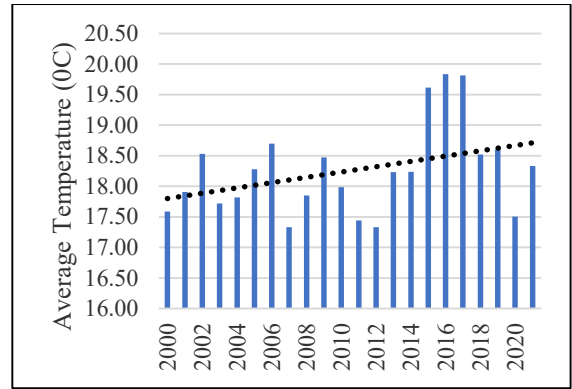
(e) Annual Winter Temperature chart

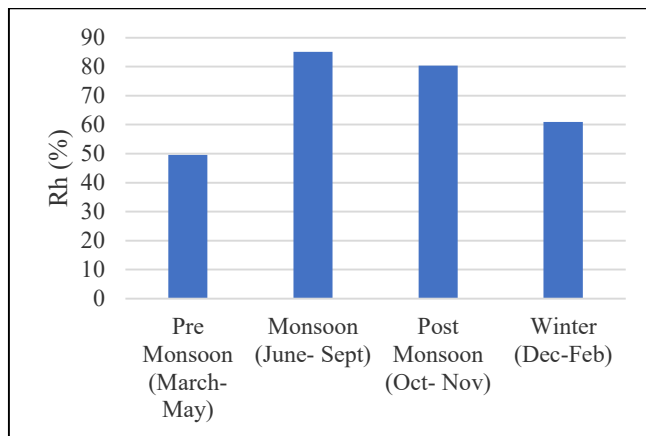**Figure A 14:** Seasonal Temperature analysis at Grid-2 from 2000 to 2021
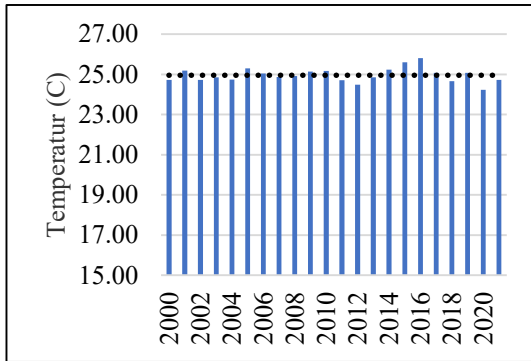
Grid-3

(a) Average Annual Temperature
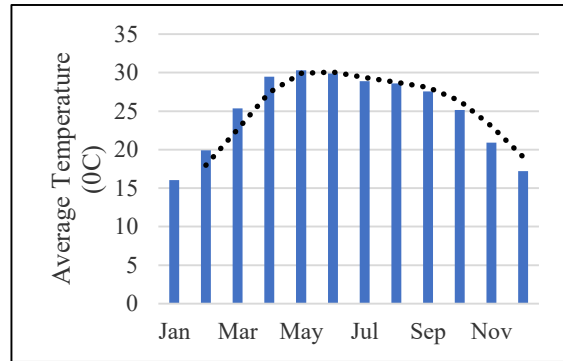
(b) Average monthly Temperature

Figure A 15: Annual and Monthly Temperature analysis at Grid 3 from 2000 to 2021
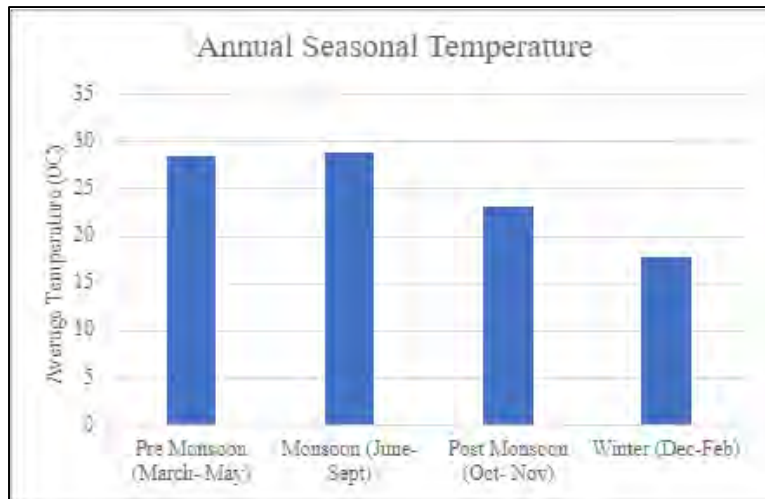
(a) Annual Seasonal Temperature chart
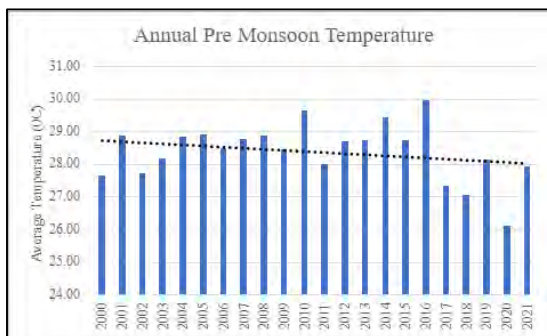
(b) Annual Pre-Monsoon Temperature chart
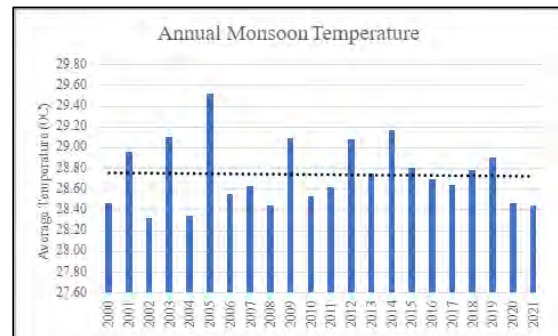
(c) Annual Monsoon Temperature chart
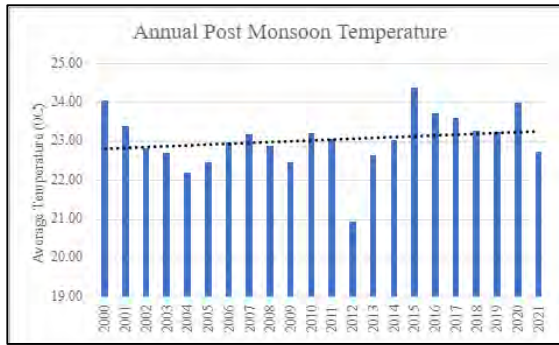
(d) Annual Post-Monsoon
Temperature chart
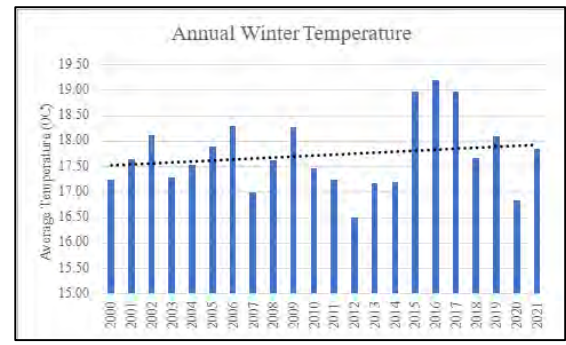
(e) Annual Winter Temperature chart

Figure A 16: Seasonal Temperature analysis at Grid-3 from 2000 to 2021
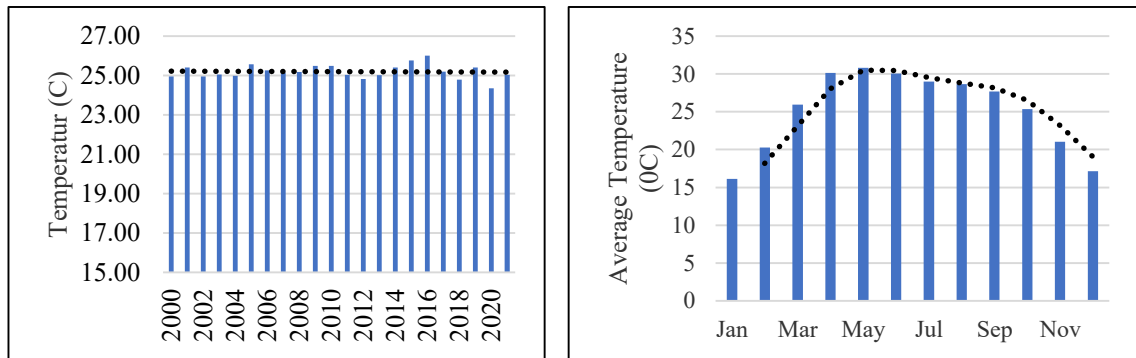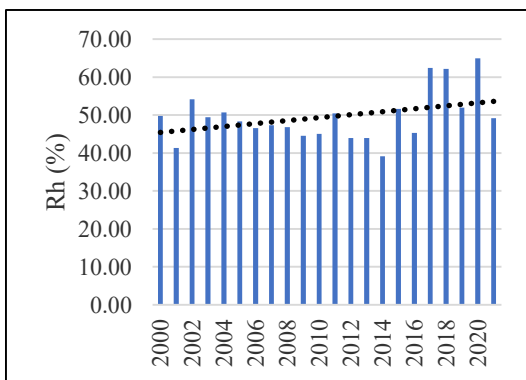
Grid-4

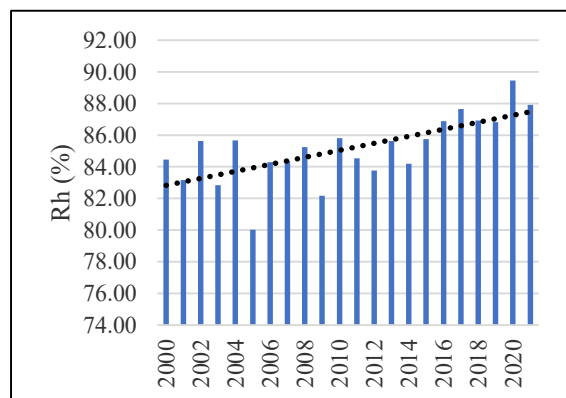(a) Average Annual Temperature

(b) Average monthly Temperature

Figure A 17: Annual and Monthly Temperature analysis at Grid-4 from 2000 to 2021
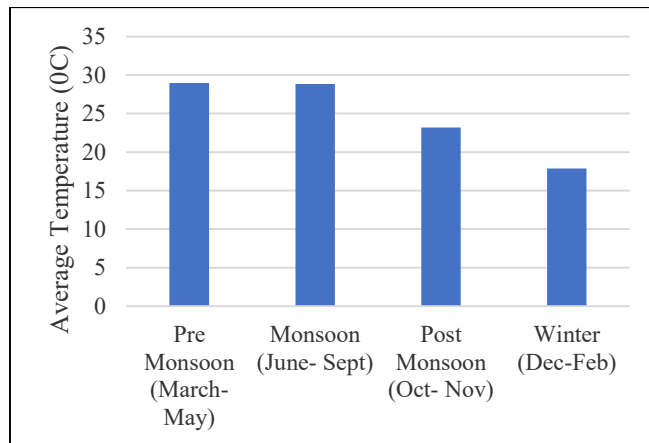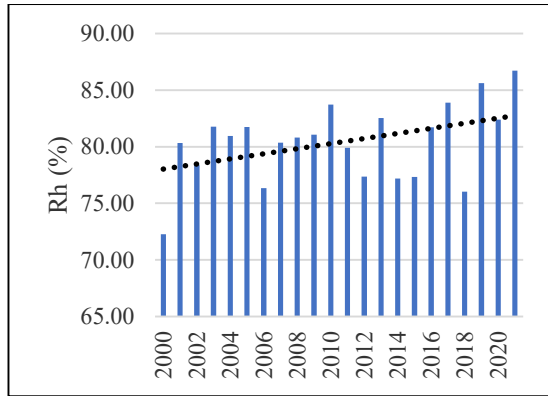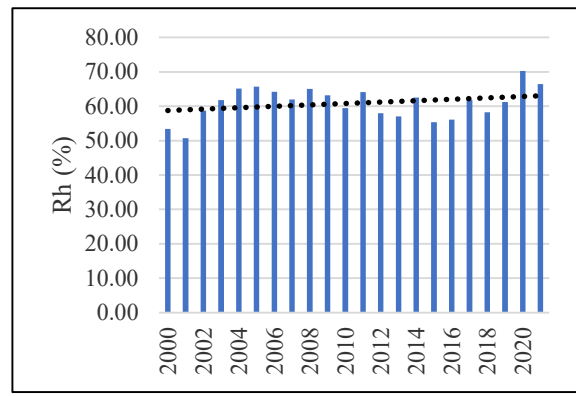

(a) Annual Seasonal Temperature chart
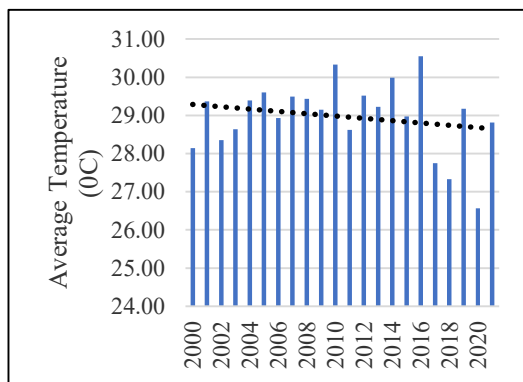
(b) Annual Pre-Monsoon Temperature chart
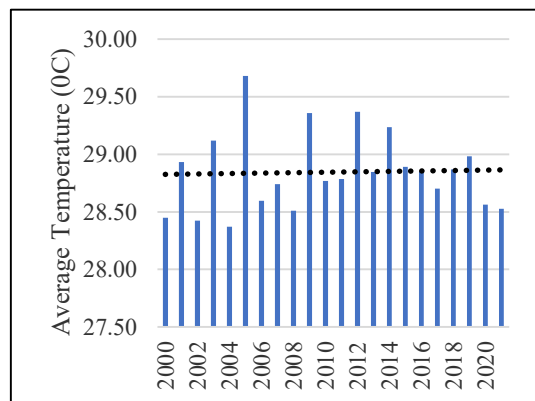
(c) Annual Monsoon Temperature chart
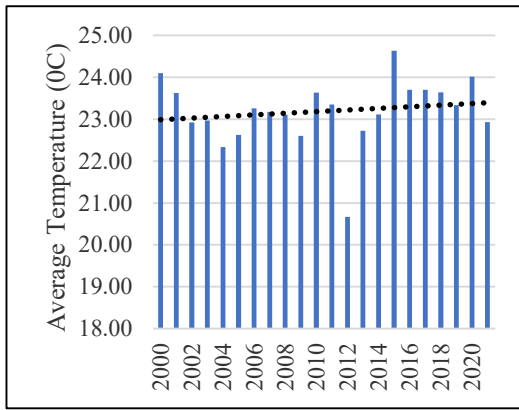
(d) Annual Post-Monsoon
Temperature chart
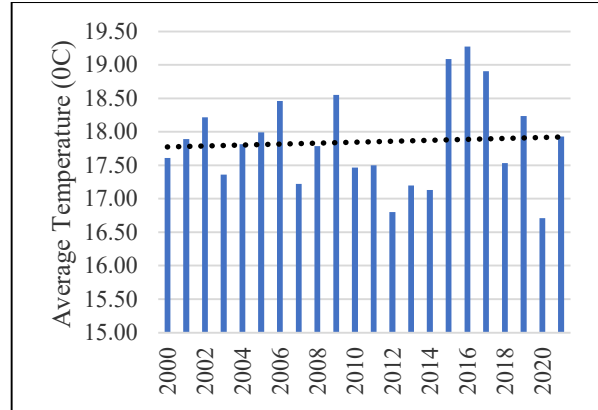
(e) Annual Winter Temperature chart

Figure A 18: Seasonal Temperature analysis at Grid-4 from 2000 to 2021
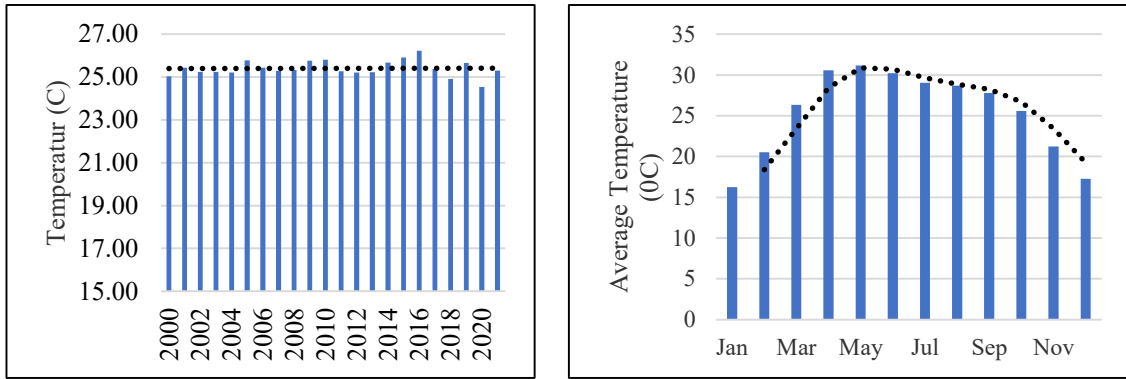
Grid-5

(a) Average Annual Temperature

(b) Average monthly Temperature

Figure A 19: Annual and Monthly Temperature analysis at Grid-5 from 2000 to 2021
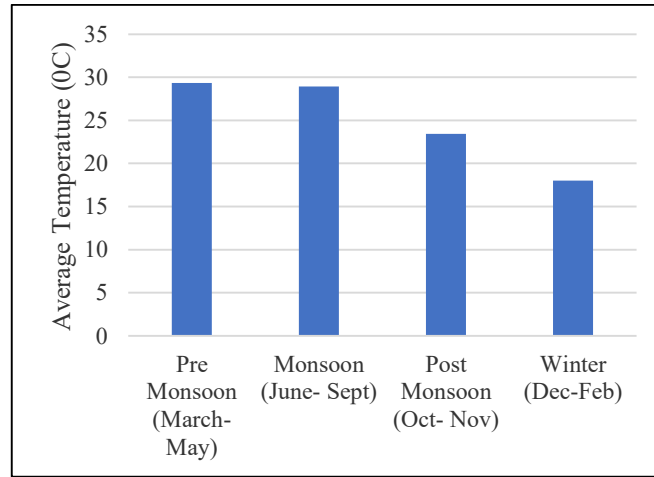
(a) Annual Seasonal Temperature chart
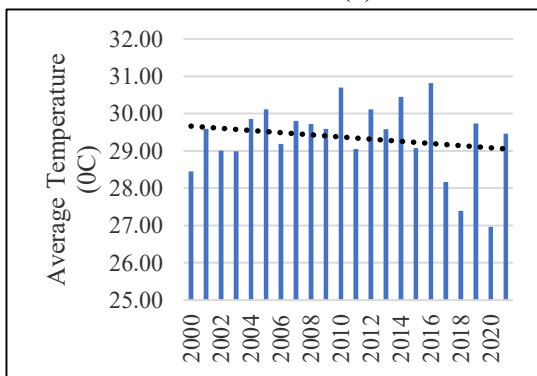
(b) Annual Pre-Monsoon Temperature chart
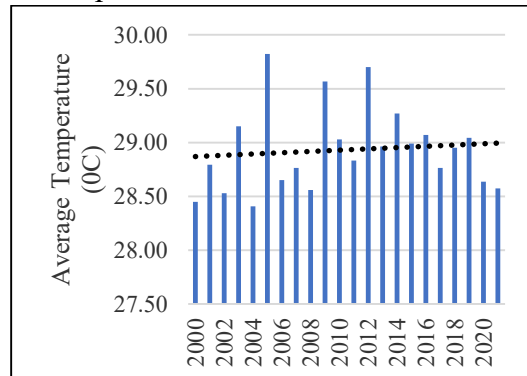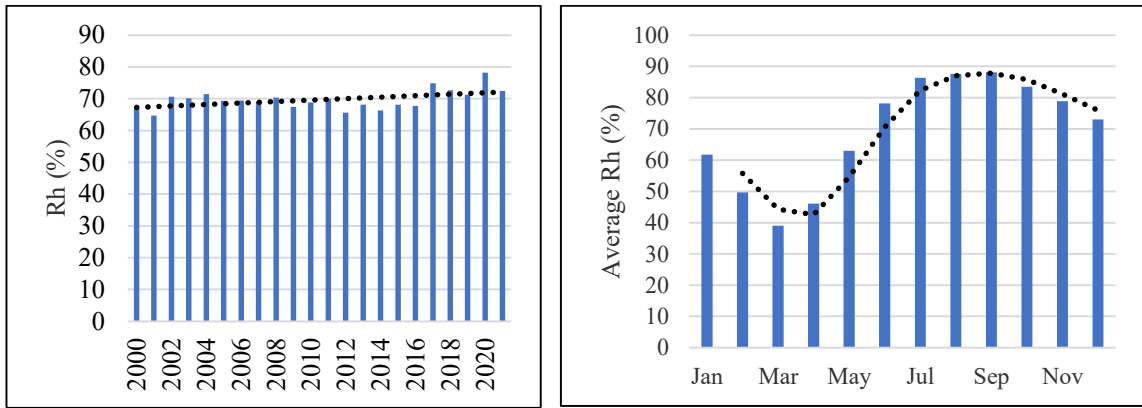
(c) Annual Monsoon Temperature chart
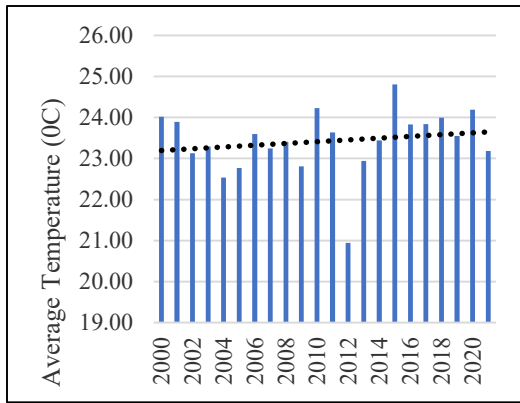
(d) Annual Post-Monsoon
Temperature chart
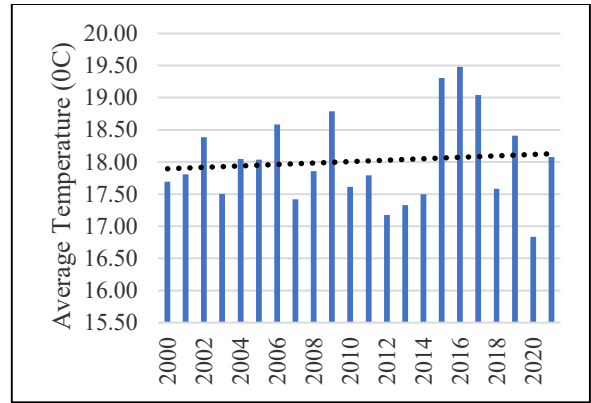
(e) Annual Winter Temperature chart

Figure A 20: Seasonal Temperature analysis at Grid-5 from 2000 to 2021
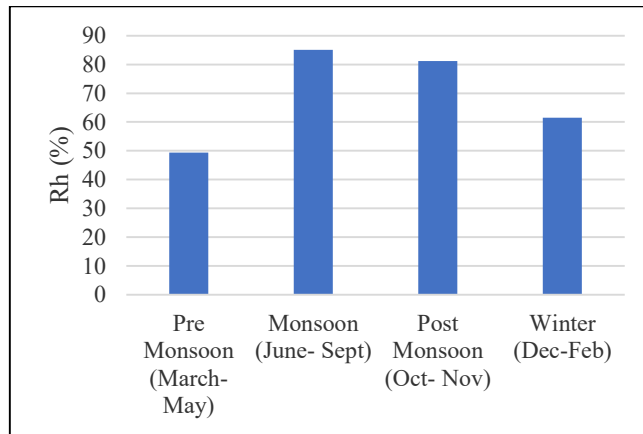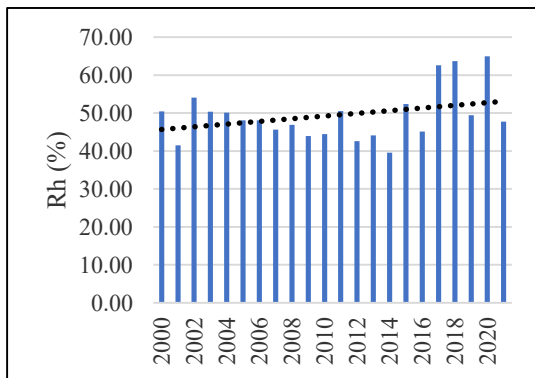
Relative Humidity

Grid-1
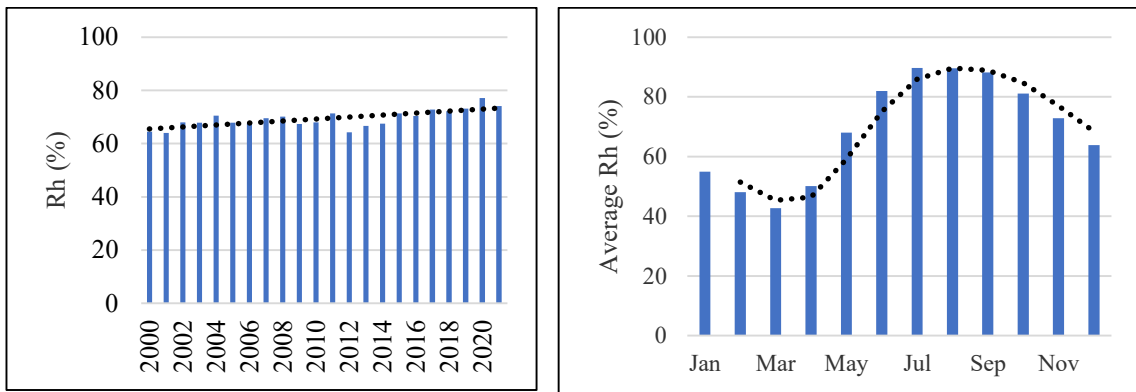
(a) Average Annual Temperature

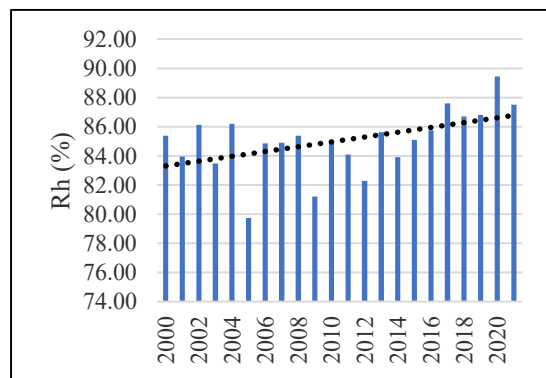(b) Average monthly Temperature

Figure A 21: Annual and Monthly Relative Humidity analysis at Grid-1 from 2000 to 2021
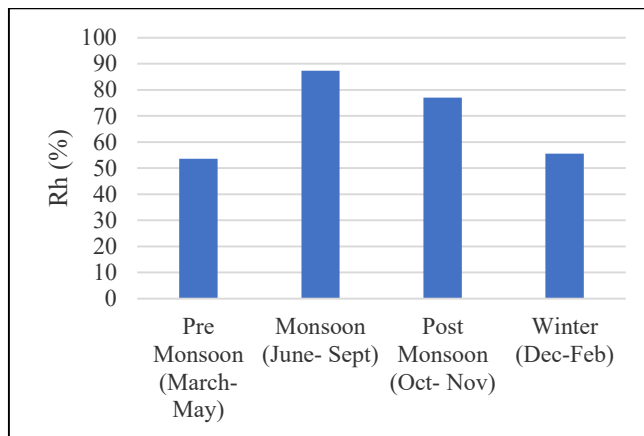
(a) Annual Seasonal Temperature chart
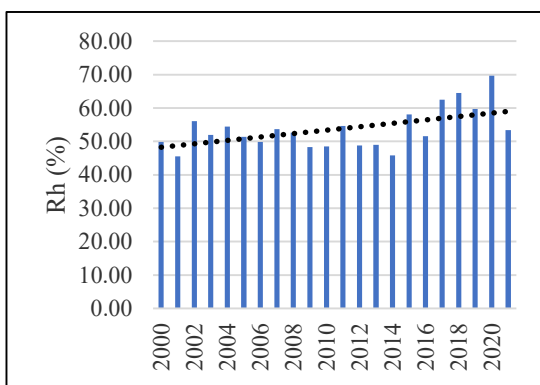
(b) Annual Pre-Monsoon Temperature chart
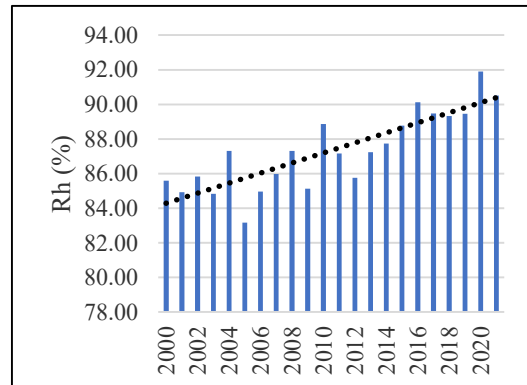
(c) Annual Monsoon Temperature chart
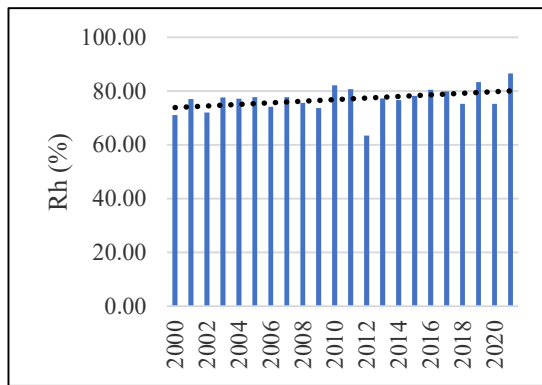
(d) Annual Post-Monsoon
Temperature chart
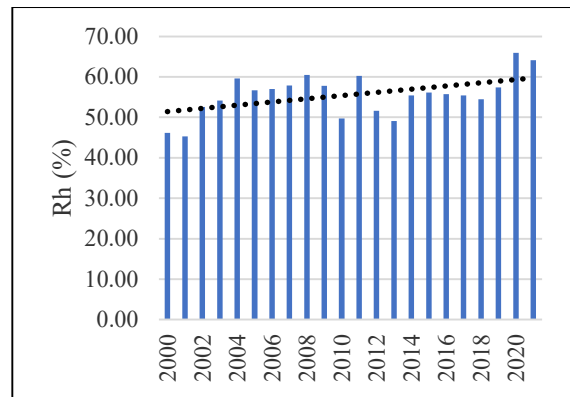
(e) Annual Winter Temperature chart

Figure A 22: Seasonal Relative Humidity analysis at Grid-1 from 2000 to 2021
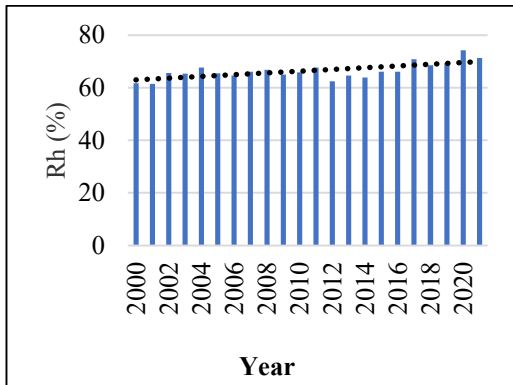
Grid-2

(c) Average Annual Temperature
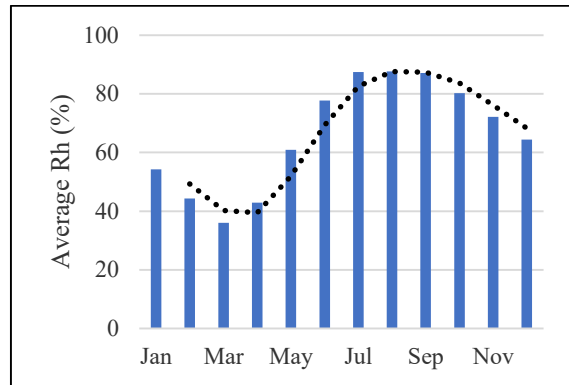
(d) Average monthly Temperature

Figure A 23: Annual and Monthly Relative Humidity analysis at Grid-2 from 2000 to 2021
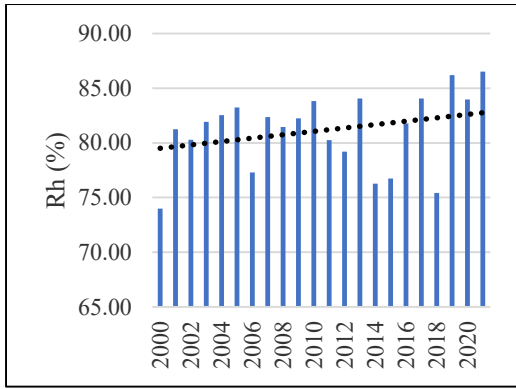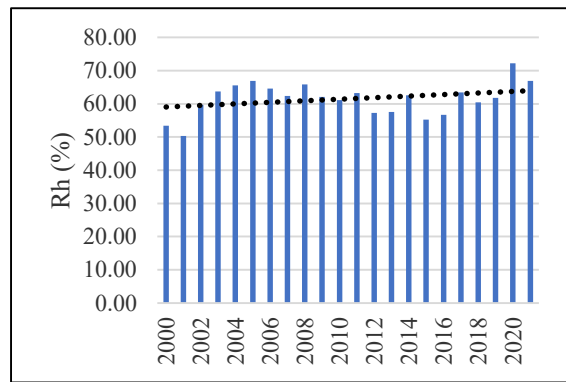

(f) Annual Seasonal Temperature chart

(g) Annual Pre-Monsoon Temperature chart

(h) Annual Monsoon Temperature chart

(i) Annual Post-Monsoon
Temperature chart

(j) Annual Winter Temperature chart

Figure A 24: Seasonal Relative Humidity analysis at Grid-2 from 2000 to 2021

Grid-3

(a) Average Annual Temperature

(b) Average monthly Temperature

Figure A 25: Annual and Monthly Relative Humidity analysis at Grid-3 from 2000 to 2021

(a) Annual Seasonal Temperature chart

(b) Annual Pre-Monsoon Temperature chart
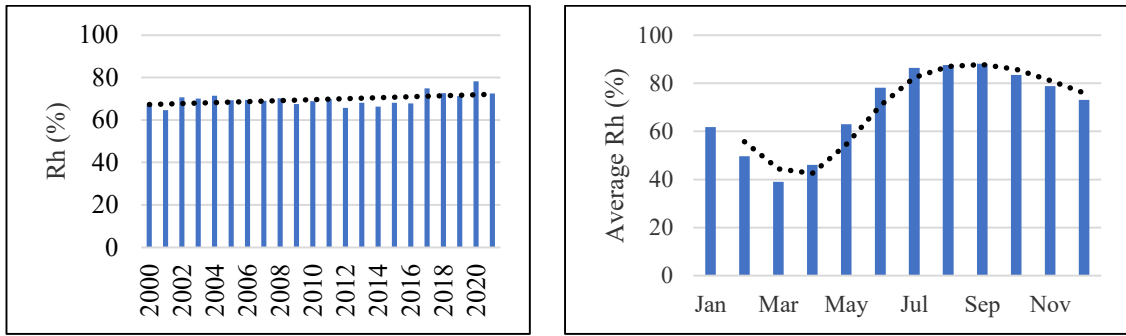

(c) Annual Monsoon Temperature chart

111

(d) Annual Post-Monsoon
Temperature chart

(e) Annual Winter Temperature chart

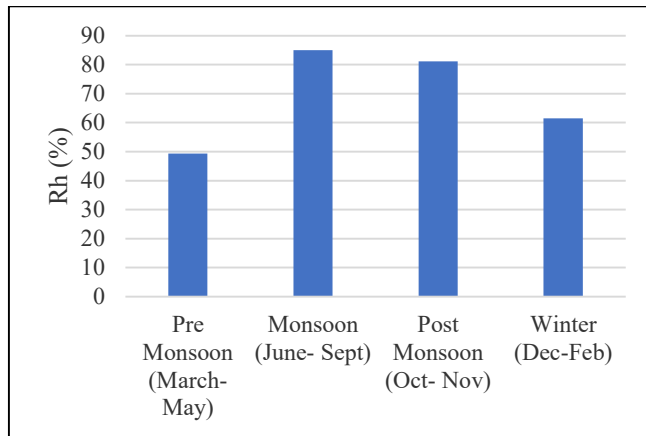**Figure A 26:** Seasonal Relative Humidity analysis at Grid-3 from 2000 to 2021

Grid-4

(a) Average Annual Temperature

(b) Average monthly Temperature

Figure A 27: Annual and Monthly Relative Humidity analysis at Grid-4 from 2000 to 2021
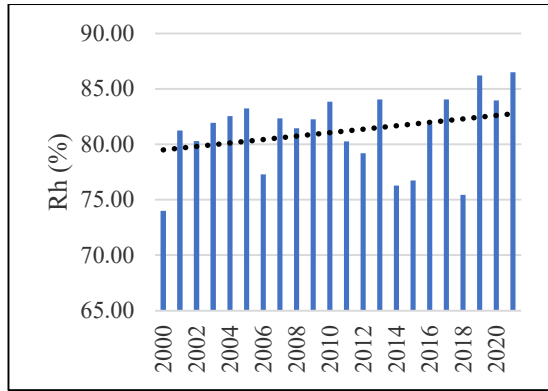

(a) Annual Seasonal Temperature chart

(b) Annual Pre-Monsoon Temperature chart

(c) Annual Monsoon Temperature chart

(d) Annual Post-Monsoon Temperature chart

(e) Annual Winter Temperature chart

Figure A 28: Seasonal Relative Humidity analysis at Grid-4 from 2000 to 2021

Grid-5

(a) Average Annual Temperature

(b) Average monthly Temperature

Figure A 29: Annual and Monthly Relative Humidity analysis at Grid-4 from 2000 to 2021

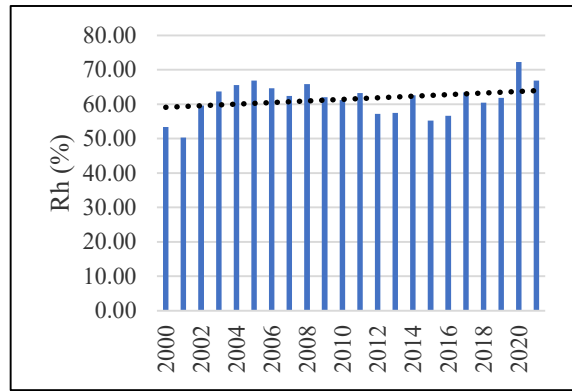

(a) Annual Seasonal Temperature chart
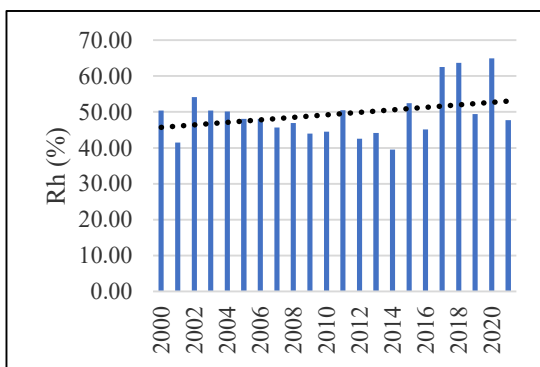
(b) Annual Pre-Monsoon Temperature chart
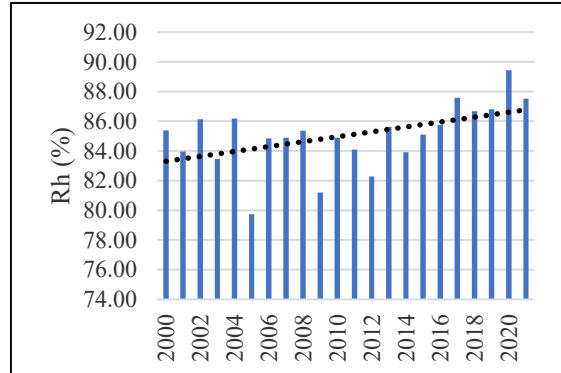
(c) Annual Monsoon Temperature chart

(d) Annual Post-Monsoon
Temperature chart

(e) Annual Winter Temperature chart

Figure A 30: Seasonal Relative Humidity analysis at Grid-5 from 2000 to 2021

APPENDIX-B

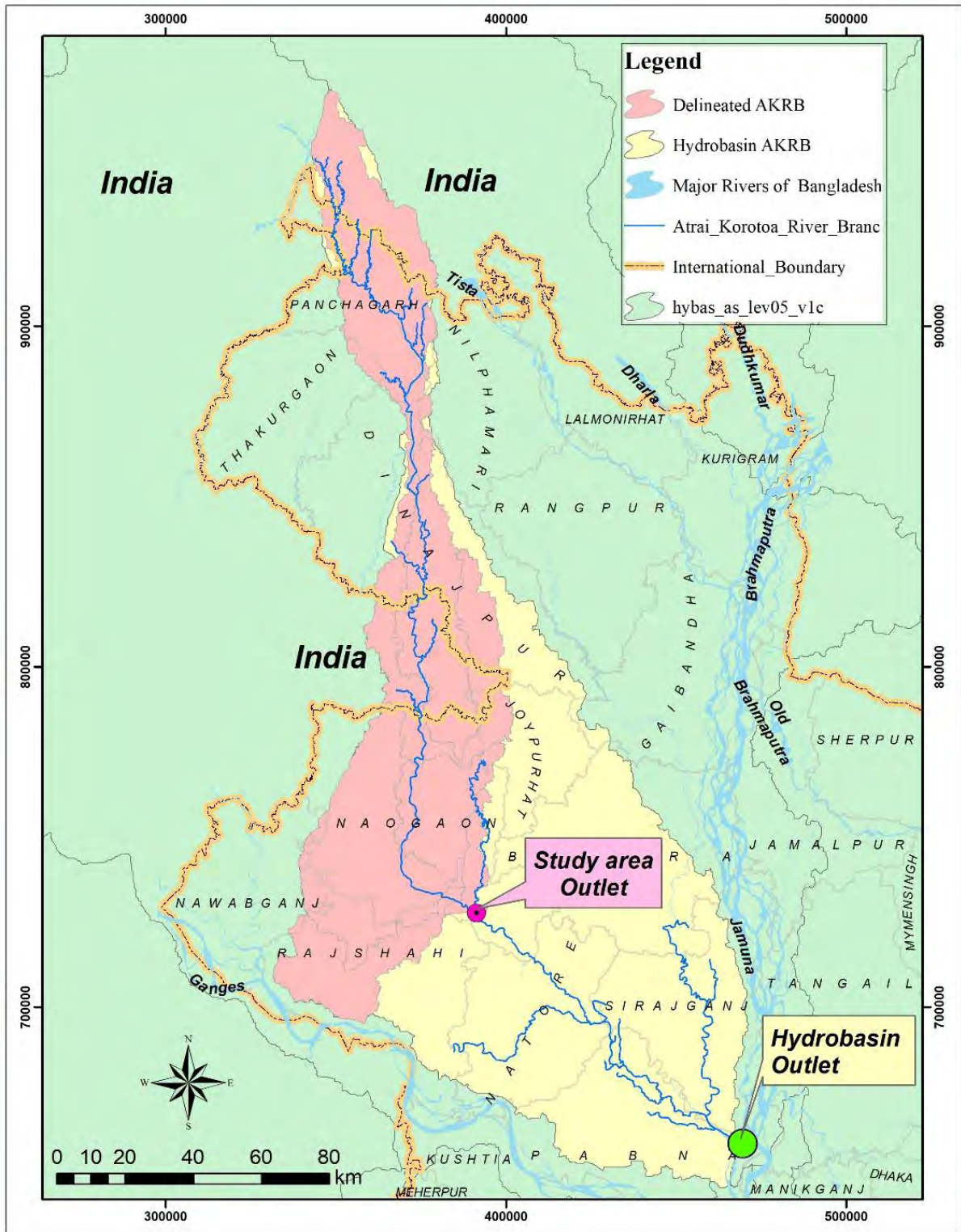**(Atrai-Karatoa River Basin Watershed Delineation Map)**

Figure B 1: Delineated AKRB watershed compared with the watershed of AKRB collected from HydroBasin